THE DEVELOPMENT OF AN ULTRASONIC BUBBLE DETECTION SYSTEM FOR USE IN ULTRASONIC CAVITATION RESEARCH

BY

ROBERT SADAO MORIMOTO

B.S., University of Illinois, 1983

THESIS

Submitted in partial fulfillment of the requirements
for the degree of Master of Science in Electrical Engineering
in the Graduate College of the
University of Illinois at Urbana-Champaign, 1985

Urbana, Illinois

ACKNOWLEDGEMENTS

I am indebted to many people for their assistance and support. Particular mention is due to the following for their exceptional interest and involvement: my parents who have offered their support throughout my education; Professor Leon A. Frizzell, my advisor, who helped to broaden my interest in engineering and offered criticism and assistance; Mike Haney, Steve Foster, Paul Embree, and Chong Lee for their technical advise; and Melanie Pan for her continued support and encouragement. I would also like to express my deepest gratitude to Joe Cobb and Bob Cicone. Special thanks are extended to Wanda Elliott for her expertise and assistance during the preparation of this thesis.

TABLE OF CONTENTS

CHAPTER 1

INTRODUCTION

Medical applications of ultrasound are numerous and diverse. The popularity of ultrasound lies in its ability to image soft tissue structures and its unique combination of convenience, comfort for the patient, noninvasiveness and a history of no known hazards to the patient. Real-time imaging and selectivity of application permit ultrasound to yield information not easily attained using other imaging techniques. Diagnostic applications of ultrasound, the most common application of ultrasonic technology, can be grouped into two categories: pulse echo and Doppler. The pulse echo technique utilizes one transducer operating alternately as a source and receiver and sophisticated electronics to process the received signals. Short pulses of ultrasound (1-3 microseconds) are transmitted into the body and the echoes from internal structures are detected by the transducer. Typically, the center frequency of the transducer lies in the low megahertz range (1-10 MHz) and the pulse repetition frequency varies from 0.5-5 kHz. The output ultrasonic intensity typically varies between 1-200 mW/sq cm SPTA (spatial peak, temporal average), and the SPPA (spatial peak, pulse average) intensity varies between 1-200 W/sq cm. The received signal contains information about the position and properties of the reflecting interface, which are obtained from the time of flight and amplitude of the signal.

The two primary modes of presentation of the echo information are the A-mode and B-mode; typically, one or both modes are

incorporated within medical ultrasound imaging systems. The A-mode (amplitude modulation) is the simplest method of displaying the received echo information. The received acoustic echo is converted to a voltage, proportional to the echo amplitude, which is displayed as a vertical deflection on a cathode ray tube. The location of the reflecting structure can be determined from the location of the signal along the baseline and a knowledge of the speed of sound within the structure. The B-mode utilizes an A-mode instrument, equipped with transducer position sensors and an intensity modulating display to map out the echoes for a two dimensional cross section. The transducer can be scanned mechanically, manually or electronically using a linear array of ultrasonic transducers.

Doppler ultrasound instruments are very common and are used to detect movement of interfaces or blood flow. The moving targets produce a backscattered signal of a different frequency than the incident ultrasound. The difference between the two frequencies is termed the Doppler frequency. It is proportional to the velocity of the moving target and is in the audible frequency range for typical blood flows. A common use of Doppler ultrasound is in obstetrics, particularly for monitoring the fetal heartbeat. The time averaged intensities of typical obstetric Doppler devices vary between 0.6-80 mW/sq cm SPTA.

Diagnostic ultrasound has been employed to image almost every region of the body, including the brain, eye, neck, heart, breast, and abdomen. In some cases, the same information can be obtained using other imaging modalities but often, ultrasound is the only technique available. Other medical applications of ultrasound

include surgery, hyperthermia, and ultrasonic therapy. In the latter case, it is desired to heat the tissue to produce beneficial effects. Ultrasound is particulary useful because it has a small wavelength and can be localized to heat tissue selectively unlike other forms of heating such as microwave or whole body hyperthermia. Therapeutic instruments operating at frequencies ranging from 0.5-3 MHz are capable of delivering acoustic intensities on the order of 1-3 W/sq cm SATP (spatial average, temporal peak). The irradiation period can vary between 5-15 minutes with the transducer moved within the treatment area to avoid excessive heating at one location.

Although no evidence exists for biological effects in mammalian tissue due to medical ultrasonic devices, it is commonly known that ultrasound can produce effects in biological systems. Small fish and frogs were killed when exposed to 300 kHz ultrasound at an intensity level believed to be in the neighborhood of 10 W/sq cm [Wood and Loomis, 1927]. The studies carried out in the 1940's by W. Fry and associates, and later by other groups on ultrasonically generated lesions in the central nervous system contributed to a large data base concerning the effects of high intensity ultrasound. Other studies range from _in vitro_ studies of the ultrasonic properties of biological tissue [Goss et al., 1978; Goss et al., 1980] to the effects on macromolecular structures [O'Brien et al., 1972; Coakley and Dunn, 1971] and _in vivo_ studies using whole organs [Dunn et al., 1975; Dunn et al., 1971; Chan and Frizzell, 1977]. This representative group of studies comprises a small part of the large data base concerning the bioeffects of ultrasound.

The research carried out within the last decade has been more concerned with the biological effects of low intensity ultrasound, similar to that used in medical applications of ultrasound. Recently, Carstensen and Gates (1984) published a review concerning studies of pulsed ultrasound on the fetus, revealing no direct evidence that diagnostic ultrasound produces any effect on the fetus. These studies, in addition to previous studies, still provide insufficient data to set numerical guidelines regarding safe levels of ultrasound to be used in medical diagnosis.

The primary mechanisms known to produce bioeffects are heat, radiation force, and cavitation. The thermal phenomenon is well understood and results from the absorption of ultrasound within the medium through which it is propagating. At low to moderate intensities, bioeffects due to thermal mechanisms have been reported [Dunn and Fry, 1971; Fry et al., 1970; Frizzell et al., 1979]. In addition to absorption, heat can develop in boundary layers and therefore small hot spots can exist within the biological media.

Radiation force can manifest itself as movement of interfaces, and flow of homogeneous viscous liquid media, called streaming. Those readers interested in a more rigorous treatment of the various mechanisms of ultrasound bioeffects are referred to, Fry (1979) and Carstensen et al., (1974). Also, an excellent collection of papers covering the areasof ultrasonic properties of biological material, interaction of ultrasound with biological media in solution and suspension, and the interaction of ultrasound with biological tissues and organs is contained in a book entitled Ultrasonic Biophysics edited by Dunn and O'Brien

(1976).

The other mechanism for effects from ultrasound in biological media is cavitation, a nonthermal mechanism known to cause biological damage at high ultrasonic intensities [Fry et al., 1970]. Ultrasonically induced cavitation activity is defined as formation of one or more pockets or cavities of gas in a liquid in response to an alternating pressure field, in this case, the irradiating acoustic field. Formation refers to the creation of a new cavity or expansion of a preexisting cavity to a size where effects can be observed. The cavity may contain either permanent gas or vapour. Two types of acoustic cavities are distinguished, stable and transient. Stable cavities are bubbles that oscillate, often nonlinearly, around some equlibrium size. They are relatively permanent and may continue oscillating for many cycles of the acoustic pressure. Transient cavities generally exist for less than one cycle or for only a few cycles of the pressure field. They expand to at least double and often to many times their original size and then collapse violently, often disintegrating into a mass of smaller bubbles [Neppiras, 1980]. The interested reader is referred to several review articles discussing the physical principles which underlie the production of acoustic cavitation [Flynn, 1964; Coakley and Nyborg, 1978; Neppiras, 1980].

The cavitation threshold is defined as the characteristic value which the sound field amplitude must exceed for cavitation to occur. For aerated gassed water, the threshold value is often found to be 1 atm (Esche, 1952) and varies depending on the experimental conditions. At higher ultrasonic frequencies, above

1 MHz, the thresholds increase sharply with increasing frequency. At 1 MHz, the threshold in tap water may be as high as 20 atm and increases to approximately 75 atm in degassed water. In optically transparent solutions, cavitation can be detected visually, but in opaque media, acoustic monitoring of harmonics, subharmonics and noise is used. Or, as suggested by the research presented herein, a bubble detection system could provide data showing the existence of bubble activity resulting from ultrasonic exposures. Experimentally, it has been found in liquids that the occurrence of cavitation requires the pre-existence of small gaseous bodies, or cavitation nuclei, generally thought of as microbubbles. It is well-known that larger bubbles tend to rise due to buoyancy, and degas the liquid and that smaller bubbles shrink and disappear due to the effects of surface tension. Harvey (1951) suggested the existence of cracks or corners in container walls or surfaces of suspended solid particles where gas could be trapped. The skin theory, especially appropriate for biological solutions or suspensions, suggests that organic molecules can collect at the surface of a gas bubble forming a sturdy skin which prevents diffusion and provides mechanical strength. Either of these mechanisms would provide stable cavitation nuclei.

Rectified diffusion is an important process by which a bubble that would ordinarily dissolve in a liquid may instead grow if it is located in a sound field of sufficient pressure amplitude. The process of growth occurs if the pressure amplitude exceeds a threshold value dependent on the amount of dissolved gas in the liquid, the bubble size, and acoustic frequency [Eller, 1969]. A bubble initially smaller than resonant size at a particular

frequency may grow by rectified diffusion to resonant size. Additional information regarding the principles of rectified diffusion has been published by Lewin and Bjorno, (1981) and Crum and Hansen, (1982).

When the sound pressure is above a critical value, the threshold for transient cavitation, the bubble expands to a maximum radius that can be many times larger than the initial radius and then collapses violently. Below this threshold, the bubble behaves as a stable cavity, oscillating in the acoustic field. Above the transient cavitation threshold, a small change in the driving pressure may result in a 1000 fold change in the size of the cavity at the moment of collapse. Calculations by Flynn (1982) show that the internal pressures in the collapsing transient cavitities generated by microsecond length pulses are of the order of 1000 to 70,000 atmospheres with accompanying temperatures approaching 1000-10,000 degrees Celsius. Shockwaves and free radicals provide the mechanical and chemical mechanisms for biological effects. Although previously it has been assumed that transient cavities do not occur under exposure conditions comparable to medical imaging, two recent developments suggest the need for further work. First, Child and Carstensen (1982) reported effects on drosophilia larvae when exposed to low level temporal average intensity ultrasound. The organism became most sensitized to ultrasound shortly before hatching, at which time the larvae has taken on air. Also, theoretical calculations reported by Flynn (1982) show that small gas nuclei in a liquid sonicated by microsecond pulses may become transient cavities. Carstensen (1982) suggests that bioeffects of low temporal,

average intensity pulsed ultrasound in tissues could be attributed to micron sized, stabilized gas bodies. He also suggests that it is the temporal peak intensity rather than the time averaged intensity that correlates with the observed effects.

That a cavitation-like mechanism may be responsible in part for a decrease in the growth rate of pea roots exposed to pulsed ultrasound was reported by Child et al. (1975). The growth rate of plant roots exposed to 10 W/sq cm ultrasound for 1 minute is reduced and has frequency and pressure dependence as reported by Carstensen et al. (1979). These observations support a postulate that a cavitation-like mechanism is at least partly responsible for the action of ultrasound. However, it should be noted that often a combination of mechanisms may contribute to a bioeffect.

Sommer and Pounds (1982) detected transient cavitation in both in vivo and in vitro studies in tissues. The cavitation threshold was reported to be 75 +/- 8 W/sq cm. ter Haar et al. (1982) using a B-scan bubble detector reportedly capable of detecting gas bubbles with diameters larger than 10 microns have detected gas filled cavities, in vivo, in the hind limb of guinea pigs during low level 0.75 MHz ultrasonic irradiations. Although most studies which suggest cavitation as a mechanism utilize higher levels of power than those typically used by medical diagnostic equipment, it has been shown by Carson et al. (1978) in a survey of diagnostic ultrasound equipment that two of the instruments examined had peak temporal and spatial intensities above 1000 W/sq cm.

Although numerous studies on non-mammalian and mammalian systems have shown that cavitation can be important in the

intensity ranges used in medical equipment, little information regarding the character and location of cavitation nuclei has been collected. Also, little data exists regarding the role of cavitation under pulsed exposure conditions.

Over thirty years ago a study was initiated at the Bioacoustics Laboratory at the University of Illinois to determine the role of cavitation as a mechanism of damage by ultrasound. In this study, the threshold for a functional endpoint, hind limb paralysis of the mouse neonate was determined using a specially constructed neonatal mouse irradiation system. The dosage relationships were determined as a function of tissue temperature and frequency [Dunn, 1956]. In these studies, neonates were irradiated at the frequencies 0.5, 0.7, and 1 MHz at temperatures ranging from 0 to 50 degrees Celsius over a broad range of exposure times and intensities [Brady and Dunn, 1974]. More recently, Lee (1982) studied the role of cavitation as a mechanism of damage in mammalian tissue <u>in vivo</u> using the neonate mouse system and a 10 degree Celsius irradiation temperature. A 1 MHz continuous wave ultrasound with intensities varying from 86-289 W/sq cm characterized the exposure parameters. Lee pointed out that there is a strong possibility that cavitation plays a minimal role in producing the functional effects for the intensity range 86-192 W/sq cm. In the range from 192-289 W/sq cm, he predicted that cavitation plays a more important role in producing the functional change. Frizzell et al. (1983) reported a factor of two increase in the exposure duration for paralysis of 50% of the mouse neonate specimens at 289 w/sq cm, 1 MHz, 10 degrees Celsius, and 16 atm hydrostatic pressure. The change in the exposure

duration for 50% paralysis was negligible at 86 and 144 W/sq cm. Pressurization suppressed the observed half harmonic signal at all intensities. Frizzell and coworkers suggest that cavitation may influence the production of the hind limb paralysis produced in the neonate when exposed to 289 W/sq cm ultrasound at ambient pressure.

To study the influence and origin of ultrasonically induced cavitation, in vivo, in the neonate mouse system, a detection system capable of detecting ultrasonically induced gas bubble activity was developed and is discussed in this thesis. Two approaches to the problem have been recognized and developed. In both cases, the incident 1 MHz ultrasound irradiates a neonatal mouse for a prescribed duration using high ultrasonic intensities, possibly causing stable or transient cavitation. To study the location and distribution of the cavitation nuclei, a pulse echo imaging technique incorporated within two data acqusition systems has been developed. The first imaging technique detects bubble activity resulting from continuous wave ultrasonic exposure. Data acquisition is achieved using a minicomputer controlled system. The second imaging technique detects bubble activity resulting from pulsed ultrasound exposures; data acquisition is achieved using microprocessor controlled hardware.

The remainder of this thesis is organized as follows. Chapter 2 presents an overview of the ultrasonic exposure system and the hardware modifications necessary to generate pulsed ultrasonic exposures. Chapter 3 discusses the imaging system incorporated within the continuous exposure data acquisition system. Chapter 4 discusses the imaging system modified for

pulsed exposures and the associated data acquisition system. Recommendations for further work appear in Chapter 5. The hardware for the system controller is discussed in Appendix A. In Appendix B, the Z80 data acquisition system controller hardware is discussed. Appendices C-I contain commented program listings.

CHAPTER 2

NEONATAL MOUSE IRRADIATION SYSTEM

2.1 Continuous ultrasonic exposure irradiation system

The block diagram in Figure 1 (see end of text for tables and figures), illustrates the neonatl mouse irradiation chamber and the associated electronics. Ultrasonic irradiations of the neonatal mouse occur in a cylindrical stainless steel chamber housed in a modified commerical deep freeze unit [Dunn, 1956]. The chamber has a vertical port allowing access to the interior, and can be pressurized up to 20 atmospheres by sealing the chamber with a steel cap. The deep freeze unit is equipped with refrigeration equipment and provides the first level of temperature regulation of the system. It is filled with propylene glycol which surrounds the chamber and is maintained at a temperature 2 or 3 degrees below the irradiation temperature, providing cooling to the irradiation chamber. The temperature of the Ringer's coupling medium within the irradiation chamber is regulated by a YSI proportional controller with a thermistor sensor, which controls a 300 W heating element. Uniformity of temperature is assured by a stirring blade driven by an electric motor.

The ultrasonic source is a 3.18 cm diameter X-cut quartz disk resonant at 1 MHz. The source is mounted at one end of the irradiation chamber and a large volume of highly absorbing castor oil is held by a thin rubber retaining wall, mounted at 45 degrees, at the opposite end. This assures that the neonate is

irradiated with essentially a traveling wave unfocused ultrasonic field. The neonate is mounted in a Plexiglas holder equipped with air lines for breathing, and is bolted to a 3 axis orthogonal coordinate system allowing accurate positioning of the neonate within the sound field. The acoustic coupling medium is degassed Ringer's solution maintained at 10 degrees Celsius, the irradiation temperature. Degassing of the coupling medium is essential to ensure that cavitation does not occur within the medium.

The electronic instrumentation as originally developed by Dunn (1956) has been considerably modified by Lee (1982). A Wavetek model 3006 synthesized signal generator produces the 1 MHZ RF signal which is gated and amplified by an ENI A-500 RF power amplifier capable of generating up to 500 W of power over its operating frequency of 0.3 to 35 MHz. The electronic gate consists of a minilabs SRA1-H RF mixer controlled by a CMC model 786C dual preset counter which is programmed for the desired duration. The output impedance of the amplifier is matched to the high input impedance of the transducer by an LC matching network. A constant voltage is maintained on the transducer by a stabilizing circuit which provides feedback to amplitude modulate the signal generator output, guaranteeing a constant ultrasonic intensity. A detailed description of the stabilizing and matching circuits can be found elsewhere [Lee, 1982].

Calibration of the ultrasound field is accomplished using the transient response of a thermocouple embedded in absorbing oil, which has been calibrated against a suspended steel ball radiometer. The interested reader is referred to Lee (1982) for

a complete description of the calibration technique and additional references.

The neonatal mice used for these experiments were acquired from a large colony maintained within the Bioacoustics Research Laboratory. The neonates, harvested daily, were less than 20 hours old, typically 2.5 cm. long and weighed between 1.5 and 1.6 grams. Since the neonate is a poikilothermic animal, it can undergo large temperature changes without adverse effects, and therefore could be used at 10 degrees centigrade. At this low temperature, the neonate is immobilized by the cold temperature and does not require any additional anesthetic. The neonate equilibrates within approximately three minutes to a temperature of 10.2 degrees Celsius in the 10 degree Celsius coupling medium [Dunn, 1956].

The functional endpoint utilized in the ultrasonic dosage studies was hind limb paralysis of the neonate resulting from the ultrasonic exposure [Frizzell, et. al., 1983]. The neonate was aligned in the irradiation chamber so that the entire third lumbar region was irradiated with an ultrasonic intensity within 5% of the peak intensity. After irradiation, the animal was removed and tested to determine if its hind limbs were paralyzed. This information, in addition to the data from the acoustical monitoring for harmonics due to bubble activity, was analyzed to determine if cavitation occurred within the neonate.

2.2 Pulsed ultrasonic exposure irradiation system

Previous studies with the neonatal mouse irradiation system used continuous ultrasonic exposures. Currently, the scientific

community has become increasingly interested in the investigation of the bioeffects resulting from exposure to ultrasonic diagnostic equipment, where pulsed ultrasound is typically used. The electronic gating system utilized for continuous wave ultrasonic exposures is not capable of generating microsecond length pulses. Therefore, the hardware controlling the ultrasonic exposure duration was modified so that short, repeated ultrasonic pulses could be generated. A digital circuit was developed to generate the control signal necessary to create short ultrasonic pulses of duration similar to the pulse lengths used in medical imaging. The remainder of the mechanical and electronic components of the neonatal mouse irradiation system remains unchanged.

The transducer must have an excellent transient response to produce wideband pulses of ultrasound. The 1 MHz ultrasonic transducer used in this research cannot generate short ultrasonic pulses (1-50 microseconds). The quartz crystal generating the ultrasound is very efficient and has low internal losses, resulting in little damping of the crystal so that ringing will occur with short pulses of ultrasound. The oscillograms in Figure 2 show the ultrasonic pulse envelopes generated by the 1 MHz transducer, as detected by a 10 MHz transducer. The pulse envelope shown in Figure 2(a) resulted from application of a 10 microsecond gated RF signal. In this case, it is clear that the transducer never achieves its full output because of its limited bandwidth. In contrast, the oscillogram in Figure 2(b) shows the pulse envelope for a 200 microsecond excitation signal. In this case the transducer reaches its full output following a finite rise time. A 1 MHz focused transducer, which uses a ceramic

crystal as the resonant element, is currently in development and will be capable of producing shorter pulses because of its greater bandwidth.

For continuous wave ultrasound experiments, the frequency, intensity, and exposure duration sufficiently describe the ultrasonic exposure parameters. In contrast, for repetitively pulsed ultrasound experiments, the pulse width, interpulse period and total exposure time replace the continuous ultrasound parameter, exposure duration. Therefore, a more complex controller is required to generate ultrasonic pulses with the desired timing. To create a short pulse of ultrasound, the continuous RF signal generated by the signal generator is pulse gated by the RF mixer for the desired duration before amplification and coupling to the transducer. To operate the RF mixer in the pulse gate mode, a control signal is required which is high for the duration of the ultrasonic exposure. For short pulses, the rise time of the pulse gated output must be small to minimize distortion of the output signal.

A TI 990 eight bit microprocessor was programmed to generate the control signals required to generate the ultrasonic pulses. Since the microprocessor operates at 2 MHz, the shortest pulse theoretically possible is 0.5 microsecond compared to the desired minimum pulse width of 0.1 microsecond. The actual minimum pulse length is larger than 0.5 microsecond because several clock cycles are required to set and reset the output signal at the microprocessors I/O port. As a result of these limitations, the microprocessor was used to generate pulses longer than 1 microsecond. Dedicated hardware was designed and fabricated to

generate ultrasonic pulses between 100 ns and 999.9 microsecond, under control of the microprocessor. This hardware was incorporated within the system controller described below.

Implementation of either bubble detection system in real time, for visual inspection of the echo data on an oscilloscope, required the design and fabrication of a multiple channel system controller. Figure 3 illustrates the output signals generated by the system controller. The PULSE GATE signal is the control signal used to drive the RF mixer. The P/R TRIGGER signal activates the pulse echo imaging system, thereby generating a short pulse of ultrasound which images the neonate. The RANGE GATE signal selectively gates the echoes received by the imaging transducer from the desired area of interest within the neonate. The SYNC signal is used to externally trigger an oscilloscope. The application of the latter three signals is discussed in Chapter 3.

Since the desired ultrasonic pulse width resolution is 100 ns, the hardware is operated synchronously at 10 MHz. The duration of the pulse gate, range gate, delay 1, and delay 2 (see Figure 3) is operator programmable. For design uniformity and increased versatility of the system controller, each of the four programmable channels was designed to generate a minimum 100 ns and a maximum 999.9 microsecond timing duration. To achieve the maximum timing duration, four stages of binary coded decimal (BCD) counters are cascaded; one set of these counters is used for each of the four channels. Since the counters are programmable, a keyboard is used to enter programmed data which are stored in latches. The BCD data loaded into each group of counters are

displayed by a digital multiplexed display system. The system controller can be operated manually via a pushbutton or may be triggered by an external trigger signal, such as a trigger signal from the microprocessor.

The four programmable channels are defined as: (1) PULSE GATE, (2) DELAY 1, (3) DELAY 2, (4) DELAYED GATE, herein abbreviated as PG, D1, D2, and DG, respectively. Channel 1 generates the control signal for the RF mixer, channels 2-4 generate the RG and P/R TRIGGER signals.

The TI microprocessor can be used to control the system controller via the external trigger input. For the repetitively pulsed experiments, the microprocessor is programmed with the ultrasonic exposure conditions. A signal is generated at the correct repetition rate by the microprocessor which triggers the system controller, generating RF pulses with the desired excitation pulse width. For ultrasonic pulses between 100 ns and 999.9 microsecond, the microprocessor assumes control over the PG channel of the system controller. The pulse width, period and exposure duration are input to the microprocessor, and data corresponding to the pulse width are down loaded to the storage latches in the system controller via the microprocessor's output port. An output signal of the microprocessor hardware triggers the system controller, which generates the repetitive ultrasonic pulses. A switch is used to select between manual or microprocessor control; when microprocessor control is assumed, the keyboard is inactivated and only the PG channel is operative.

The pulse gate circuit generates as output, a TTL signal, TTL* signal, and PG-RF signal. The asterisk (*) following a

signal name indicates an active low TTL signal, a convention followed herein. The TTL signal can be used to drive the control input to an RF mixer. The RF mixer incorporated within the system controller requires, as input, the continuous RF signal and generates the pulse gated RF output, available at the PG-RF output. The range gate circuit generates as output, a TTL signal, TTL* signal, P/R TRIGGER signal, and DG-RF signal. The received 10 MHz RF signal input to the RF gate, incorporated within the range gate circuit, generates the pulse gated RF signal available at the DG-RF output. A Sync signal is available for oscilloscope external triggering.

Three subcircuits comprise the system controller: (1) control and timing, (2) data entry, (3) display and data storage. Figure 4 illustrates the integration of each subcircuit into the complete design and illustrates the microprocessor interface. A detailed explanation of the hardware implementing each subcircuit is included in Appendix A. Circuit schematics, component layouts, and connector pinouts are included in Appendix A.

CHAPTER 3

CONTINUOUS ULTRASONIC EXPOSURE BUBBLE DETECTION SYSTEM

3.1 Pulse-echo imaging system

An ultrasonic pulse-echo imaging system was developed to detect bubbles within the neonatal mouse. The imaging system consists of pulser-receiver electronics, an oscilloscope, and an imaging transducer mounted on a three axis coordinate system. The block diagram in Figure 5 shows the principal components of the system, illustrating pulser-receiver configuration A, one of three configurations implemented. The transducer acts as a source when transmitting the pulse and as a receiver until the next pulse is sent. By using the imaging system, ultrasonic A-scans can be generated within the region of interest in the neonate. A short pulse of ultrasound is transmitted into the biological medium and the reflected energy resulting from scattering is received and amplified. In complex biological media (for example, a neonatal mouse), a returned echo could be due to acoustic reflection from normal tissue or bubble activity within the neonate. If bubble activity at the intensity levels used in this study is a result of stable cavitation, the bubbles should exist long enough to be detected. The location of the reflector can be determined from the time delay (time of flight) between the transmitted and returned echo signals. Since the time of flight, T (microsecond), corresponds to the round trip travel time, the distance from the transducer to the reflector, d (mm) is given by

$$d = 1.54\ T/2$$

where the velocity is taken as 1540 m/s.

The frequency of the imaging transducer should be higher than the 1 MHz irradiating transducer for two reasons. First, this allows frequency separation between the irradiating ultrasound and the frequency of the imaging pulse. This frequency separation is especially important when high intensity ultrasound is used for irradiation because the high power signal can be detected by the imaging transducer. Also, harmonic generation resulting from the nonlinear finite amplitude effect generates additional acoustic "noise" detectable by the imaging transducer. If the frequency difference is large enough, these effects will be minimized. The harmonics of the irradiating wave decrease in amplitude with frequency, so their amplitude would be low in the frequency range of maximum sensitivity for the imaging transducer.

The range resolution capability of the system is constrained by the precision with which the position in time of the arrival of an echo can be measured. This depends on the pulse width and the sensitivity of the receiver electronics. Since the pulse width decreases with frequency, the resolution increases with frequency, so it is desirable to use the highest possible frequency for the imaging transducer. The transducer must be broadband to accurately reproduce the wideband excitation signal and physically small enough to fit in the irradiation chamber. The highest frequency transducer available commercially, satisfying these requirements, is 20 MHz but it was not used due to data acquisition hardware constraints.

The two transducers picked for use in the bubble detection

system were the Panametrics V311 and V319 immersion transducers with center frequencies at 10 and 15 MHz, respectively. The 15 MHz transducer is suited only for qualitative studies because digitization of the echoes as required for quantitative analysis requires complex hardware which was not readily available at this frequency. Both transducers are designed to have a 1.27 cm aperture and 2.54 cm focal length. These two dimensions impose a lower limit on the volume of material that is imaged. Figure 6 illustrates the parameters describing the focal region. Dt is the transverse diameter (half power beam width) perpendicular to the direction of propagation at which the acoustic pressure amplitude squared is reduced to one half its peak value. The lateral resolution is determined by the beam width, which depends on the distance from the transducer to the imaged object and the receiver radius. The transverse diameter can be approximated as,

$$Dt = \frac{FL}{R}$$

where R is the radius of the transducer, F is the focal length and L is the wavelength in the medium. Da, the axial length of the focal region, is the distance between points along the axis of propagation at which the pressure amplitude squared is reduced to one half its peak value and is computed using the expression,

$$Da = Qa*Dt$$

The quantity Qa is dependent on the half aperture angle of the transducer, and a value of 12.5 is used [Fry and Dunn, 1962]. Using these expressions, the transverse and axial diameters of the 10 MHz transducer are estimated to be 0.60 mm and 7.50 mm, respectively. The transverse and axial diameters for the 15 MHz transducer are estimated to be 0.40 mm and 5.0 mm, respectively.

To determine the actual beam profile for the 10 MHz transducer, a pulse echo technique and a needle point reflector were used. The transducer, mounted stationary in the water tank, transmitted and received the echoes from the needle tip mounted in the moving tank. The tank was mounted on an automated millbase such that it could be moved in three orthogonal directions with a resolution of 25.4 microns. The needle tip was moved to the position where the received signal was largest, then scans in each of the three perpendicular coordinate directions were done. The two coordinates perpendicular to the direction of propagation from the transducer yielded similar beam plots as expected from the cylindrical symmetry of the imaging transducer. The 95% beamwidth was determined to be approximately 0.11 mm, and the transducer was found to be focused at 2.41 cm as measured from the front plane of the transducer to the focal point. The diameter of the needle tip determines the resolution of the beam profile measurement, but is not easily measurable.

The Panametrics model 5052PR ultrasonic pulser-receiver integrates all the electronics necessary to generate short pulses of ultrasound and amplify the returned echoes. To create the short pulses of ultrasound, the pulser must produce a short duration, high voltage spike waveform to drive the transducer. To control the amplitude of the pulse, the wideband waveform is sent through a matched attenuator before it is applied to the transducer. The amplifier used to process the received signal has good overload tolerance and a short recovery time because the high voltage pulse is coupled directly to the amplifier with only a small amount of attenuation. The amplifier has a wide dynamic

range and a low noise level to receive echoes from weak reflectors.

The pulser section of the device can be driven externally via an external trigger input (+5 volts into 50 ohms) when synchronizing of the pulser output is necessary. The internal trigger signal (200-5000 Hz) was not used in this study. The energy switch controlling the output energy contains four positions, and is used to select the optimum pulse width and excitation amplitude for a given transducer. The pulser was typically operated with an energy setting of 1, maximizing the range resolution. As the energy is increased, the system sensitivity increases but the range resolution degrades because the pulse width increases. Panametrics specifies a maximum pulse amplitude of -220 volts into 50 ohms; however, the input impedance to the transducer typically has resistive and reactive components. The input impedance of the transducer was measured with a Hewlett Packard model 4193A Vector Impedance meter. The impedance was measured with water and air coupling; the difference in the measurements was negligible. Over the range of frequencies for which the input impedance was measured, the phase angle of the impedance was negative. The nonzero phase angle implies that the input impedance of the transducer has real and reactive components. Therefore, it is likely that the delivered voltage is much lower than the value specified by Panametrics.

It was also possible with the pulser-receiver to adjust the damping applied to the transducer. Maximum damping is typically used for maximum range resolution. As the level of damping is decreased, the pulse width of the received signal increases.

Although maximum sensitivity is typically achieved with zero damping, a tradeoff exists between range resolution and system sensitivity. The sync signal output provides a 3 microsecond synchronizing pulse each time the imaging transducer is excited; this signal is used to trigger an oscilloscope. The receiver has a maximum 40 dB gain and a 0 - 68 dB attenuator adjustable in 2 dB steps. Since the received echo amplitudes resulting from bubble activity are very small, maximum gain is obtained.

The Panametrics device can be operated in two modes. When operated in mode 1 (see Figure 5), the transducer is connected to the TRANSMIT/RECEIVE (T/R) BNC connector for transmit/receive operation. In mode 2 (see Figure 5), only the excitation pulse is available at the T/R BNC; the received signal applied to the RECEIVE (RCVR) BNC connector is amplified and available at the SIGNAL OUTPUT BNC connector.

In pulser receiver configuration B (illustrated in Figure 7), the Panametrics generates the high voltage signal to excite the imaging transducer; the receiver portion of the device was not used. The Panametrics is operated in mode 2 to eliminate signal loading by the Panametrics receiver electronics. The received signal decoupled from the excitation pulse is preamplified using an Aydin Vector MHD-175 31 dB amplifier. An additional 20 decibels of amplification is achieved using a Hewlett Packard 461-A amplifier.

Pulser receiver configuration C, shown in Figure 8, eliminates use of the Panametrics device. The high voltage excitation signal is generated by a high output pulser circuit designed and fabricated by Paul Embree. The decoupled, received

signal is amplified using the same amplifier configuration shown in Figure 7.

To accurately position the imaging transducer in the irradiation chamber, the transducer is mounted on a three axis coordinate system. The coordinate system utilizes three Daedal, Inc. series 3900 linear translation stages integrated to provide 3-axes (X-Y-Z) of movement. Each stage is adjustable using micrometer screws to a resolution of 2.54 microns.

3.2 Continuous ultrasonic exposure data acquisition system

A technique to detect cavitation induced bubble activity *in vivo* resulting from continuous wave ultrasonic irradiation has been developed utilizing the three pulser-receiver configurations described in the previous section. Figure 9 shows a schematic of the irradiation chamber and a block diagram of the system electronics. A Perkin-Elmer 7/32 minicomputer was used to process the data and generate the signals controlling all aspects of the experiment. The minicomputer is a 32 bit machine with 384 kilobytes of memory and four 5 megabyte hard disks. The neonatal mouse is mounted in a holder, aligned using a microscope, and mounted in the irradiation chamber. After the controlling program is initialized with the specific experimental parameters, i.e., baseline and ultrasound exposure times, the acquired data corresponding to the received echo signals are stored in the computer for further processing. The data taken during the baseline period, when the neonate is not exposed to ultrasound, are processed to generate the mean reference echo. The data taken during the ultrasonic exposure are compared to the mean echo to

identify new echoes that may arise from bubble formation, resulting from cavitation activity. The software and associated hardware were originally developed by Foster (1984).

The FORTRAN program NEO, listed in Appendix C, controls the hardware required to acquire and store the data in the computer. The parameters: (1) intensity, (2) baseline, (3) experiment duration, (4) pulser energy, (5) range, and (6) width are entered as input to the program. The parameters, intensity and pulser energy are output variables, stored in the output file generated by the program. The first three parameters characterize the ultrasonic exposure; intensity has dimensions of W/sq cm, the baseline and experiment durations are entered in seconds. The ultrasonic exposure duration is equal to the difference between the experiment duration and the baseline. The fourth parameter, pulser energy, is input to the program because the pulser was sometimes operated with an energy setting larger than 1, sacrificing range resolution for increased system sensitivity. The last two parameters, range and width, determine the delay and width of the range gate relative to the pulser trigger signal. The range gate determines the portion of the reflected echoes to be stored for further processing. The range gate parameters are used internally by the 7/32 DAS during data acquisition and the RANGE GATE signal is available for oscilloscope display. Figure 10(a) shows the RANGE GATE signal and the relation among the range and width parameters. The oscillogram in Figure 10(b), generated during an experiment, shows the actual range gated signals reflected from the neonate. The two parameters characterizing this signal, range and width have units of microsecond and can be

converted to an equivalent distance by multiplying by the velocity of sound in the medium. Range determines the delay between the P/R TRIGGER signal and initiation of data acquisition. Width determines the duration for which data are acquired and stored in the computer. The RANGE GATE signal is displayed on the second trace of a dual trace oscilloscope and shows explicitly which portion of the data is stored. The output of the receiver is displayed on channel one and the scope is triggered externally by the P/R TRIGGER signal.

3.3 Description of the 7/32 data acquisition system hardware

Analog to digital (A/D) conversion necessary for data storage and computer processing is accomplished using a computer controlled A/D converter [Foster, 1984]. The block diagram in Figure 11 shows the components comprising the A/D converter, which consists of two TRW TDC1007J 8 bit flash A/D's operating in parallel at 25 MHz, for a net 50 MHz digitizing rate. The converter contains dedicated memory capable of storing the digitized data at high speeds. An ECL oscillator running at 25 MHz generates a two phase clock allowing each A/D to operate off alternate clock edges. In this way, two samples are generated during each period of the clock, thereby allowing digitization of a wider bandwidth signal than is possible using one A/D. The swing of the input data is limited to +/- 500 mV to guarantee accurate conversion and no saturation of the A/D's. The eight bit parallel conversion has a resolution of 3.096 mV. Ideally, any received noise signal should be limited to less than +/- 3.096 mV so that the noise is not detected when the input signal is

quantized. If over or under range inputs are encountered, the output of the A/D is clipped and the inputs are represented at FFH and 00H, respectively, where 'H' indicates a hexadecimal number. The eight bit output of each digitized sample is stored in a dedicated block of high speed memory. Each memory block utilizes the INTEL model 2115A static memory chip, organized as a 4 kilobyte memory block addressable by the A/D and 7/32 minicomputer. The address lines of the A/D's are strobed by the outputs of a 12 bit counter clocked synchronously with the A/D when the range gate is high or when the computer requires access to the stored data. The A/D converter is controlled by assembly language program ATD3, a subroutine called by NEO. A listing of ATD3 is provided in Appendix D.

The hardware necessary to generate the RANGE GATE signal and the P/R TRIGGER signal is now described. A digital circuit made up of four cascaded counter blocks (see Figure 11) and additional combinational logic comprise the hardware. Each block of counters has an associated block of storage latches, containing the computer programmed data. The four counter blocks are called P/R trigger, range, range gate, and echo, respectively.

The pulser is externally triggered periodically by the computer controlled P/R TRIGGER signal. The pulse repetition rate is determined by the length of the experiment and the total number of frames of echoes to be digitized. Since the size of memory accessible by each A/D is fixed, the width of the range gate determines how many echoes can be digitized and stored in memory. The pulse repetition rate is equal to the experiment duration divided by the total number of echoes minus one. The P/R TRIGGER

signal is generated by a free running 24 bit counter operating at 5.005 MHz. Twenty-three bits of the counter are available to generate the delay between successive triggers, allowing a minimum repetition rate of 0.59 Hz. The counter must be free running so that the pulser generates consecutive pulses and a flicker free oscilloscope display of the received echoes, as required to align the imaging system during an experiment. Once the repetition rate is determined from the input parameters, the appropriate digital data are stored in latches and presented to the data inputs of the P/R trigger counter. At the end of each P/R trigger timing cycle, the counter reloads and generates the P/R TRIGGER pulse. At this time, bit 23 of the P/R trigger counter, driving the input to a flipflop, changes state, enabling the 16 bit range counter after the next clock edge. At the end of the range gate, the flipflop is cleared and is not reset until the next P/R trigger is sent. The 16 bit range counter, loaded with data contained in latches previously loaded under program control, operates at 5.005 MHz and can generate a maximum 13.09 ms delay. After the range counter has counted the programmed amount, the 16 bit range gate counter is enabled. After the range counter has counted the programmed amount, the 16 bit echo counter is incremented. The echo counter is loaded with data corresponding to the total number of echo frames to be digitized. When the echo counter overflows, the computer is flagged, indicating that the data acquisition sequence is completed. Until this counter overflows, the sequence of P/R trigger, enable range counter, enable range gate counter and increment echo counter continues. The digital data for the P/R trigger and echo counters are loaded into the appropriate latches

under the control of assembly language program ATD3. A listing of ATD3 is provided in Appendix D. The data loaded into the range counter and range gate counter are calculated from the appropriate values entered into the program and loaded into the latch by assembly language program CURSOR, a subroutine of NEO, listed in Appendix D.

The control input to the RF mixer, controlling the baseline and ultrasonic exposure duration, is generated by the 7/32 computer. The parameters, baseline and experiment duration are used by assembly language program RF to control one channel of the digital input-output (DIO) board, generating the control signal. A listing of RF is included in Appendix D.

3.4 Problems encountered during application of the system

Several problems were encountered during the various phases of system development. Since the propagating acoustic wave transports momentum, it exerts a steady force on interfaces within the medium called radiation force. Longevin radiation force results from the difference between the mean pressure at an absorbing or reflecting wall and in the same acoustic medium, at rest, behind the wall. When the ultrasound is turned on, radiation force causes a small movement of the neonate within the acoustic field, even though the neonate's limbs and head are securely positioned in the holder.

For all experimental intensities, the movement of the neonate was detectable by the 7/32 DAS since the system can ideally detect a 30 micron movement of the neonate, corresponding to the distance

between two A/D samples. The actual threshold for detection depends on the system's sensitivity and the characteristics of the echo being tracked. During continuous ultrasonic exposures, the neonate moves shortly after the sound is turned on to a new equilibrium position. This movement is easily detectable during exposures of 1 s or longer if the position of one echo as displayed on an oscilloscope is followed during the transition between sound on and sound off. Since the neonate moves in the direction of propagation, the echoes will be shifted toward increased time of flight, and the echo from an interface with the sound off would be received before the same echo with the sound on. In terms of the data acquired during the data window, the range parameter appears shorter but the width parameter is not affected, as illustrated in Figure 12. Therefore, if the movement at a given intensity can be determined, the range parameter can be adjusted to ensure that the desired data are acquired. This is assuming that the movement is not so severe that the desired echoes are moved completely out of the window. The reason for concern lies in problems encountered during data processing, a topic not yet discussed.

The movement of the neonate can be dealt with in two ways. First, if the amount of movement is known for the desired intensity, the transducer can be moved to compensate for the movement of the target. As illustrated in Figure 13, the imaging transducer undergoes a linear translation in one direction. In this way, the focal region of the transducer can be adjusted to cover the target region during the time that the sound is turned on and the neonate moves to its new equilibrium position. This

allows collection of the desired data when the sound is on, but the data acquired during the baseline period are shifted and only the overlapping portions of the data can be used for processing. This solution is dependent on the uniformity of weight and size of the neonates. Although the neonates are carefully monitored to ensure correct age and weight, there are subtle anatomical differences resulting in different responses to the same intensity ultrasound which does not allow the necessary generalization of the solution.

The second solution utilizes software to shift the data to compensate for the movement. This is accomplished by designating an echo to be a "landmark" echo. If the "landmark" echo is identified in each group of echoes affected by radiation force, the shift can be determined by noting the location of this echo within the frame of the mean echoes and in the echoes acquired during the ultrasonic exposure. The concept of the mean echo is introduced in a later chapter. Basically, it is the frame of echoes obtained when each sample within each frame of baseline echoes is averaged over all the frames of baseline echoes. Herein, a frame of echoes corresponds to the data acquired resulting from the returned echoes from one imaging pulse transmitted into the neonate.

The landmark echo is selected using the criteria that it is easily detected in both the baseline and ultrasound exposure echoes and is not greatly affected by the ultrasonic exposure. The amplitude of the echo must be very large to ensure that false alignment of the echoes does not occur. The ideal echo to use which satisfies the requirements is the first reflected echo from

the interface between the coupling medium and the neonate. The signal amplitude of this echo is the largest obtainable and typically will saturate the A/D because of the difference in dynamic range as compared to the echoes of interest.

This technique is implemented by shifting the mean echo along each of the echoes obtained during the ultrasonic exposure until the landmark echoes from each frame are aligned. Then the shift is measured and stored for later use. This technique does not require modification of the system geometry and is done using a quantitative process resulting in precise and reproducible data processing. To process the data, while compensating for the effects of radiation fore, a larger range gate must be used, resulting in an increased number of samples for each frame of echoes. As long as the window length is picked, such that no echoes of interest which are present in the baseline case are missing when the sound is on, no data are lost. However, increasing the window length decreases the total number of echoes that can be taken. For example, if the window length is doubled, the number of echoes is halved. Decreasing the number of echoes will decrease the accuracy of the system from a statistical point of view.

The 10 MHz ultrasonic transducer is utilized in the ultrasonic imaging system as both a transmitter and receiver of ultrasound. Since the transducer is broadband, it can receive a range of frequencies including the desired 10 MHz signal. Throughout the range of ultrasonic intensities used in previous studies with the mouse neonate system (44.84 W/sq cm - 289 W/sq cm), the 1 MHz signal was distorted by finite amplitude effects,

producing higher harmonics which increased in magnitude with the intensity of the irradiating ultrasound. The source of these "noise" signals is discussed and different filtering techniques are presented to try to minimize the effect of the "noise" on the data.

Even at the lowest ultrasonic intensity (44.84 W/sq cm), a slightly distorted 1 MHz signal can be detected in addition to the desired 10 MHz signal. Figure 14(a) is an oscillogram taken of the signal detected by the 10 MHz imaging transducer when 44.84 W/sq cm ultrasound is incident on a small diameter, reflecting metal cylinder. The cylinder is positioned to emulate the neonate spinal cord, but generates a larger reflected signal than the neonate would, so the noise signals detected are typically larger than what normally occurs. Another advantage of using the cylinder is that spectral analysis will not be affected by cavitation related noise signals. The signal is essentially periodic with frequency 1 MHz and has a peak to peak swing of approximately 190 mV. It is slightly distorted and therefore is comprised of several frequency components in addition to 1 MHz. A Hewlett Packard 8553B spectrum analyzer was used to determine the frequency spectrum of the observed signal. As illustrated in Figure 14(b), the second through seventh harmonics of the 1 MHz signal have nonzero Fourier coefficients in the Fourier series describing the signal. Therefore, the detected signal is comprised of several frequencies, the dominant frequency being the 1 MHz fundamental frequency. The signals are displayed using a log scale because of the large amplitude fluctuations between any two adjacent frequency components. For an intermediate ultrasonic

intensity of 144 W/sq cm, the detectable noise signal is still periodic but it has increased in amplitude. As shown in Figure 15(a), the peak to peak amplitude has increased to approximately 340 mV and is further distorted. The oscillograms of the frequency spectrum shown in Figures 15(b) and 15(c) illustrate an increase in the number of detected frequency components to 11. At 256 W/sq cm, the highest intensity used, the peak to peak amplitude increased to approximately 440 mV. The increased level of distortion is shown by the oscillogram in Figure 16(a). The corresponding oscillograms of the frequency spectrum (Figures 16(b) and 16(c)) show the increased frequency content of the signal. In Figure 16(b), the center frequency of the oscillogram is 10 MHz and 18 harmonics are detected. Figure 16(c) illustrates the higher frequency spectra detected when the center frequency of the spectrum analyzer was increased to 20 MHz and the input signal was amplified. It is very difficult to obtain a composite oscillogram illustrating all the frequency components because of dynamic range and bandwidth limitations of the spectrum analyzer. It should also be noted that the relative magnitude of each harmonic is not appropriately represented in Figures 14-16 because the receiving transducer has a very nonuniform frequency response. However, the data clearly illustrate an increase in the amplitude and distortion of the noise signal as the ultrasonic intensity increases. For any of the ultrasonic intensities, the noise levels are much higher than the resolution of the A/D. When pulser-receiver configuration A (mode 1) is used, the noise signal is amplified along with the desired 10 MHz signal, resulting in clipping of the A/D and loss of the 10 MHz signal. Although the

tenth harmonic (i.e., 10 MHz noise) is detectable for the higher intensities, its amplitude is very small and is ignored.

Since the 1 MHz signal is at a much higher power level than the 10 MHz signal transmitted by the imaging transducer, it is reasonable to expect detection of some 1 MHz noise. This has been experimentally observed along with broadband noise which was not predicted.

Digital and analog filtering techniques have been applied to the imaging system to reduce the "noise" content of the received signal. The most obvious solution might be an analog bandpass filter centered around 10 MHz. This type of filter will reduce the amplitude of all the harmonics except those in the pass band of the signal, thereby reducing the "noise." However, reducing the bandwidth of the signal results in ringing and loss of range resolution. Therefore, a bandpass filter is an effective means for eliminating much of the harmonic "noise" signal but results in loss of range resolution.

The 10 MHz bandpass filter design is shown in Figure 17(a). This filter has half power frequencies at 8.78 MHz and 11.78 MHz and provides 26 dB rejection at 1 MHz. This filter was used extensively during the development of the continuous wave exposure imaging system.

An alternate approach is to use a high pass filter. Since the amplitude of the harmonics decreases with frequency, a high pass filter can reduce most of the harmonic noise (below 10 MHz) without decreasing the bandwidth of the imaging signal as much as a bandpass filter.

Two five pole doubly terminated high pass Butterworth filters

were designed with lower half power frequencies at 6 MHz and 8 MHz. As shown in an earlier discussion, for the lowest intensity (44.84 W/sq cm), only the first six harmonics contribute significantly to the noise spectra. Therefore, the highpass filter with a half power frequency at 6 MHz would be effective in removing most of the noise. For higher intensities where more harmonics are detected, the filter with a half power point at 8 MHz would be used. At these intensities, an engineering tradeoff exists between a high frequency lower half power cutoff and an acceptable level of attenuation at 10 MHz. The attenuation at 10 MHz increases because the frequency response begins to drop off well above the half power frequency. Figures 17(b) and 17(c) illustrate the two highpass filter designs. The highpass filter, with a designed 6 MHz lower 3 dB point, was found to have -3 dB points at 6.25 MHz and 30.25 MHz. The attenuation at 1 MHz is 50.45 dB and at 10 MHz is 0.72 dB. The highpass filter, with a designed 8 MHz lower 3 dB point, was found to have -3 dB points at 8.79 MHz and 32.9 MHz. The attenuation at 1 MHz is 52.04 dB and at 10 MHz is 0.91 dB. Figure 18 illustrates the distortion of the filtered signal relative to the input signal for each of the three filter designs. The upper trace of each oscillogram displays the input signal, the filtered signal is displayed by the lower trace. The signal filtered by the 10 MHz bandpass filter shown in Figure 18(a) has a longer effective pulse length, resulting from the ringing generated by the filter. The same signal filtered by the highpass filters, illustrated in Figures 18(b) and 18(c) are less affected by ringing, although the 8 MHz filter results in some signal ringing. The 6 MHz filter shows the best response, minimal

ringing and loss of signal amplitude.

To minimize the effect of the noise signal, the received RF signal from the imaging transducer is filtered before amplification. For the case of pulser-receiver configuration A, the Panametrics device is operated in mode 2. Now the T/R output generates the excitation signal and the received RF signal is applied to the RCVR BNC connector. This is illustrated in Figure 5, where a decoupler circuit is inserted between the T/R BNC connector and the transducer. One output of the decoupler is connected to the transducer, the filter is inserted between the other output and the RCVR BNC connector. For pulser-receiver configurations B and C, the analog filter is inserted between the decoupled, received RF signal and the external amplifier.

Still another approach is to use a digital filter to attenuate the harmonic noise. This is convenient because the quantized data are stored in computer memory. A digital filter is a linear shift-invariant discrete-time system that is realized using finite-precision arithmetic. The precision of the implementation depends on the word length used by the computer, in this case 32 bits. Design of digital filters involves three steps: (1) the specification of the desired properties of the system; (2) the approximation of these specifications using a causal discrete-time system; (3) the realization of the system using finite-precision arithmetic. The digital filters were designed and implemented for this application using a program developed by Parks and McClellan (1972). This program computes the coefficients required to implement a finite impulse response (FIR) linear phase filter. Using this program, the coefficients

for an N tap linear phase FIR filter were computed. The designed filter is characterized by equiripple behavior in both the passband and stopband. The unquantized and eight bit quantized frequency response can be plotted if desired. Input variables are: (1) filter length; (2) type of filter; (3) bandedge array; (4) desired function array for each band; and (5) weight function array in each band. To generate highpass filters, two bands are required where the weight is 0 in the stopband and 1 in the passband. The digital filter can be implemented in the frequency domain using the fast Fourier transform (FFT) or in the sequence domain using convolution. The coefficients for four digital highpass filters were obtained; the respective lower and upper band frequencies for each filter were 2.5 MHz/7.5MHz, 4.0 MHz/6.0 MHz, 6.0 MHz/8.0 MHz, and 7.0 MHz/9.0 MHz. The unquantized frequency response of the digital filter with bandedges at 7.0 and 9.0 MHz is illustrated in Figures 19(a) and (b). Program DIGFIL computes the convolution of the discrete input data and the filter coefficients. The coefficients for the four filters are stored in a file that can be accessed by the program; one set of coefficients is selected by the operator. The input and output data are stored in files accessed by the program. The file containing the filter coefficients and a listing of DIGFIL are provided in Appendix E.

The filter responses were obtained for each of the digital filters, using constant input data. Figure 20 shows the filtered response for the digital filter with bandedges at 2.5/7.5 MHz; the top plot is the input data and the bottom plot is the filtered output. Figure 21 shows the filtered response for the filter with

bandedges at 4/6 MHz. Figures 22 and 23 show the filtered response for the digital filter with bandedges at 6/8 MHz and 7/9 MHz, respectively. For the first two filters, minimal signal attenuation and ringing are observed. But the remaining two filters introduce considerable signal ringing and signal attenuation. This is expected because these two filters have cutoff frequencies very close to 10 MHz resulting in loss of signal bandwidth. To illustrate the effectiveness of digital filtering, a 1 MHz and 10 MHz sine wave were digitized and filtered using the digital filter with bandedges at 2.5/7.5 MHz. Figure 24 shows the 1 MHz input signal and the filtered output, which was reduced to zero. Figure 25 shows the 10 MHz input signal and the filtered output which differs in phase but differs only slightly in amplitude.

3.5 Data processing

After the acquired data are stored in the 7/32 computer, additional programs are used to pre-process the data compensating for the radiation force and "noise" effects. Program DIGFIL implements a digital highpass filter, further attenuating the analog filtered noise signal. One of the four sets of filter coefficients is used, depending on the ultrasonic intensity level. Program INTERP, 1:5 interpolates the analog and digital filtered data, providing better reconstruction of the quantized data, especially when plotting of the data are desired. Although it is possible to list and inspect the data in a numerical form, it is often difficult to determine the relation between frames of

echoes. Program ECHO utilizes a plotting package to generate hardcopy plots of specific frames of data. The data are processed by program ANALYZ to determine if bubble activity exists. The data processing involved in programs INTERP, ECHO, and ANALYZ are now discussed; DIGFIL was discussed in the previous section of this chapter.

It is desired to translate the data sampled at 50 MHz to a higher sampling rate; this process is illustrated in Figure 26(a). The sampling rate increase is basically an interpolation process and can be efficiently implemented using a FIR digital filter. The process of interpolating a signal x(n) by an integer ratio L is depicted in Figure 26(b). The sampling rate of x(n) is increased by L by inserting L-1 zero valued samples between each sample of x(n). This creates a signal w(n) whose frequency components are periodic with a period equal to the original sampling frequency as shown in Figure 26(b). To eliminate the periodic components and retain only the baseband frequencies, it is necessary to filter w(n) with an appropriate lowpass filter. The resulting signal y(n) with sampling frequency L*f is the desired interpolated signal. The Fourier transform of y(n) is shown at the bottom of Figure 26(b). The FIR filter, in a standard direct form implementation, is chosen as the digital lowpass filter. The magnitude and phase of the digital lowpass filter are shown in Figures 27(a) and (b). In this case, the output of the filter y(n) can be computed by the relation

$$y(n) = h(m)w(n-m)$$

where $h(m),(m=0,...N-1)$ are the filter coefficients and N is the duration of the unit sample response of the filter. The

computation is causal; the computation of an output point depends only upon past and present values of w(n) and not upon past values of any internal filter variables. The filter computations need be made only once for every five points because the other points are zero. A more detailed explanation of the interpolation process can be found elsewhere [Crochiere et al., 1975]. The coefficients for the desired linear phase lowpass FIR filter were obtained using the digital filter design program.

Program INTERP listed in Appendix F implements the interpolation process, convolving the input data and the filter coefficients. Also included in the interpolation program is the capability to generate plots of the input data and the interpolated data. Figure 28 is a sample output of the program, the upper plot is the input data, and the lower plot is the interpolated data. Hardcopy plots of the data at various points of data processing are useful for visual inspection of the acquired data and the effects of digital filtering and the interpolation process.

Plots of the data acquired by program NEO are generated by the program PLOT. Since only specific frames of data are typically examined, the desired frames of echoes to be plotted are selected and stored in a file accessed by the plotting program. The approximate echo amplitude (mV) is determined for each quantized sample and is plotted versus the sample position within the range gate (microsecond) over which the data were collected. Up to nine different frames of echoes can be selectively plotted by PLOT. A fully commented listing of PLOT is provided in Appendix G.

During execution of DIGFIL, a specified number of samples of the input data and the filtered data are stored in a file accessed by program ECHO. This program generates a pair of plots, allowing a direct comparison of the input and the filtered output data. The amplitude of both the input data and the filtered data are plotted in millivolts versus the echo position within the range gate. A listing of ECHO is provided in Appendix H.

To determine if ultrasonically induced cavitation occurs within the neonate, the following data analysis is performed on the preprocessed data. Program ANALYZ listed in Appendix I performs the data processing. Under ideal conditions, i.e., no "noise" or radiation force effects, an echo acquired during the baseline exposure could be subtracted from each of the echoes acquired during the ultrasonic exposure. New components or increased amplitude for existing components in echoes detected during the ultrasonic exposure might be attributed to reflection from bubbles created by ultrasonic cavitation activity.

Rather than using only one frame of the baseline echoes as the reference echo, the "mean" echo is computed using all of the baseline data. The value of each sample comprising the "mean" echo is computed as the mean of the corresponding sample over all of the frames of echoes acquired during the baseline exposure. Each sample in the mean echo is subtracted from its corresponding sample within each frame of the ultrasonic exposure data. The root mean square (RMS), difference as defined by

$$\left[\sum_{\text{samples}} (\text{DATA ECHO} - \text{MEAN ECHO})^2\right]^{1/2}$$

is the measure used to quantify the difference between the echoes collected with and without ultrasound. The accuracy of this

analysis technique depends on the variability observed in the echoes collected during the baseline period. The effects of noise and radiation force will decrease the accuracy of the technique, the level of which depends on how well the data are preprocessed to compensate for these problems. The variability that is observed would determine the noise floor threshold which must be well below the actual mean difference in order for it to be considered a valid difference between the mean echo and the data. The noise floor was experimentally determined by analyzing the data taken during an experiment when the ultrasound was not turned on so that only baseline data were acquired. The mean echo was computed and the RMS mean difference was computed for each frame of the baseline data. The plot of the RMS difference shown in Figure 29 illustrates the noise floor for a 2 microsecond range gate. As the width of the range gate increases, the noise floor also increases. To determine the noise floor when data are acquired during the baseline and ultrasonic exposure period, the RMS difference for the baseline echoes is examined. To accurately approximate the noise level, a large number of baseline echoes should be acquired, but due to memory constraints this cannot be achieved.

Consideration of either noise or radiation force effects complicates the data processing and the determination of the noise floor. If it is assumed that the combination of analog and digital filtering effectively removes the noise content of the 10 MHz signal, the effects on the noise floor should be minimal and can be ignored. It is extremely difficult to experimentally determine the noise floor with these complications because if

cavitation is occurring, the additional signal resulting from bubble activity could not be differentiated from noise.

The power contained in each frame of echoes is also computed, using

$$P = \frac{1}{K_2 - K_1} \sum_{K_1}^{K_2} s(K)^2$$

where k1 and k2 are the limits bounding the sequence and x(k) is the value of sample k. This power is expressed in decibels as

$$P(db) = 10 \text{ LOG } \frac{P}{PREF}$$

where Pref corresponds to the power contained in a +/- 500 mV 10 MHz sine wave where

$$F(t) = 128 \sin \omega_o t$$

and Pref is computed using

$$PERF = \frac{1}{T} \int_o^T f^2(t)dt$$

$$= \frac{16384}{T} \int_o^T \sin^2 \omega_o t dt$$

$$= 8192$$

During the baseline period, the power should be constant but if additional echoes are detected during irradiation resulting from scattering from ultrasonically induced bubble activity, the power contained in each frame will increase. Therefore, an increase in the RMS difference should be accompanied by an increase in power. Figures 30(a) and (b) show a sample output of program ANALYZ illustrating the parameters computed by the program. ANALYZ generates a plot of the RMS difference and power versus frame number which is examined for evidence of bubble activity.

Figure 31(b) illustrates an echo detected by the imaging transducer, resulting from acoustic reflection from an interface within the neonate. Figure 33(a) shows the echo acquired during

the ultrasonic exposure. The detected signal is the sum of the desired 10 MHz signal and the noise signal. The noise signal, periodic at 1 MHz, is attenuated after digital filtering as shown in Figure 32. After application of the digital filter with bandedges at 2.5/7.5 MHz, the desired echo is recovered. The interpolated, filtered echo is shown in Figure 33.

CHAPTER 4

PULSED ULTRASONIC EXPOSURE BUBBLE DETECTION SYSTEM

4.1 Introduction to the technique

To avoid several of the problems encountered using the continuous wave pulse echo technique i.e., broadband noise, and movement of the neonate due to radiation force, a technique utilizing pulsed ultrasonic exposure was developed. The block diagram in Figure 34 shows each element required to implement this technique. To aid the description of the technique, the geometry of the acoustic fields generated by the two transducers and the relation between the system parameters are illustrated in Figure 35.

If a short pulse of 1 MHz ultrasound irradiates the neonate periodically, the fundamental signal and its harmonics will be contained within a temporal packet, constantly changing in position as the pulse propagates away from the source. Therefore, it is possible to temporarily separate the irradiating pulse and the range gated echoes resulting from the imaging pulse. In this way, the problems of 1 MHz noise and harmonic generation due to the nonlinear acoustic properties of the neonatal mouse system are avoided. During a specified temporal slot, the imaging transducer will receive the reflected 1 MHz energy and during the next slot, the 10 MHz echoes are received. Therefore, by adjusting the range gate, either or both of the received signals can be examined. If the pulse irradiating the neonate is short and has a low duty

cycle, the neonate is affected less by radiation force, since it takes the neonate a finite amount of time to respond to the force. The drawback of this technique results from the complications of temporarily separating the irradiating ultrasound and the received echoes detected by the imaging transducer. Also, the echoes received by the imaging transducer do not contain information about the initial formation and steady state behavior of the bubble activity. Rather, the information pertains to events occurring after irradiation of the specimen has ceased.

A timing diagram of the technique is illustrated in Figure 36, where the time variation of the signals present at the 1 MHz transducer, neonate, and imaging transducer are shown. The neonate is irradiated with a short pulse of ultrasound, typically longer than 100 microseconds. In this example the pulse width is 100 microseconds and the repetition rate is 7.14 kHz. The 100 microsecond lower limit on the ultrasonic pulse width results from the characteristics of the 1MHz irradiating transducer, as discussed previously. The pulse propagating toward the neonate is partly absorbed and partly reflected from the surface and the interfaces within the neonate. The initial edge of the 100 microsecond pulse arrives at the neonate at time T1. T1 is given by

$$T1 = D1 / V$$

where D1 is the distance from the 1 MHz transducer to the neonate and V is the speed of sound in the coupling medium. For D1 equal to 9.5 cm and V given approximately as 1500 m/s, T1 is approximately 63 us. As shown in Figure 36, for x=9.5 cm, the pulse is present at the neonate between T1 and T1+100. The next

pulse is present from t equal to 203-303 us. The energy reflected from the neonate is received by the imaging transducer at a time T2 later, where T2 is given by

$$T2 = D2 / V$$

and D2 is the distance between the spinal cord region of the neonate and the imaging transducer. For D2 equal to 2.54 cm and V equal to 1500 m/s, T2 is approximately equal to 17 us. The velocity of sound in the neonate has been approximated to be the same as in the coupling medium. As shown in Figure 36, for x=12 cm, the pulse is detected at the receiver from T1+T2 until T1+T2+100. The second pulse is detected from 230-330 us. The temporal window unaffected by the 1 MHz noise signal exists from 180-230 us. The imaging pulse is timed such that the pulse of 1 MHz ultrasound with its harmonics has ended before the range gated echoes are received by the imaging transducer. In the ideal case where the 1 MHz transducer instantaneously creates an ultrasonic pulse, zero rise and decay times, the maximum duty cycle possible is

$$tp / (tp + \text{width of gate})$$

where tp is the 1 MHz ultrasonic pulse duration.

The greatest information is obtained when the duty cycle is very close to 100%, but this increases the problems associated with radiation force. Therefore, a compromise must be made between the radiation force problems and the maximum duty cycle. When the duty cycle is close to 100%, the ultrasonic exposure will be nearly continuous so that the cavitation activity occurs continuously. When the nonzero effects of the rise and decay,

times of the 1 MHz transducer are considered, the maximum permissible duty cycle is decreased drastically.

To accurately define the timing required to implement the system, the rise and decay times of the 1 MHz transducer as seen by the imaging transducer were measured. The PG channel of the system controller was used to drive the control input to the RF mixer, generating short pulses of ultrasound. The temporal response of the 1 MHz transducer was monitored using the 10 MHz imaging transducer. The rise and decay times of the interrogating transducer were not measured because it is the net contribution from both transducers that must be characterized. The rise time was measured using the following definition: the time required for the output to swing from 10%-90% of its final value. The rise time of the transducers was found to be approximately 20 microseconds. The decay time was longer because reflections were detectable at the end of the pulse. This reflected signal is presumed to be a result of scattered ultrasound propagating in the sound tank.

4.2 Pulsed ultrasonic exposure data acquisition system

The pulsed ultrasonic exposure imaging technique was implemented utilizing a dedicated Z80 based microprocessor controlled data acquisition system interfaced to the 7/32 microcomputer. An A/D controlled by the microprocessor is capable of storing large quantities of data and has a 50 MHz bandwidth. The acquired data are transferred to the 7/32 minicomputer for data processing, although many of the data processing operations

can be implemented using the specalized hardware integrated within the system.

A Z80 data acquisition and signal processing system (Z80 DAS) as developed by Paul Embree for two dimensional pulsed ultrasonic flow meter research was adapted to collect data acquired by the imaging system. The system as used for data acquisition is comprised of a 6 MHz Z80 microprocessor based central processing board interfaced to 128 kilobytes of bank selectable memory and four banks, each bank with 32 kilobytes of memory. Analog to digital conversion of the data is accomplished using a TRW TDC1025E1C A/D converter interfaced to the Z80 and associated memory. The A/D is an 8 bit, fully parallel flash converter capable of digitizing an analog signal at rates from DC to 50 megasamples per second. It will accurately sample analog input signals with frequency components as high as 12.5 MHz and will quantize a signal as large as 1 V p-p. The conversion is encoded in a 2's complement representation which varies between 7FH (+0.5V) and 80H (-0.5V) where DC is represented as 00H. The resolution of the A/D is 3.096 mV, and when the input signal is overrange, the sampled output is clipped.

Signal processing is accomplished using a TRW TDC1028 digital filter/correlator operating at 10 MHz. The device is a video speed TTL compatible bit-slice building block for Finite Impulse Response (FIR) digital filters and multi-bit digital correlators. It provides eight delay stages, eight multipliers and eight adders in a single integrated package. Using the signal processing hardware, digital filter implementation and sophisticated signal processing is possible.

Parameters which are entered into the microprocessor at the beginning of each experiment are (1) starting address, (2) period, (3) delay, and (4) gate. Since a large amount of memory is available, several experiments can be stored in the Z80 DAS before it is necessary to transfer the data to the 7/32. The first parameter, starting address, determines where the first byte of data is stored, the remainder of the data follows sequentially. This parameter is entered as a hexadecimal number limited between 8000H and FFFFH for each of the four banks of memory. The second parameter, the period, is set as an integer times 0.32 us and determines the frequency of the P/R TRIGGER signal. A twelve bit counter generates the delay between P/R triggers, a maximum of 1.31 ms (763 kHz). The third and fourth parameters, delay and gate, determine the location and width of the data window. The hardware implementation and purpose of the data window are similiar to the range gate incorporated within the continuous ultrasonic exposure data acquisition system. Each unit of range corresponds to 0.32 us and can be converted to an equivalent distance by multiplying by the velocity of sound in the acoustic coupling medium. Each unit of gate corresponds to 16 samples; the equivalent length of the gate can be calculated since a sample occurs every 0.02 microseconds and the velocity of propagation is known. After all the parameters are entered, the system generates one frame of echoes so that the alignment of the system can be checked. If the alignment of the system is satisfactory, the number of frames of echoes desired and the starting address are entered into the program. The acquired data are stored in memory and the echo data can be displayed graphically on a CRT.

Advantages of this data acqusition system over the 7/32 DAS system include increased data storage, a wider bandwidth data converter, and a real time display of the digitized echoes utilizing the graphics capabilities of the system.

To attenuate any residual 1 MHz and broadband noise, an analog filter can be used to process the RF signal before digitization. Digital filtering techniques are used to attenuate low level noise signals. After the data are uploaded to the 7/32 computer, the data can be digitally filtered and interpolated as discussed in Chapter 3. The data are digitally filtered using program DIGFIL and interpolated by program INTERP. To determine if ultrasonic cavitation occurs, the data are processed by program ANALYZ.

The Z80 DAS can be adapted to acquire data for either the case of continuous ultrasonic exposure or pulsed exposure using the temporal technique. In either case, additional hardware is required because the Z80 DAS was designed for use with only one transducer. This hardware is required to control the 1 MHz irradiation transducer. Figure 37 illustrates the relation among the signals generated by the Z80 DAS and shows the additional signals required for the Z80 DAS to be used with either technique. Figure 37(a) illustrates the free running P/R TRIGGER signal, used to trigger the pulser electronics. Figure 37(b) illustrates the timing of the P/R TRIGGER and RANGE GATE signals generated during data acquisition. The timing of the delay and gate parameters are referenced to the P/R TRIGGER signal. Figure 37(c) illustrates the signal required to drive the control input to the RF mixer for data acquisition during continuous ultrasonic exposures. In this

case, the ultrasound is turned on for the desired exposure duration and echoes are taken during the baseline and ultrasonic exposure. For continuous ultrasonic exposures, the required control signal is low for the duration of the baseline and high for the duration of the ultrasonic exposure. This signal directly drives the control input of the RF mixer, maintaining the RF signal off during the baseline, the low state of the signal, and pulse gating the RF when the control signal is high. The hardware is activated by the Z80 DAS at the beginning of data aquisition. This activation is triggered by the first positive edge of the DMA signal which is generated as an output signal of the hardware and has the same timing as the data window. This signal is high when the A/D takes control of the data bus, indicating storage of the echoes. This is the only signal available as an output of the Z80 DAS which can be decoded to determine when data acquisition begins. The number of echoes in the baseline and the ultrasound on portions of the experiment are determined by the period between P/R triggers, the baseline duration, the exposure parameters, and the number of echoes specified. For the specific timing relation implied by Figures 37(c) and 37(d), the data acquired during gate 1 correspond to baseline data, and the data acquired during gates 2-3 correspond to ultrasound exposure data.

Pulsed ultrasonic exposures required for the temporal imaging technique necessitate synthesis of a more complex signal to trigger the system controller to generate the pulsed irradiation during the correct temporal slot. As illustrated in Figure 37(d), the required control signal for the RF mixer is delayed relative to the P/R TRIGGER signal, and changes state at the end of the

delay for the duration of the exposure. During the baseline the control signal is disabled so that the ultrasound is not turned on. Since the external trigger signal to the system controller is generated after each P/R trigger is detected, it is gated so that during the baseline the signal is suppressed but during the ultrasonic exposure, the signal is passed to the output so that the ultrasound is generated in a pulsed fashion. For the excitation signal shown in Figure 37(e), and the Z80 DAS signal relationship shown in Figure 37(f), the data acquired during the first gate correspond to baseline data. The data acquired during gates 2-3 correspond to ultrasonic exposure data. The hardware design, including circuit schematics, component layout and timing diagrams, is provided in Apppendix B.

CHAPTER 5

SUGGESTIONS FOR FURTHER WORK

The 7/32 DAS and Z80 DAS provide quantitative information regarding the role of cavitation in the production of hind limb paralysis of the mouse neonate. Hardware limitations restrict the exposure duration when using high ultrasonic intensities. Therefore, it is not possible to visually detect any variation in the received echo signal while the experiment is in progress. A real time implementation of both bubble detection systems previously discussed can be accomplished utilizing the system controller and a 100 MHz storage oscilloscope. If the proper trigger signal is applied to the system controller, continuous or pulsed ultrasonic exposures can be generated. The P/R TRIGGER signal generated by the system controller triggers the pulser, generating the imaging pulse. The reflected energy is received by the imaging transducer and is range gated by the system controller electronics. The echo data is stored in real time by the storage oscilloscope for analysis. Each frame of data can be examined for evidence of cavitation activity; and oscillograms of the data provide hard copy documentation. The combination of the quantitative analysis technique and the qualitative technique discussed result in a powerful bubble detection system.

An alternative to using the developed imaging system utilizes a commercial A/B-scan diagnostic instrument to image the neonate. The B-scan capability of the instrument can locate cavitation sites within the neonate with increased resolution over an A-scan

system. The storage display element of the instrument stores the data in real time for further processing. The stored images can be studied qualitatively for evidence of bubble activity. By developing additional hardware, the video signal generated by the scanner can be digitized and stored for computer processing. Similiar techniques as discussed in Chapter 3 can be applied to detect bubble activity resulting from ultrasonic exposure. The 7/32 DAS hardware would benefit from the following enhancement. The size of memory available to the A/D should be increased so that more data can be collected during an experiment. A DAS similar to the Z80 DAS should be developed to control the continuous and pulsed ultrasonic bubble detection systems. The hardware developed for the Z80 DAS should be incorporated within the new design so that all the experimental parameters are keyboard selectable.

More sophisticated analog filters and digital signal processing techniques should be developed to process the data. Statistical processing techniques should be extensively used during signal processing.

TABLES

TABLE 1. IC IDENTIFICATION FOR THE CONTROL AND TIMING CIRCUIT BOARD

C1 - 74LS00
C2 - 74LS04
C3 - 74LS162
C4 - 7414
C5 - 74LS04
C7 - 74LS00
C8 - 74LS10
C9 - 74LS162
C10 - LM311
C13 - 74LS74
C14 - 74LS74
C15 - 74LS162
C19 - 74LS10
C20 - 74LS20
C21 - 74LS162
C22 - 74LS10
C23 - 74LS163
C24 - 74LS10
C25 - 74LS162
C26 - 74LS10
C27 - 74LS162
C28 - 74LS162
C29 - 74LS163
C30 - 74LS04
C31 - 74LS162
C32 - 74LS20
C33 - 74LS162
C34 - 74LS162
C35 - 74LS10
C36 - 74LS74
C37 - 74LS162
C38 - 74LS10
C39 - 74LS162
C40 - 74LS162
C41 - 74LS20
C43 - 74LS162
C44 - 74LS74
C45 - 74LS162
C46 - 74LS162
C47 - 74128
C48 - 74128

TABLE 2. SIGNAL IDENTIFICATION FOR EDGE CONNECTOR 1 (EC1)

PIN	SIGNAL/CONNECTION
1	+5
2	+5
3	NC
4	NC
5	POWER ON/C10-7
6	LOCAL TRIGGER (NO)/C1-1
7	LOCAL TRIGGER (NC)/C1-5
8	TRIGGER SELECT/C1-10
9	TRIGGER SELECT/C1-12
10	EXTERNAL TRIGGER/C4-1
11	GND
12	PULSE GATE/C44-5
13	P/R TRIGGER/GND
14	DELAYED GATE TTL/C47-4
15	DELAYED GATE TTL_/C48-10
16	GND
17	DELAYED GATE/C44-9
18	PULSE GATE TTL/C47-10
19	PULSE GATE TTL_/C47-13
20	GND
21	GND
22	GND
A	+5
B	+5
C	NC
D	NC
E	NC
F	NC
H	NC
J	SYNC/C47-1
K	SYNC/GND
L	EXTERNAL TRIGGER/GND
M	GND
N	GND
P	P/R TRIGGER/C48-1
R	DELAYED GATE TTL/GND
S	DELAYED GATE TTL_/GND
T	GND
U	NC
V	PULSE GATE TTL/GND
W	PULSE GATE TTL_/GND
X	GND
Y	GND
Z	GND

TABLE 3. SIGNAL IDENTIFICATION FOR SCOTCHFLEX CONNECTOR 3&4 (SFC3-4)

SFC3		SFC4	
PIN	CONNECTIONS	PIN	CONNECTIONS
1	M5-17 TO C25-3	1	M7-5 TO C32-3
2	M5-19 TO C25-4	2	M7-7 TO C32-4
3	M5-21 TO C25-5	3	M7-9 TO C32-5
4	M5-23 TO C25-6	4	M7-11 TO C32-6
5	M5-5 TO C31-3	5	M3-17 TO C38-3
6	M5-7 TO C31-4	6	M3-19 TO C38-4
7	M5-9 TO C31-5	7	M3-21 TO C38-5
8	M5-11 TO C31-6	8	M3-23 TO C38-6
9	NC	9	M3-5 TO C44-3
10	M1-17 TO C37-3	10	M3-7 TO C44-4
11	M1-19 TO C37-4	11	M3-9 TO C44-5
12	M1-21 TO C37-5	12	M3-11 TO C44-6
13	M1-23 TO C37-6	13	NC
14	M1-5 TO C43-3	14	M8-17 TO C28-3
15	M1-7 TO C43-4	15	M8-19 TO C28-4
16	M1-9 TO C43-5	16	M8-21 TO C28-5
17	M1-11 TO C43-6	17	M8-23 TO C28-6
18	NC	18	M8-5 TO C34-3
19	M6-17 TO C2-3	19	M8-7 TO C34-4
20	M6-19 TO C2-4	20	M8-9 TO C34-5
21	M6-21 TO C2-5	21	M8-11 TO C34-6
22	M6-23 TO C2-6	22	NC
23	M6-5 TO C8-3	23	M4-17 TO C40-3
24	M6-7 TO C8-4	24	M4-19 TO C40-4
25	M6-9 TO C8-5	25	M4-21 TO C40-5
26	M6-11 TO C8-6	26	M4-23 TO C40-6
27	NC	27	M4-5 TO C46-3
28	M2-17 TO C14-3	28	M4-7 TO C46-4
29	M2-19 TO C14-4	29	M4-9 TO C46-5
30	M2-21 TO C14-5	30	M4-11 TO C46-6
31	M2-23 TO C20-6		
32	M2-5 TO C20-3		
33	M2-7 TO C20-4		
34	M2-9 TO C20-5		
35	MC-11 TO C20-6		
36	NC		
37	M7-17 TO C26-3		
38	M7-19 TO C25-4		
39	M7-21 TO C25-5		
40	M7-23 TO C25-6		

TABLE 4. IC IDENTIFICATION FOR THE DATA ENTRY CIRCUIT BOARD

W0 - 74LS125
W1 - 74C922
W4 - 74LS74
W5 - 74LS74
W6 - 74LS83
W8 - 74LS10
W9 - 74LS10
W11 - 74LS374
W12 - 74LS374
W13 - 74LS74
W14 - 74LSO4
W15 - 74LS190
W16 - 74LS125
W18 - 74LS155
W19 - 74LS00
W20 - 74LS04
W21 - 74LS190
W22 - 74LS490

TABLE 5. SIGNAL IDENTIFICATION FOR SCOTCHFLEX CONNECTOR 2 (SFC2)

PIN	SIGNAL/CONNECTION
1	R4/W1-4
2	R3/W1-3
3	R2/W1-2
4	R1/W1-1
5	NC
6	NC
7	C1/W1-11
8	C2/W1-10
9	C3/W1-8
10	C4/W1-7

TABLE 6. SIGNAL IDENTIFICATION FOR EDGE CONNECTOR 2 (EC2)

PIN	SIGNAL/CONNECTION
1	+5
2	NC
3	P8/SFC1-29
4	P9/SFC1-28
5	NC
6	D1/W13-3
7	D2/W13-6
8	D3/W13-8
9	D4/W13-11
10	NC
11	POWER ON/EC1-5
12	G2 CONTROL/W9-6
13	2Y3/W18-12
14	2Y2/W18-11
15	2Y1/W18-10
16	2Y0/W18-9
17	1Y3/W18-4
18	1Y2/W18-5
19	1Y1/W18-6
20	1Y0/W18-7
21	NC
22	GND
A	+5
B	P9_/SFC1-17
C	NC
D	NC
E	NC
F	NC
H	NC
J	P13/SFC1-19
K	NC
L	NC
M	NC
N	1KHZ/W22-9
P	NC
R	H/W11-9
S	G/W11-6
T	F/W11-5
U	E/W11-2
V	D/W12-9
W	C/W12-6
X	B/W12-5
Y	A/W12-2
Z	GND

TABLE 8. SIGNAL IDENTIFICATION FOR SCOTCHFLEX CONNECTOR 1 (SFC1)

PIN	SIGNAL
1	GND
2-8	NC
9	P0 BIT E
10	NC
11	P1 BIT F
12-16	NC
17	P9_ BYTE SELECT_
18	NC
19	P13 TRISTATE OUTPUT CONTROL
20-24	NC
25	P12 EXTERNAL TRIGGER OUTPUT
26	P10 EXTERNAL TRIGGER INPUT
27	P10 RF GATE TRIGGER
28	P9 BYTE SELECT
29	P8 DATA ACCEPT
30	NC
31	P2 BIT A
32	NC
33	P7 BIT D
34	NC
35	P3 BIT H
36	NC
37	P6 BIT C
38	P4 BIT A
39	P5 BIT B
40	NC

TABLE 9. IC IDENTIFICATION FOR THE DISPLAY AND DATA CIRCUIT BOARD

M1-M8 - 74116
M9-M16 - 74LS157
M17-M20 - 74LS153
M21 - 74LS83
M22 - 74LS04
M23 - 74LS47
M24 - 914C500X5SR
M25 - 74LS47
M26 - 914C500X5SR
M29 - 74LS83
M30 - 74LS04
M31 - 74LS190
M32 - 74LS155
M36 - DIP HEADER
M37 - 4 6562 PNP TRANSISTORS
M38 - 4 6562 PNP TRANSISTORS

TABLE 10. SIGNAL IDENTIFICATION FOR SCOTCHFLEX CONNECTOR 5 (SFC5)

PIN	SIGNAL/CONNECTION
1	a/M24-16
2	b/M24-15
3	c/M24-14
4	d/M24-13
5	e/M24-12
6	f/M24-11
7	g/M24-10
8	NC
9	a/M26-16
10	b/M26-15
11	c/M26-14
12	d/M26-13
13	e/M26-12
14	f/M26-11
15	g/M26-10
16	NC
17	D1/M33-7
18	D2/M33-6
19	D3/M33-5
20	D4/M33-4
21	D5/M33-9
22	D6/M33-10
23	D7/M33-11
24	D8/M33-12
25	DECIMAL POINT/D4-6
26	DECIMAL POINT/D8-6

TABLE 11. SIGNAL IDENTIFICATION FOR EDGE CONNECTOR 3 (EC3)

1	GND
2	1Y0/EC2-20
3	1Y1/EC2-19
4	1Y2/EC2-18
5	1Y3/EC2-17
6	2Y0/EC2-16
7	2Y1/EC2-15
8	2Y2/EC2-14
9	2Y3/EC2-13
10	G2 CONTROL/EC2-12
11	NC
12	POWER ON/EC1-5
13	1KHZ/EC2-N
14	NC
15	NC
16	NC
17	NC
18	NC
19	NC
20	NC
21	NC
22	GND
A	GND
B	A/EC2-Y
C	B/EC2-X
D	C/EC2-W
E	D/EC2-V
F	E/EC2-U
H	F/EC2-T
J	G/EC2-S
K	H/EC2-R
L	NC
M	DISPLAY SELECT/M14-1
N	DISPLAY SELECT/M10-1
P	NC
R	NC
S	NC
T	NC
U	NC
V	+5
W	+5
X	+5
Y	+5
Z	GND

TABLE 12. IC IDENTIFICATION FOR THE Z80 DAS RF CONTROLLER BOARD

UA1	74LS74
UA2	74LS74
UA3	74LS162
UA4	74LS85
UA5	74LS00
UA6	74LS10
UB1	74LS00
UB2	74LS14
UB3	74LS162
UB4	74LS85
UB5	74LS190
UB6	74LS85
UC1	74LS490
UC2	74LS04
UC3	74LS162
UC4	74LS85
UC5	74LS190
UC6	74LS85
UD1	74LS490
UD2	74LS00
UD3	74LS162
UD4	74LS85
UD5	74LS190
UD6	75LS85
UD7	74LS10
UE1	74LS490
UE2	74LS00
UE3	74LS10
UE4	74LS00
UE5	74LS74
UF2	74LS74
UF3	74LS74

TABLE 13. SIGNAL IDENTIFICATION FOR EDGE CONNECTOR 4 (EC4)

1	GND
22	+5
A	GND
Z	+5

FIGURES

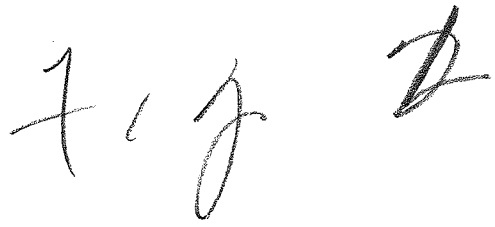

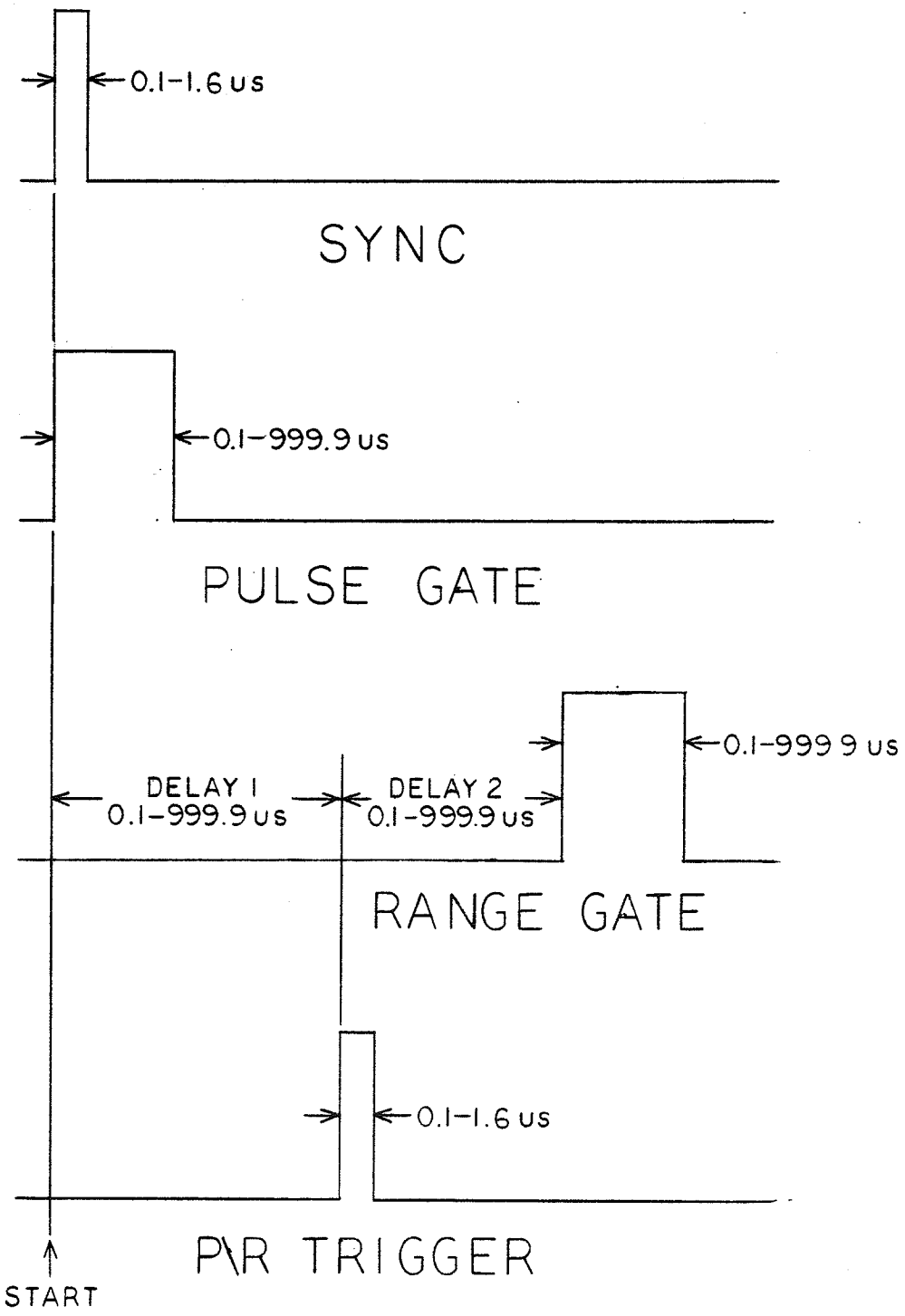

Figure 3. System controller output signals.

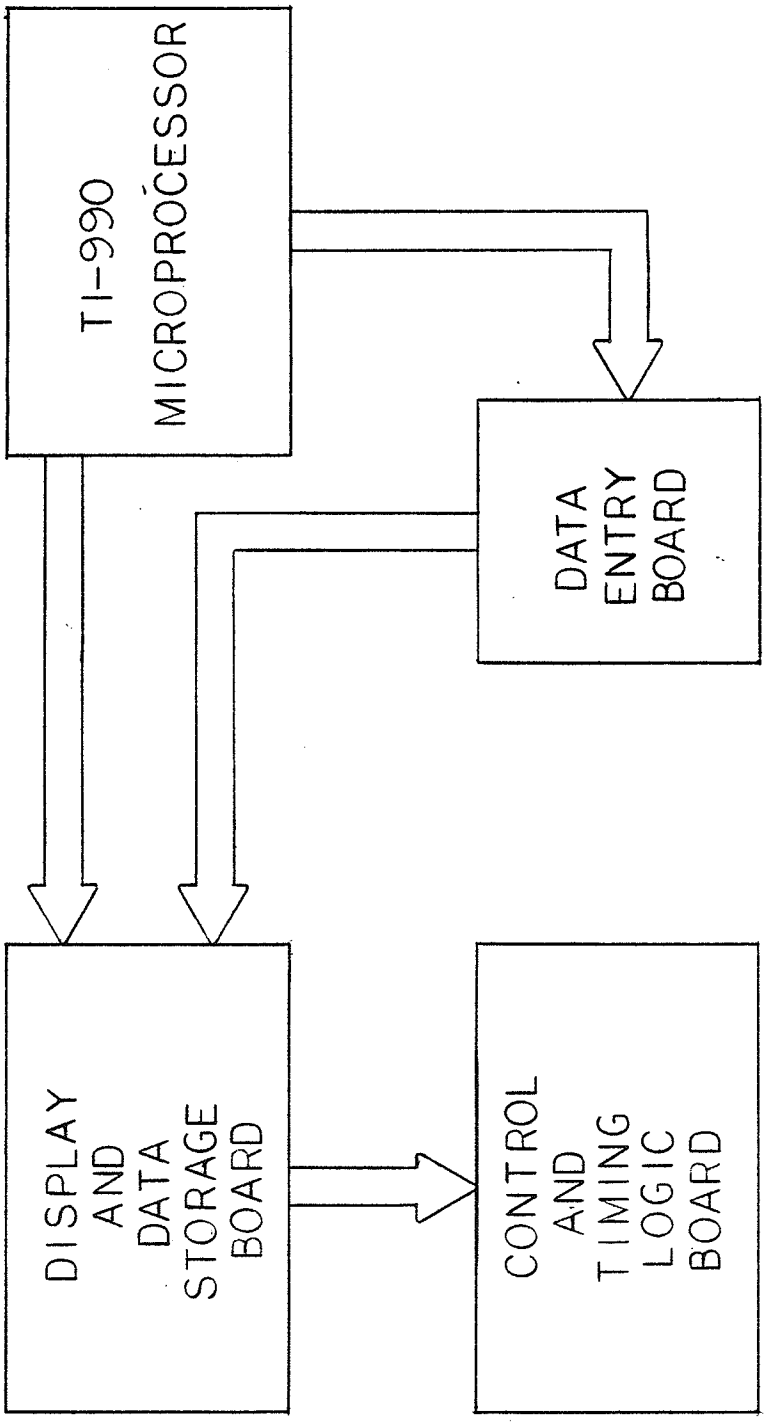

Figure 4. Subcircuits of the system controller.

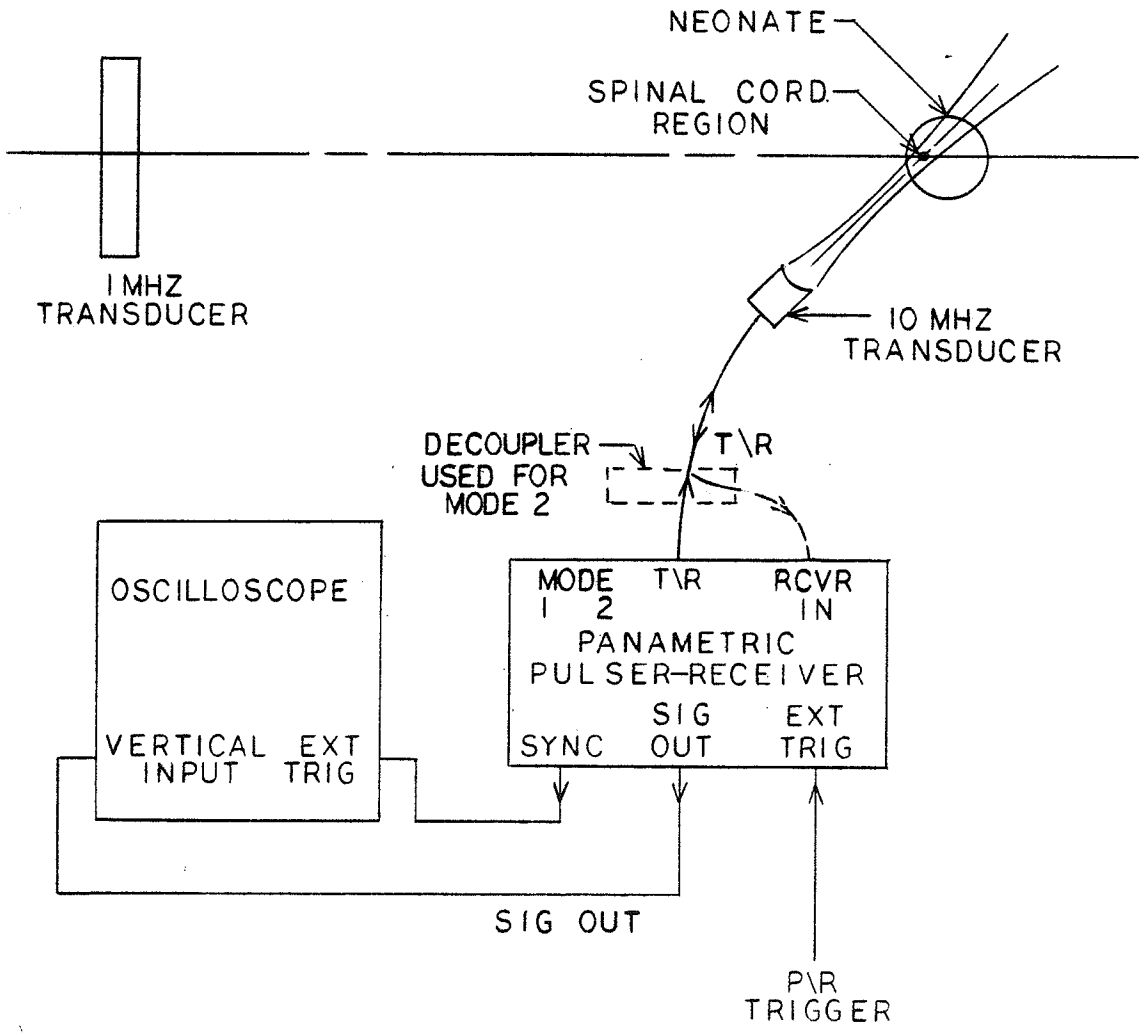

Figure 5. Pulser-receiver configuration A.

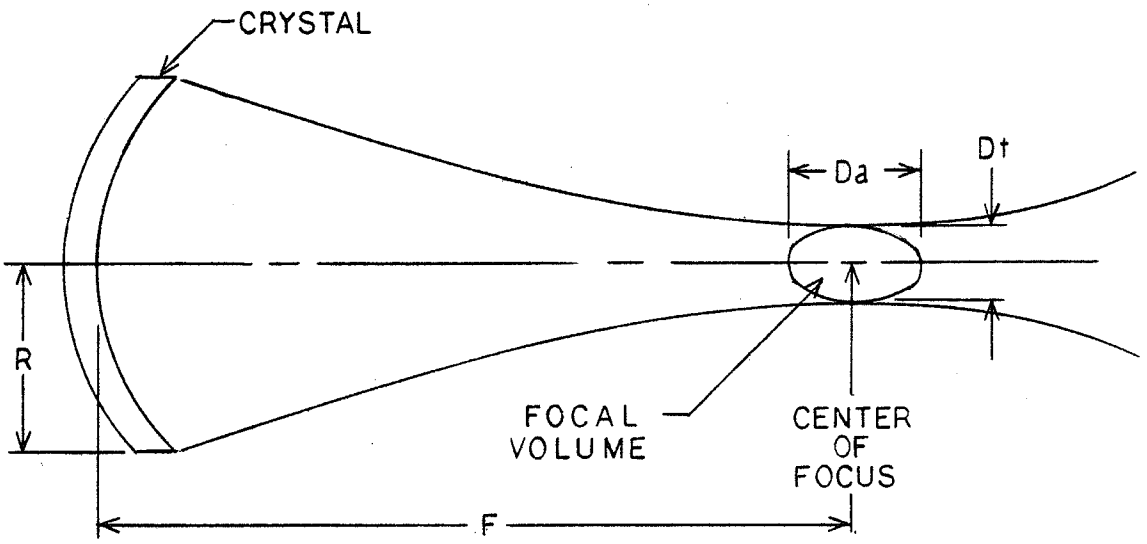

Figure 6. Relation among the parameters describing the half power dimensions of the focal volume.

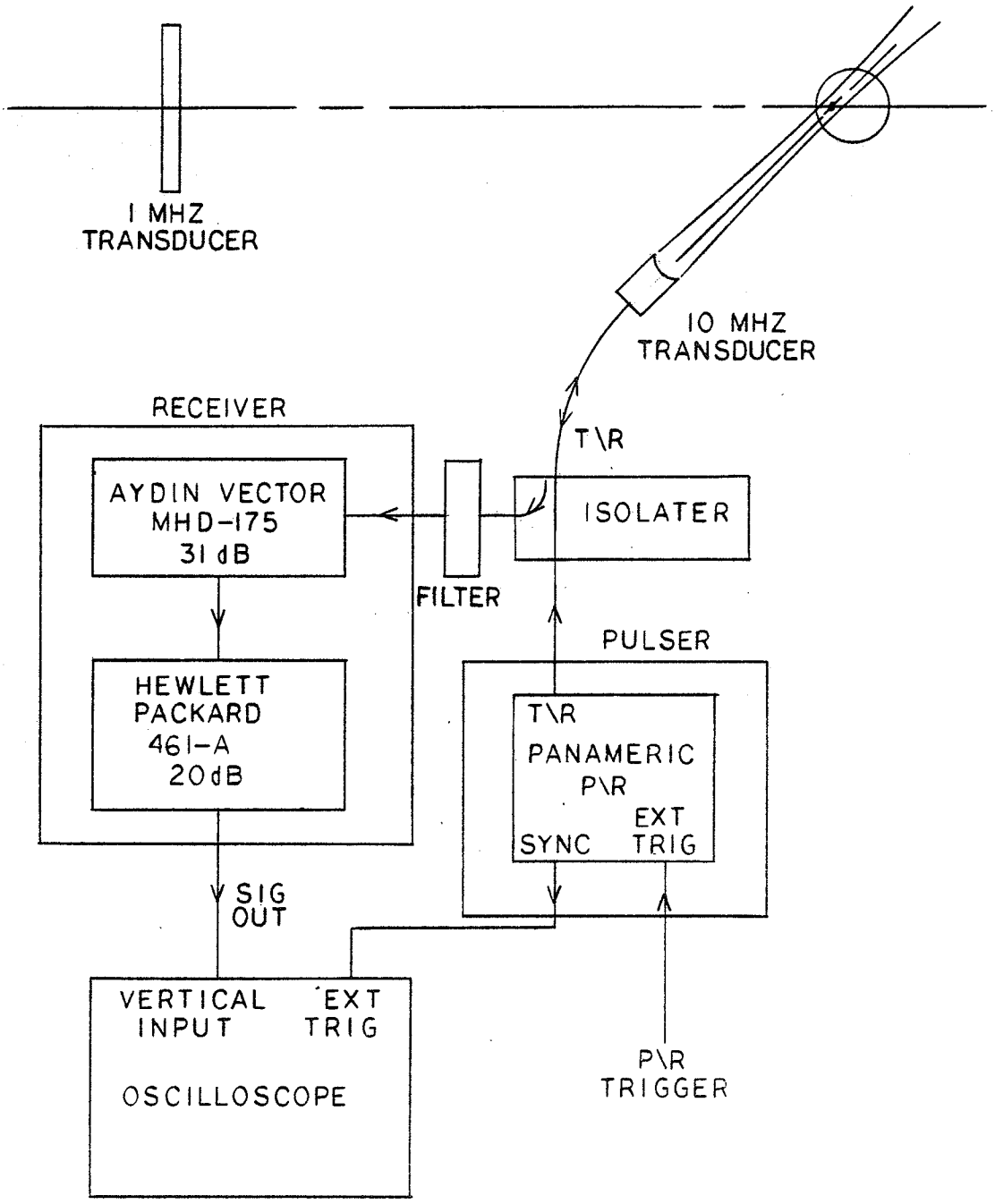

Figure 7. Pulser-receiver configuration B.

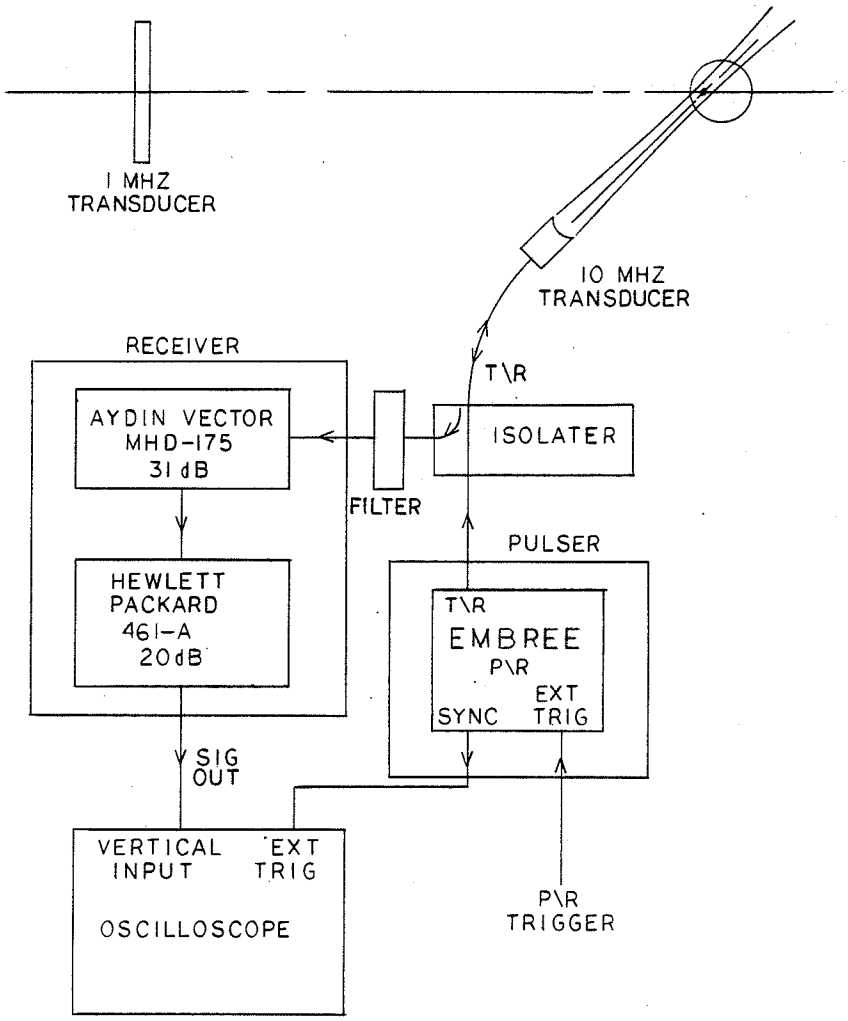

Figure 8. Pulser-receiver configuration C.

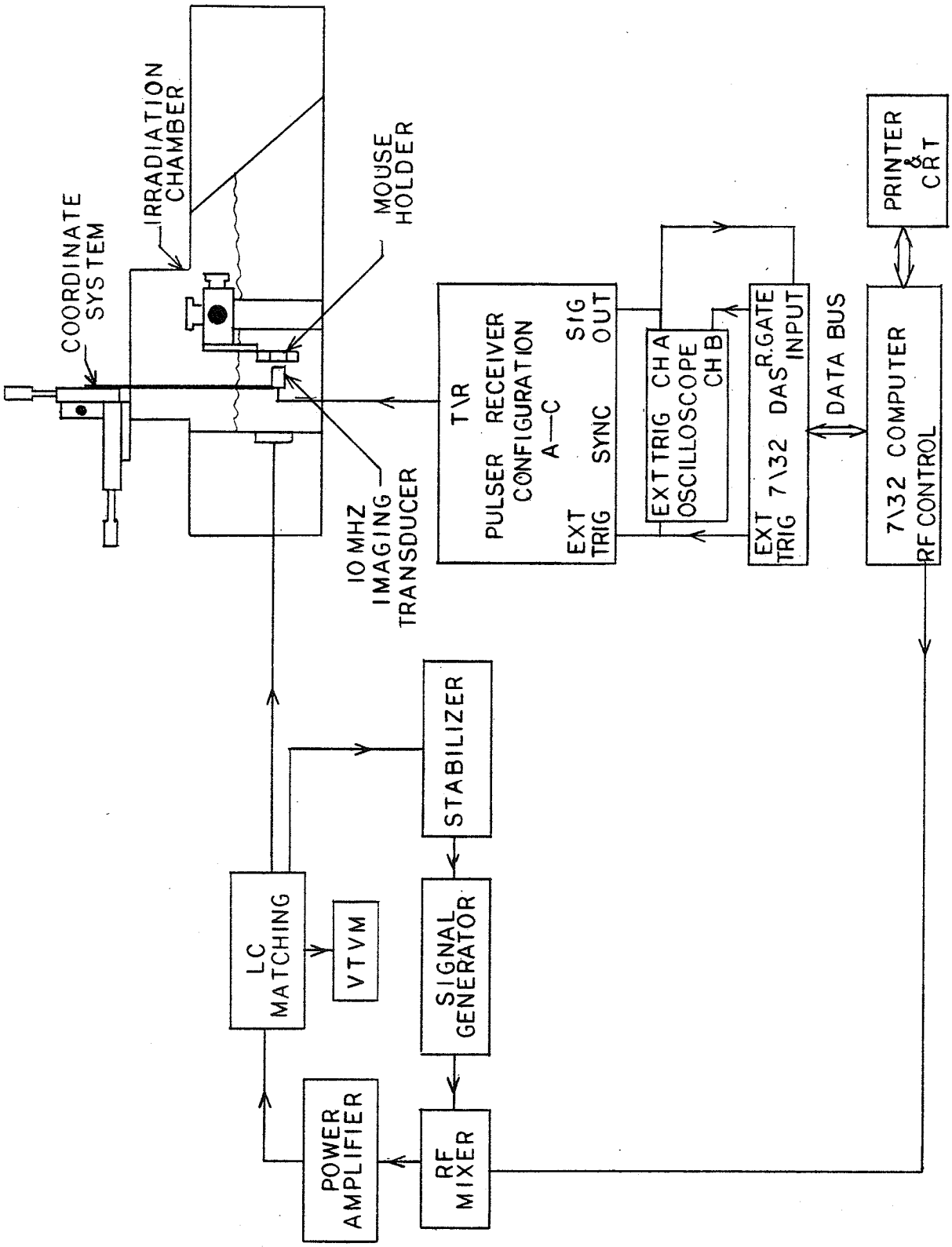

Figure 9. Block diagram of the continuous ultrasonic exposure system electronics.

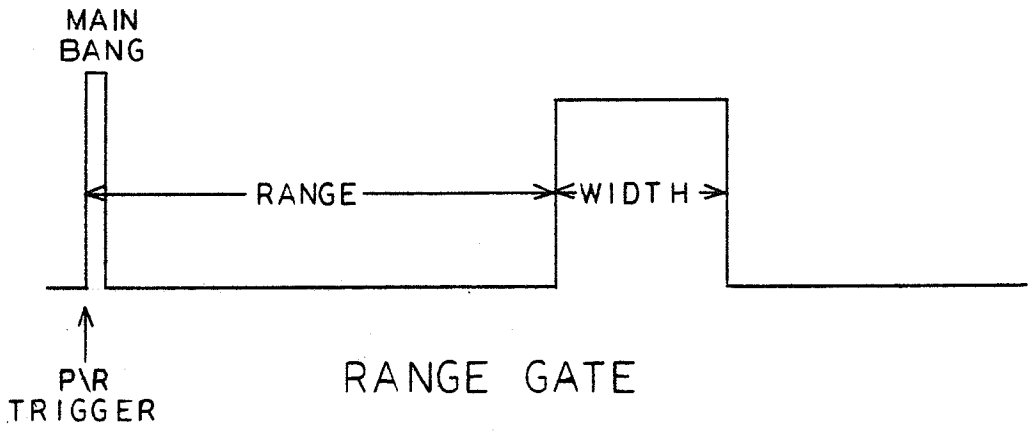

(a)

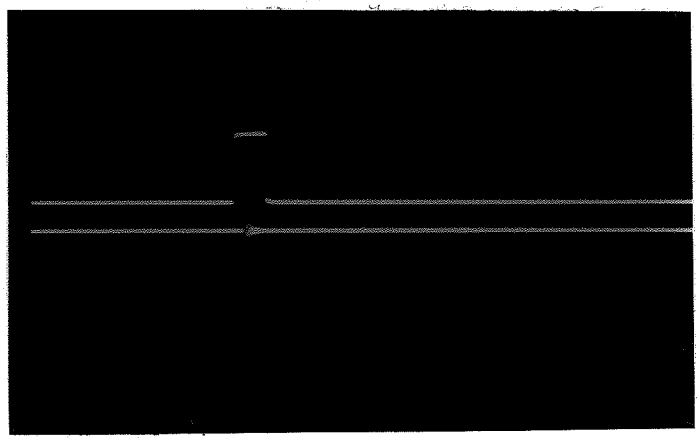

(b)

Figure 10. (a) Relation among the parameters describing the range gate signal, (b) oscillogram of the range gate signal superimposed over the received echo signal.

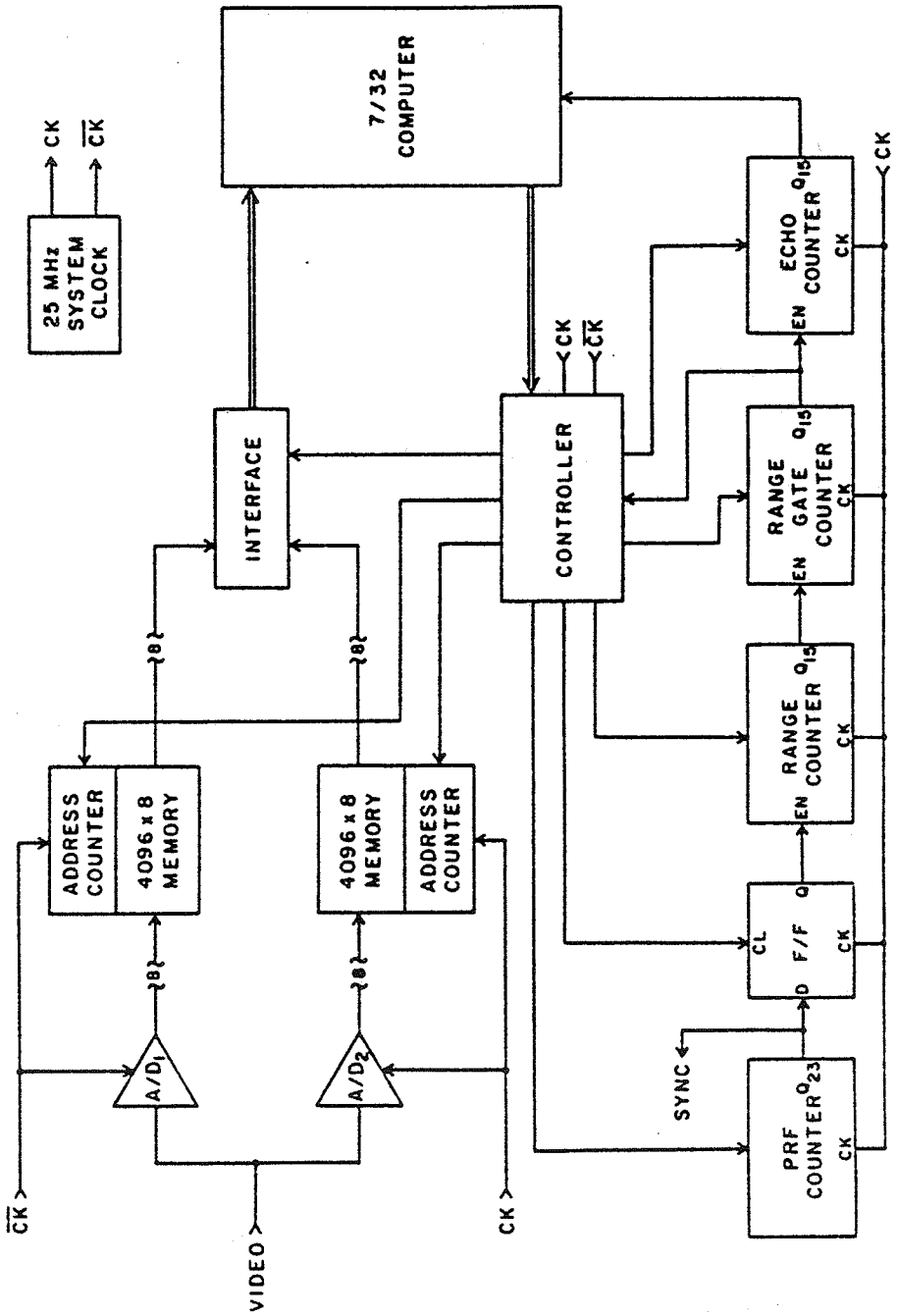

Figure 11. Block diagram of the 7/32 DAS.

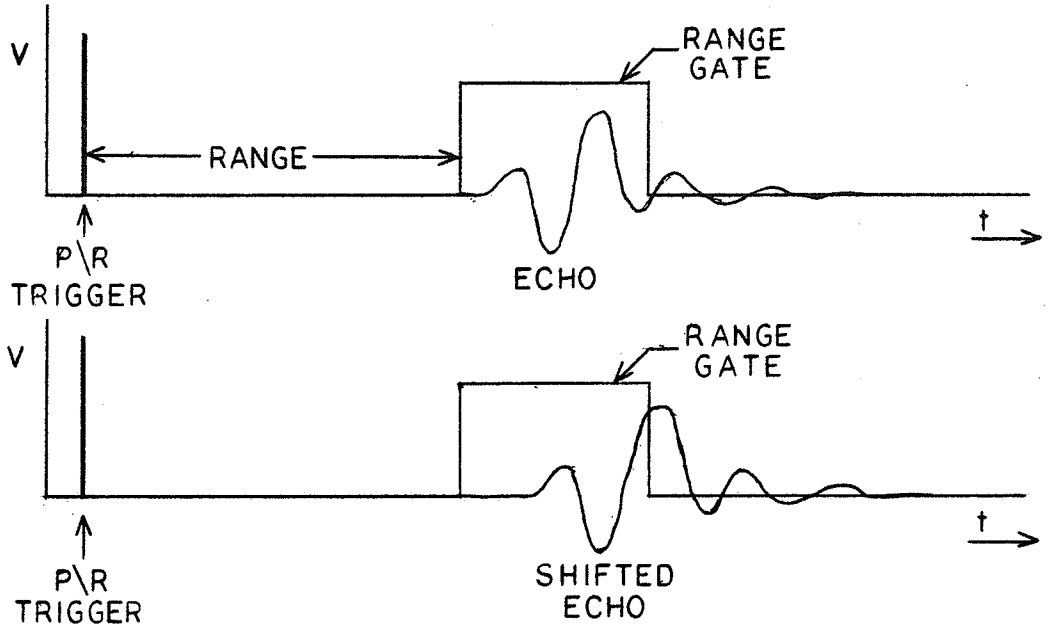

Figure 12. Effect of radiation force on the range gated data.

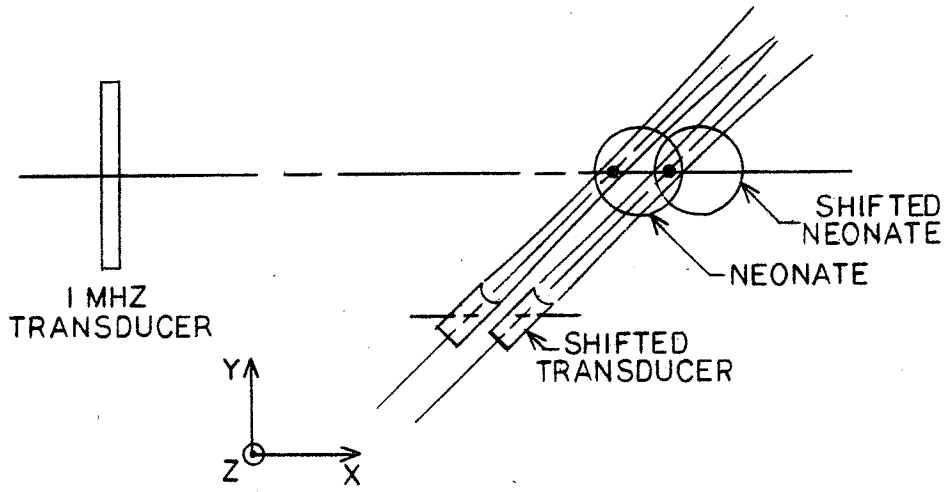

Figure 13. Translation of the imaging transducer to compensate for radiation force effects.

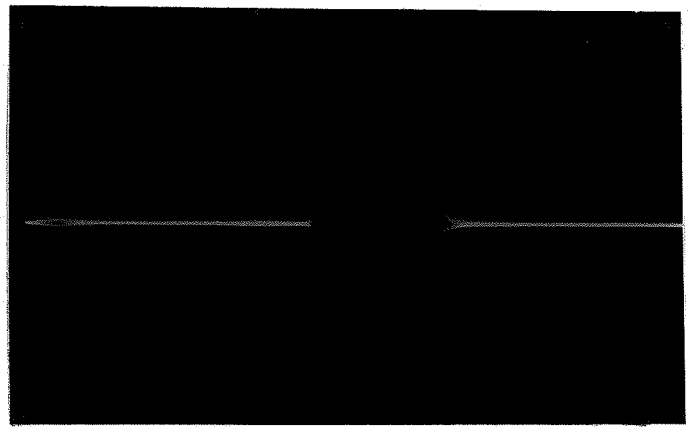

(a)

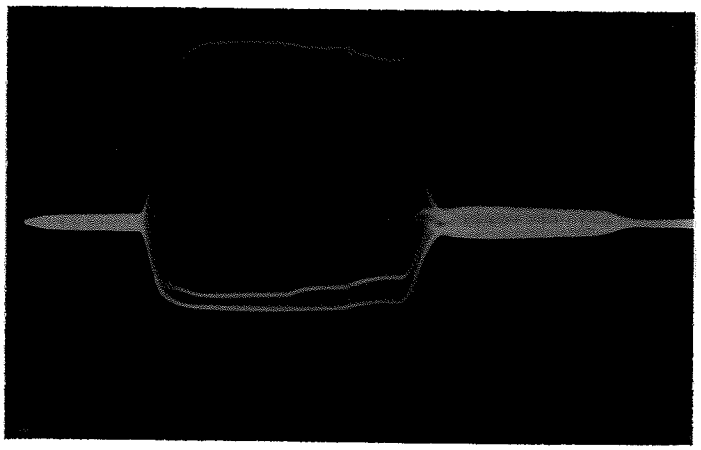

(b)

Figure 2. (a) Ultrasonic pulse generated by a 10 microsecond excitation signal, (b) ultrasonic pulse generated by a 200 microsecond excitation signal.

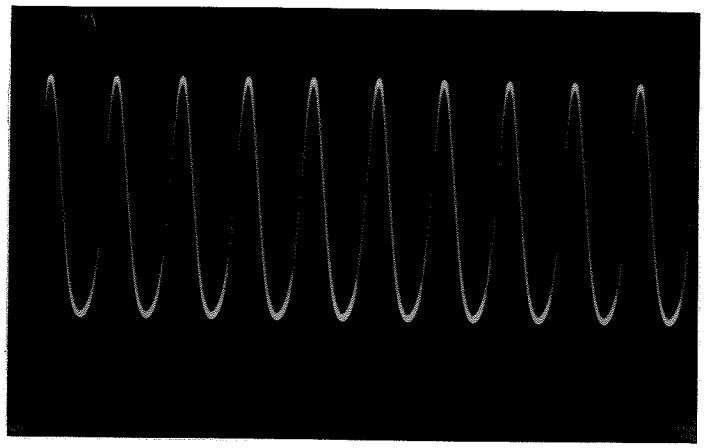

(a)

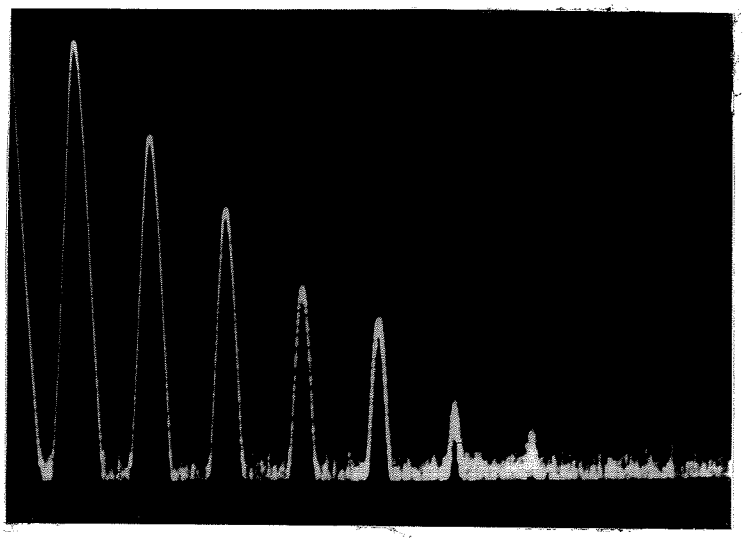

(b)

Figure 14. (a) Noise signal for I = 4.4.84 W/cm sq., (b) spectral components of the noise signal.

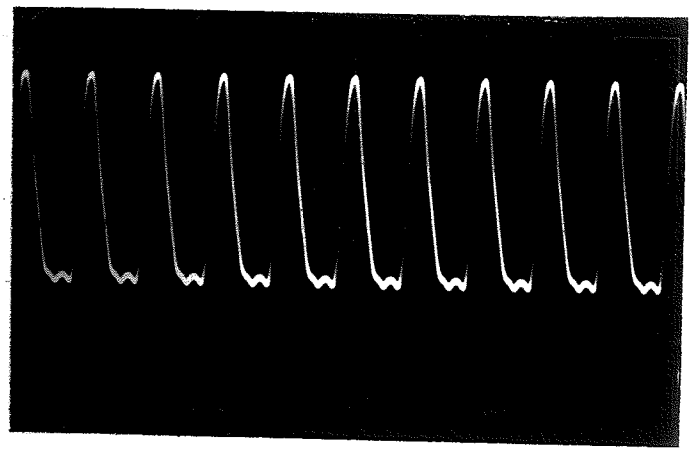

(a)

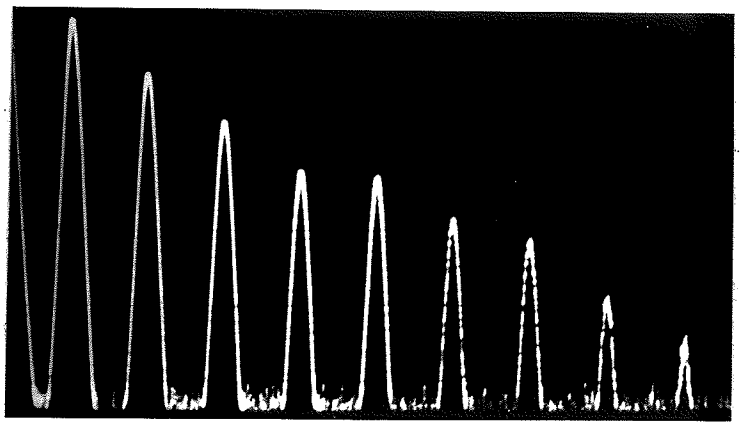

(b)

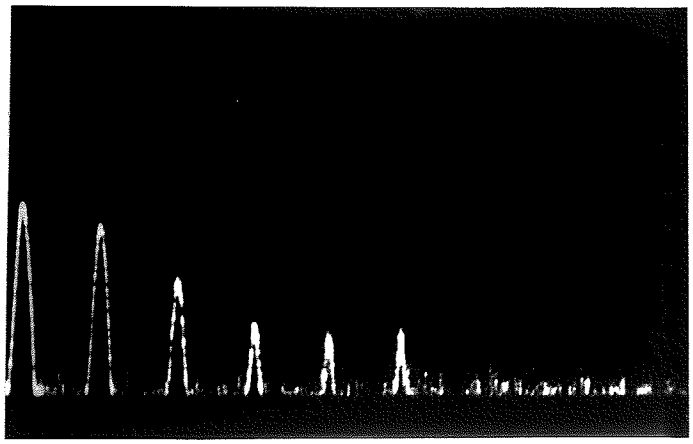

(c)

Figure 15. (a) Noise signal for I = 144 W/cm sq., (b) spectral components of the noise signal (center frequency = 5 MHz), and (c) spectral component of the noise signal (center frequency = 10 MHz).

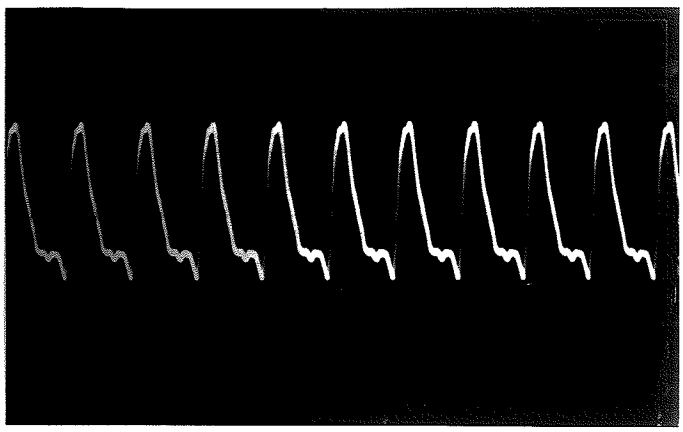

(a)

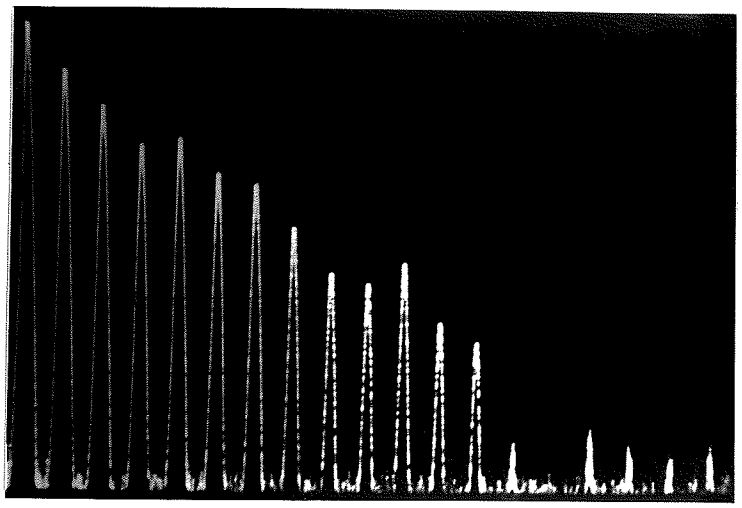

(b)

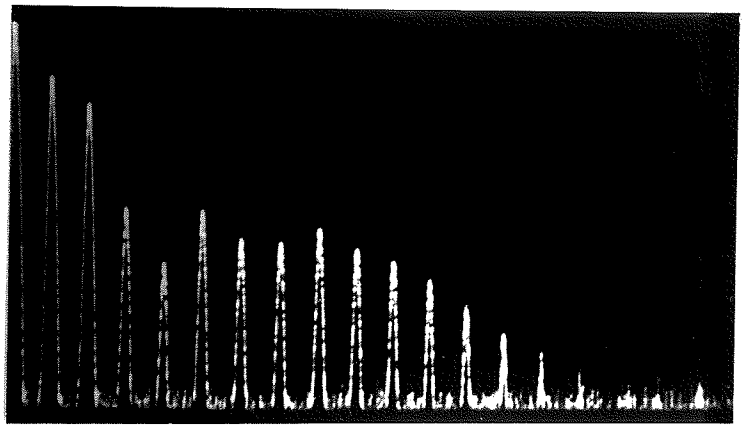

(c)

Figure 16. (a) Noise signal for I = 250 W/cm sq., (b) spectral components of the nose signal (center frequency = 10 MHz), and (c) spectral components of the noise signal (center frequency = 20 MHz).

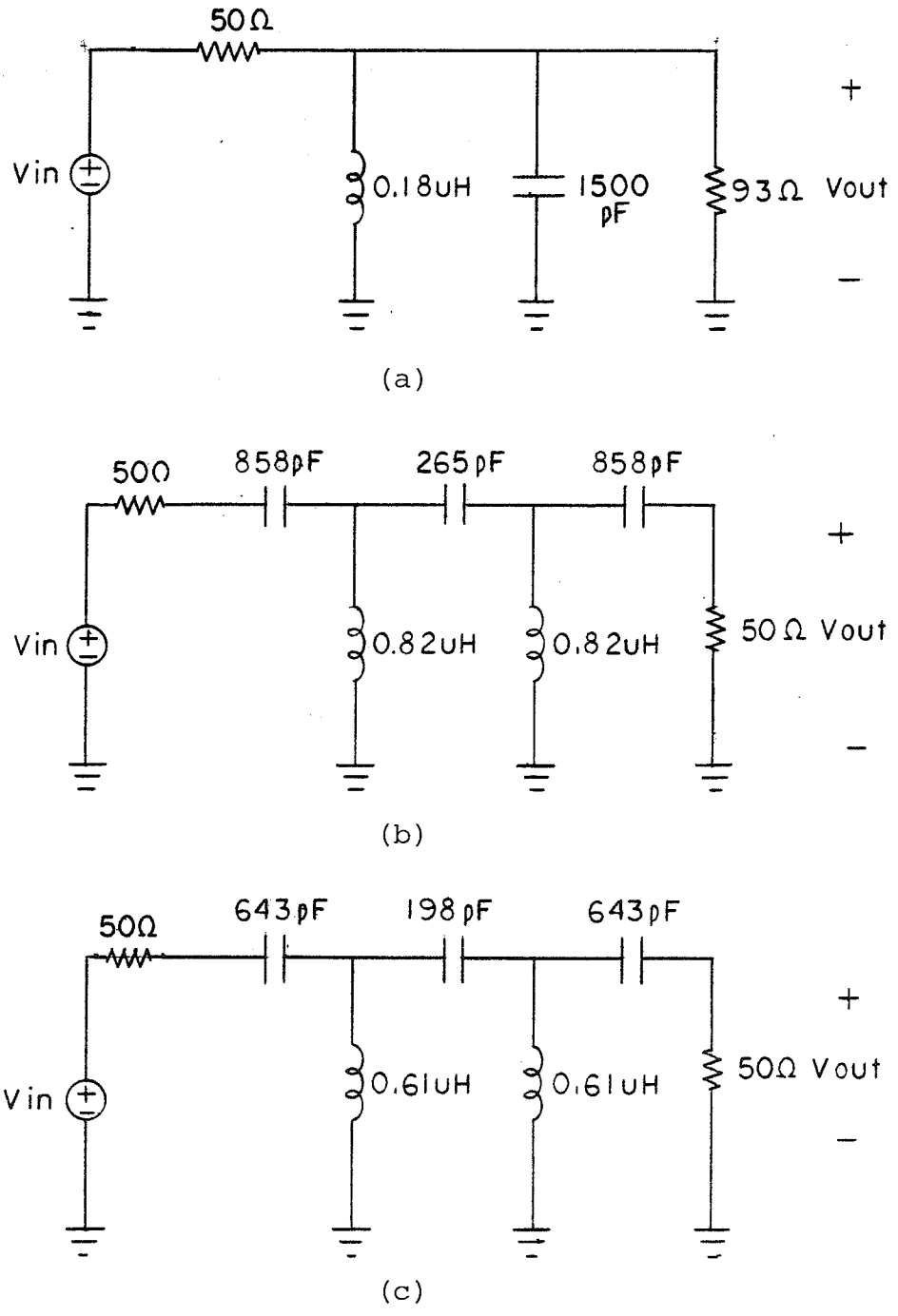

Figure 17. (a) 10 MHz bandpass filter, (b) 6 MHz highness filter, and (c) 8 MHz highpass filter.

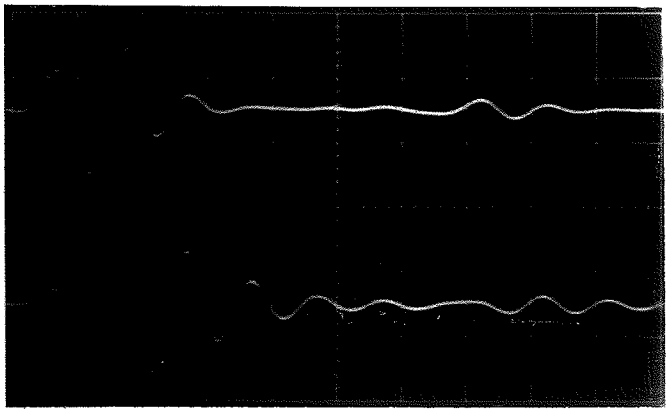

(a)

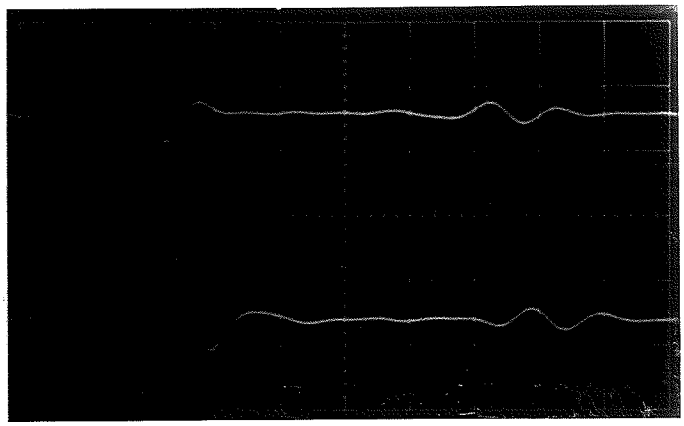

(b)

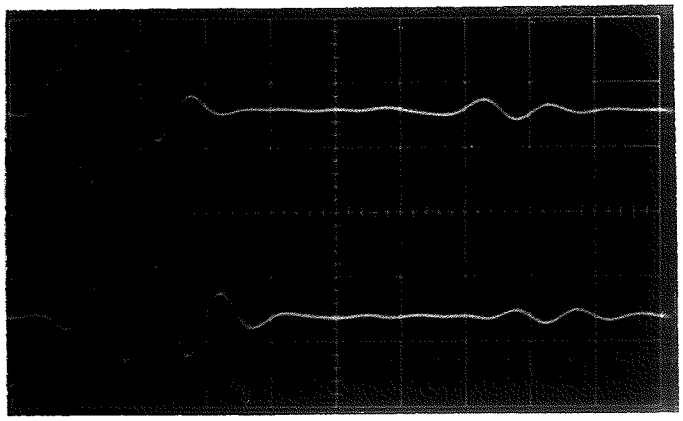

(c)

Figure 18. (a) Filter response for the 10 MHz bandpass filter, (b) filter response for the 6 MHz highpass filter, and (c) filter response for the 8 MHz highpass filter.

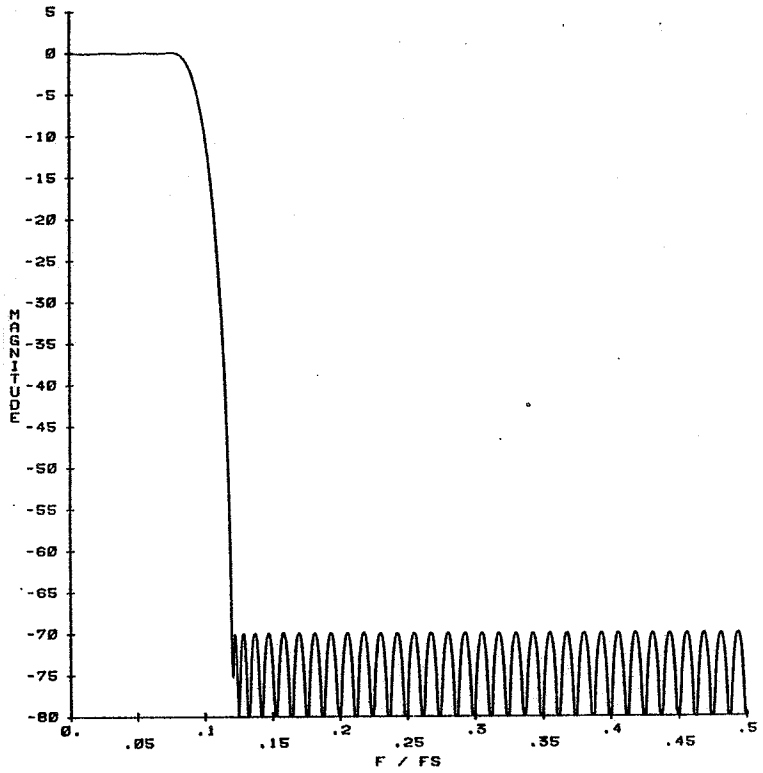

(a)

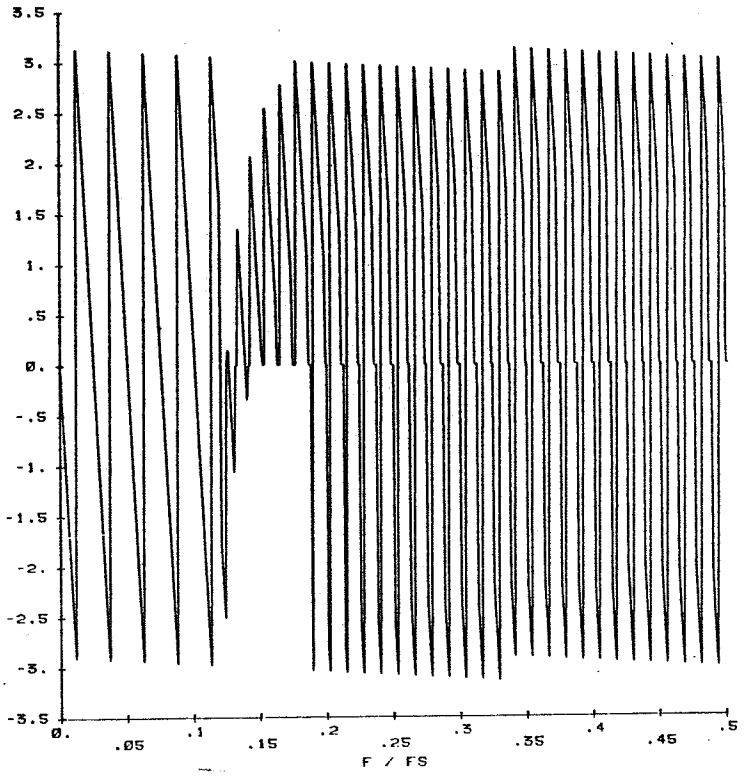

(b)

Figure 19. (a) Magnitude of the frequency response for the high-pass digital filter with bandedges at 7.0 and 9.0 MHz, (b) phase of the frequency response for the highpass digital filter with bandedges at 7.0 and 9.0 MHz.

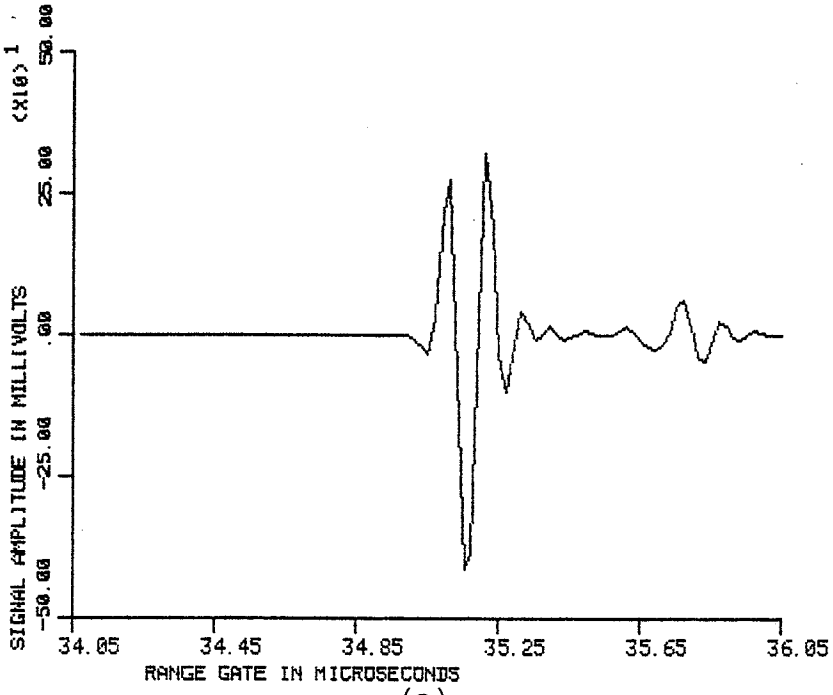

(a)

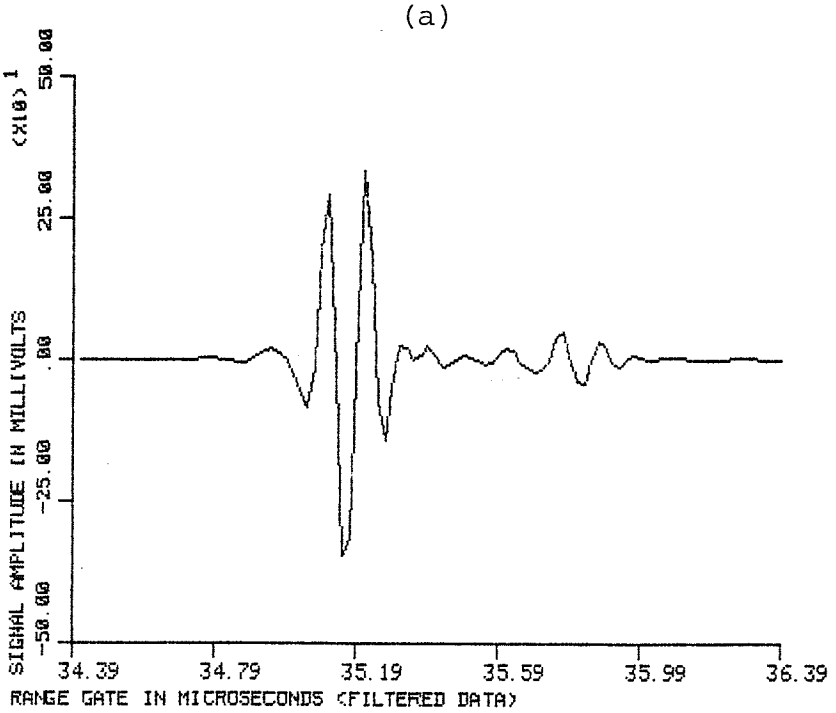

(b)

Figure 20. (a) Signal input to digital filter, (b) output of digital filter with bandedges at 2.5/7.5 MHz.

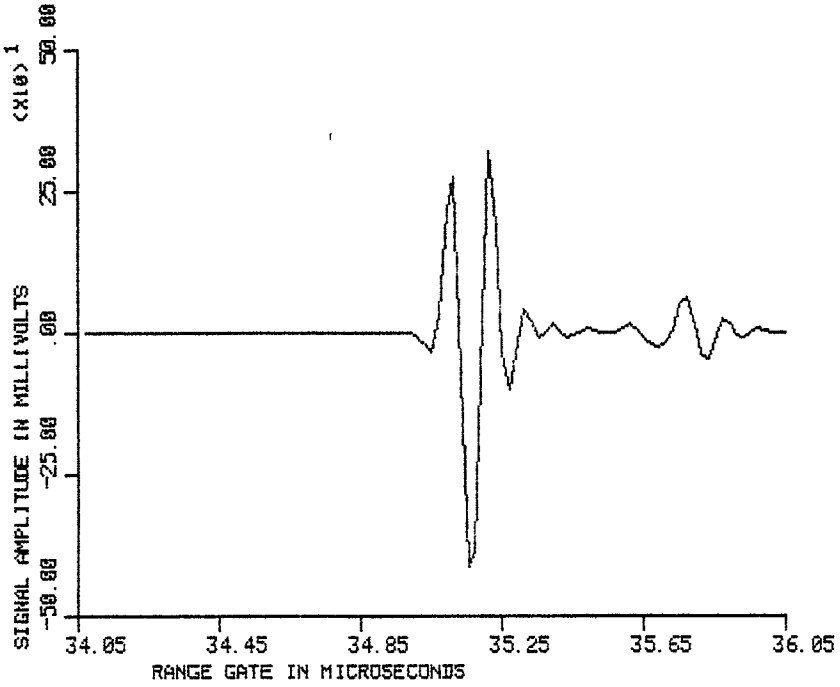

(a)

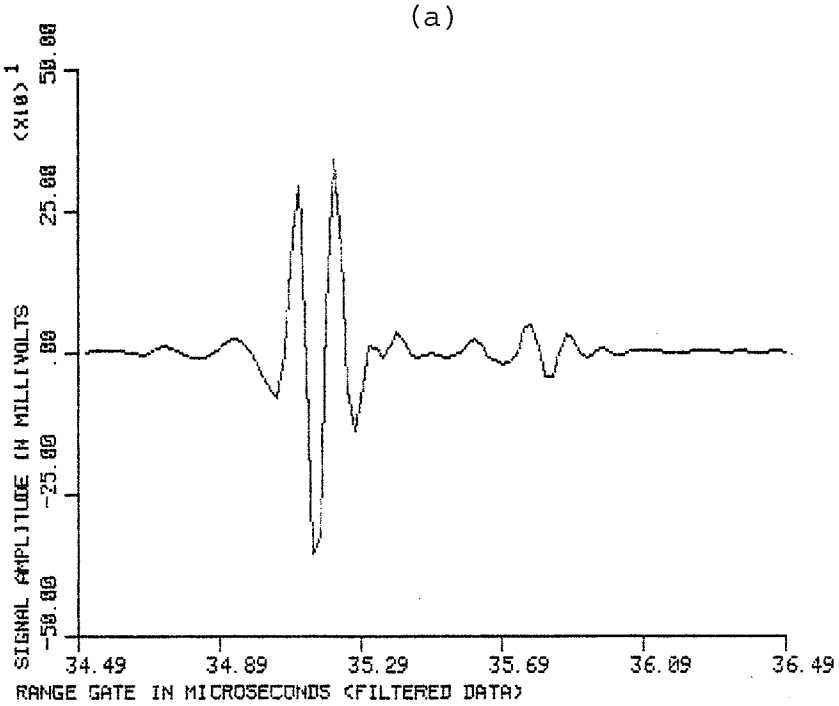

(b)

Figure 21. (a) Signal input to digital filter and (b) output of digital filter with bandedges at 4.0/6.0 MHz.

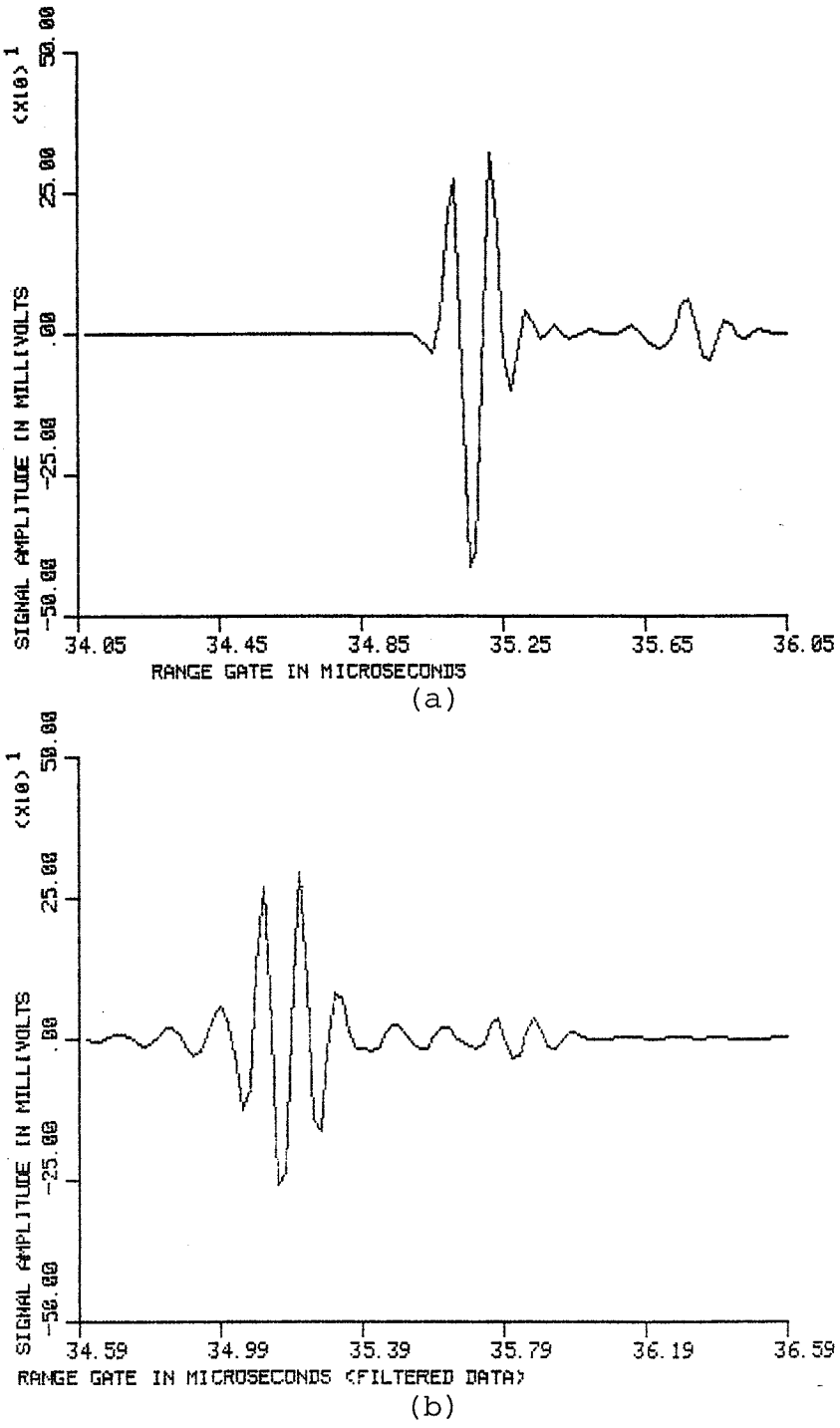

Figure 22. (a) Signal input to digital filter and (b) output of digital filter with bandedges at 6.0/8.0 MHz.

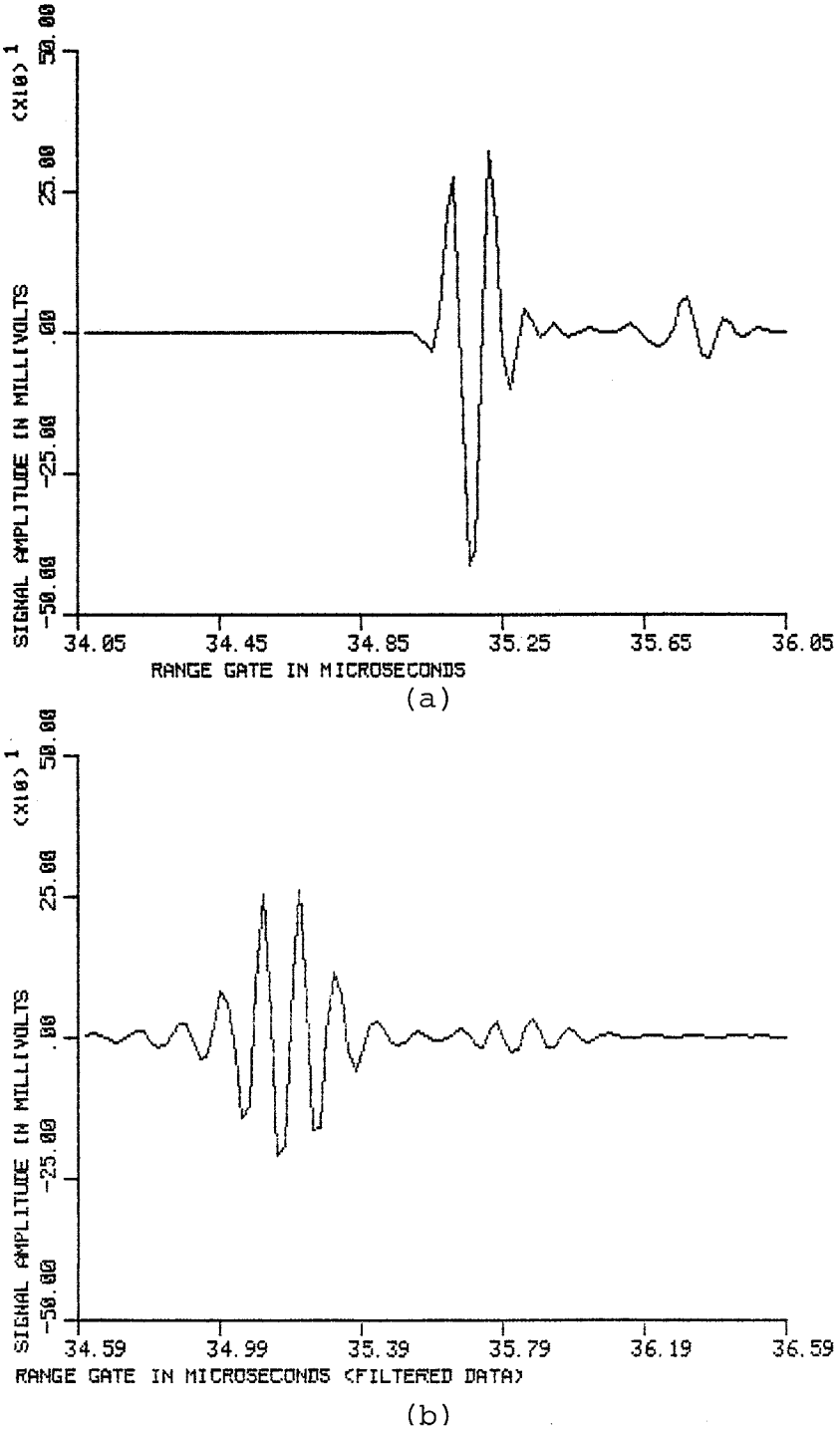

Figure 23. (a) Signal input to digital filter and (b) output of digital filter with bandedges at 6.0/8.0 MHz.

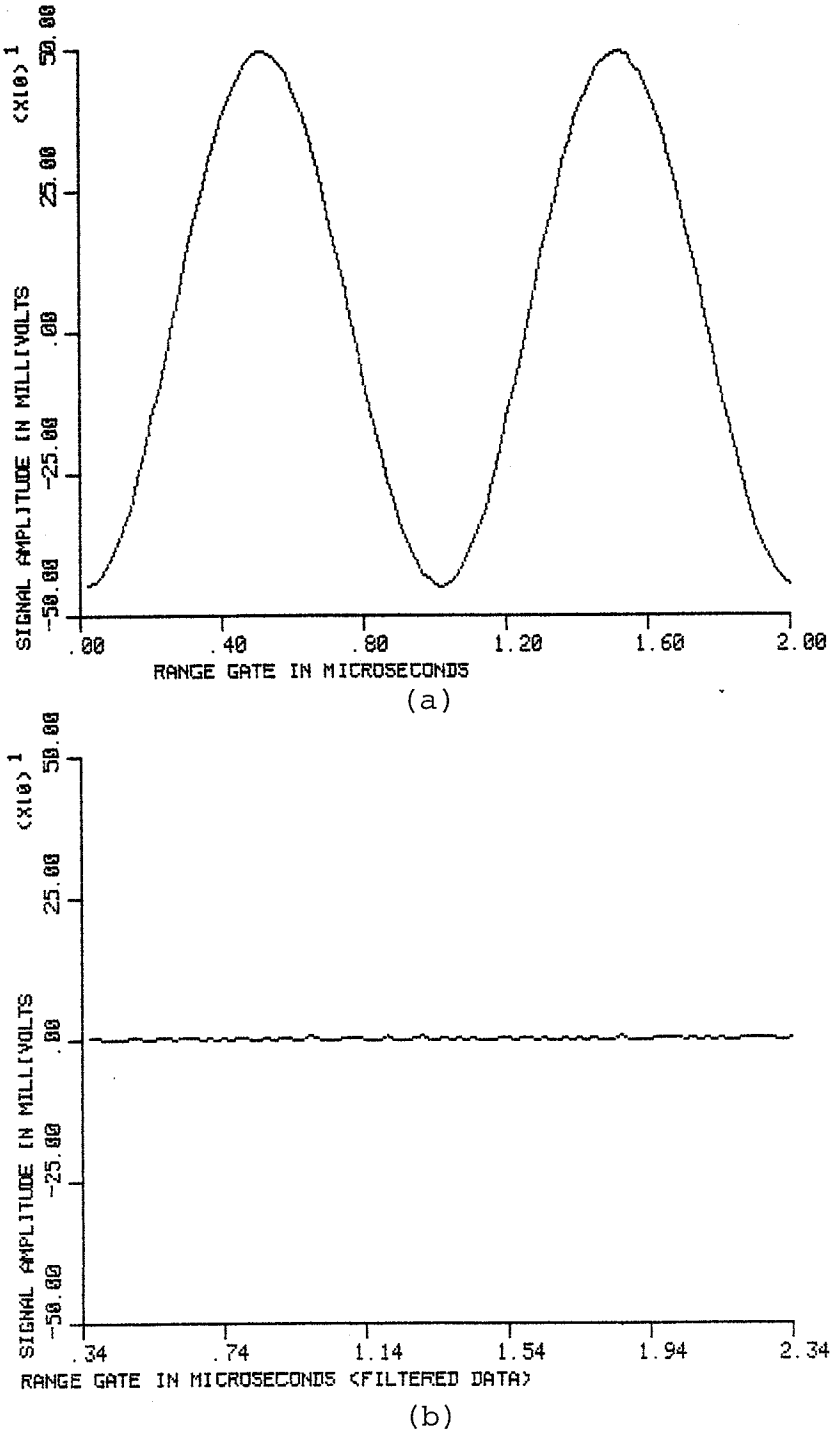

Figure 24. (a) 1 MHz signal input to digital filter and (b) output of digital filter with bandedges at 2.5/7.5 MHz.

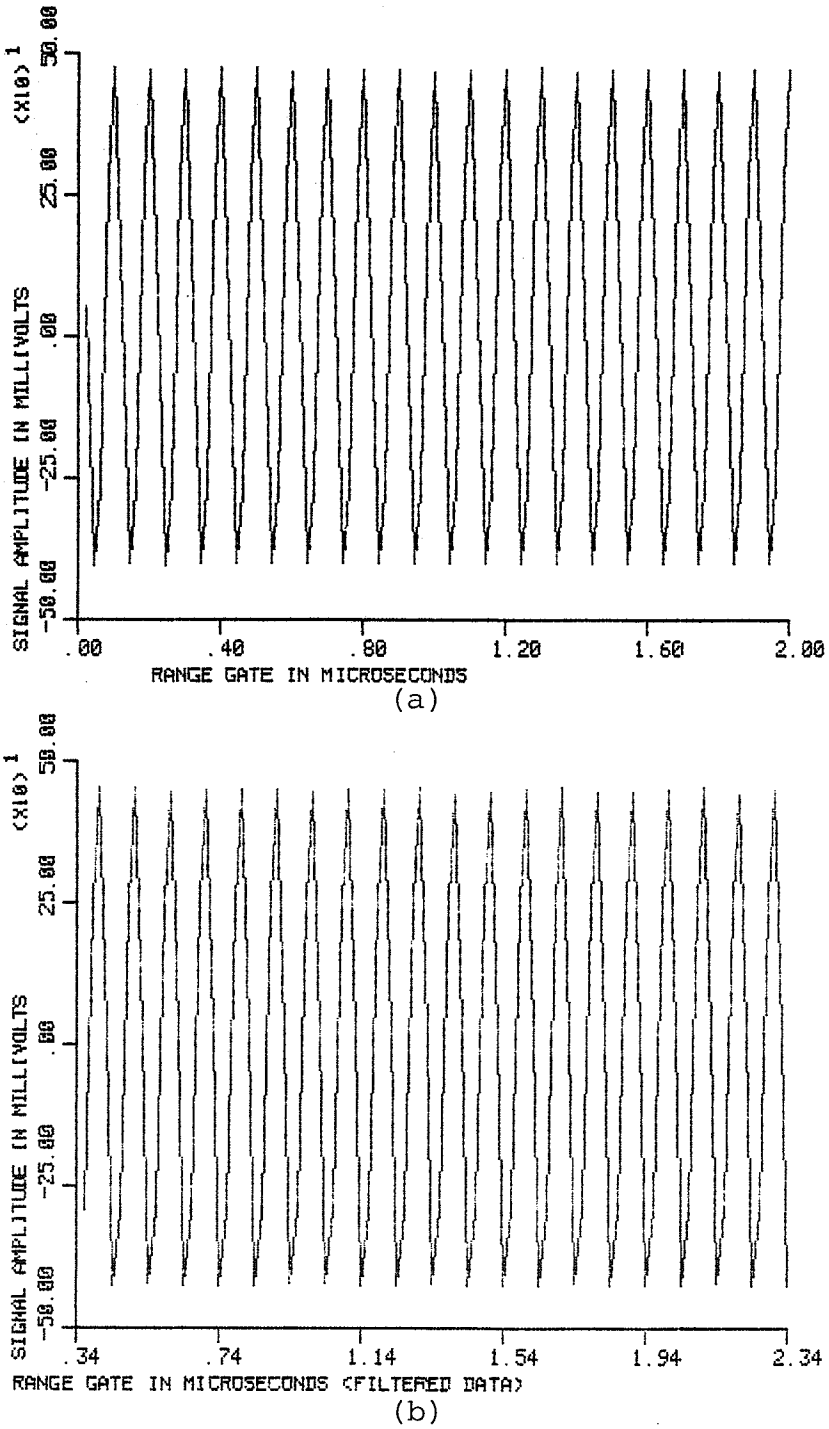

Figure 25. (a) 10 MHz signal input to digital filter and (b) output of digital filter with bandedges at 2.5/7.5 MHz.

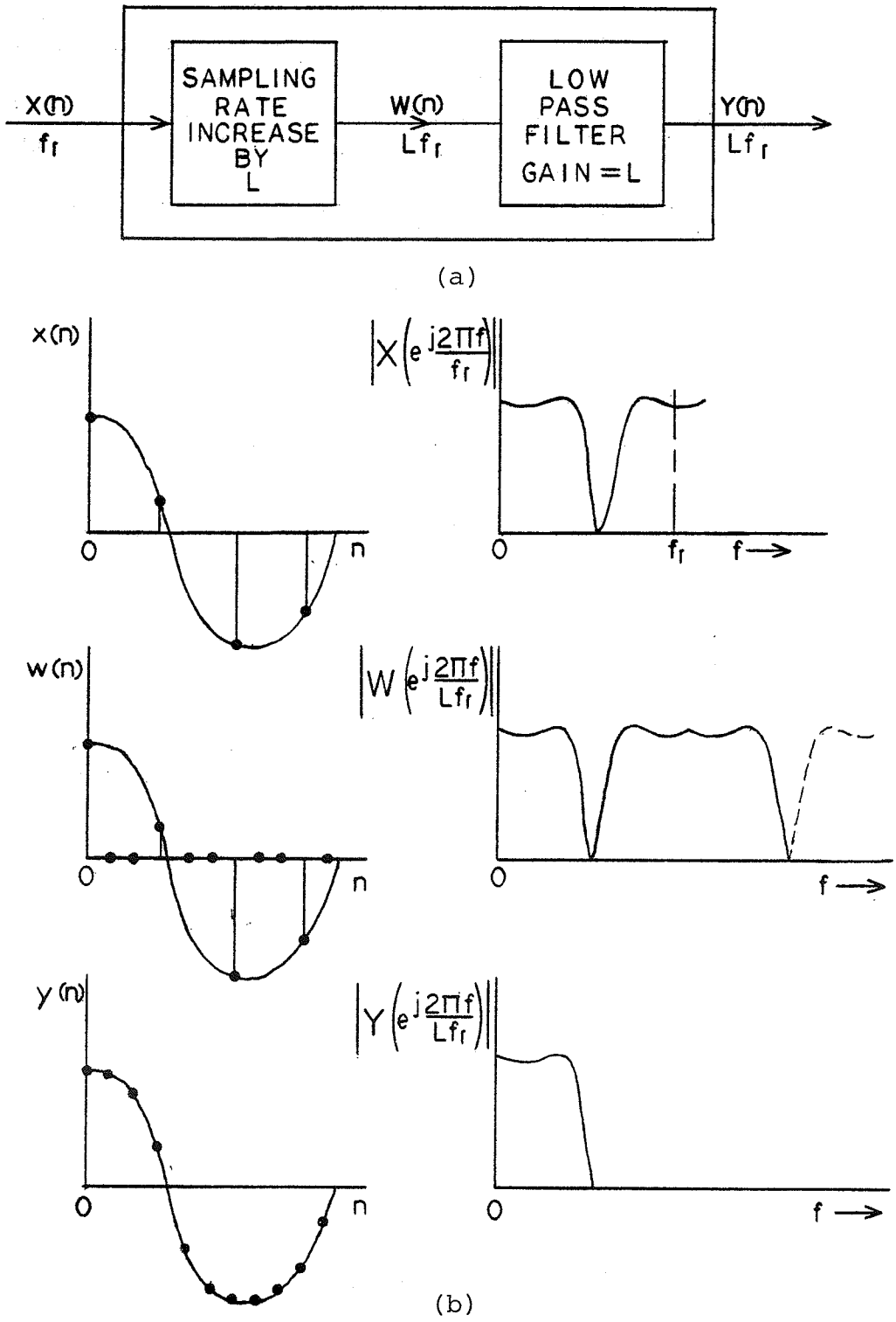

Figure 26. (a) Interpolation process and (b) frequency response and waveform interpretation.

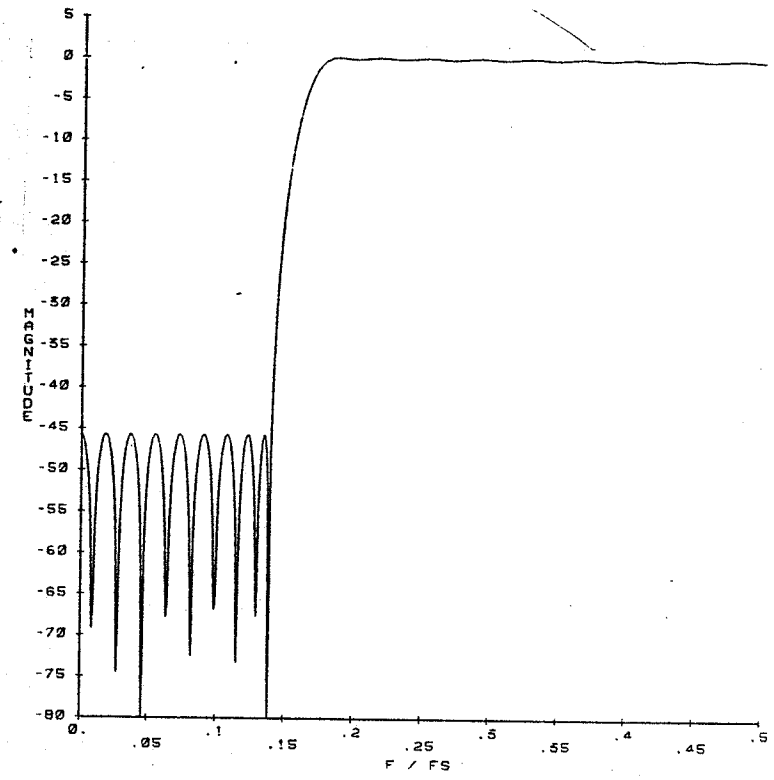

(a)

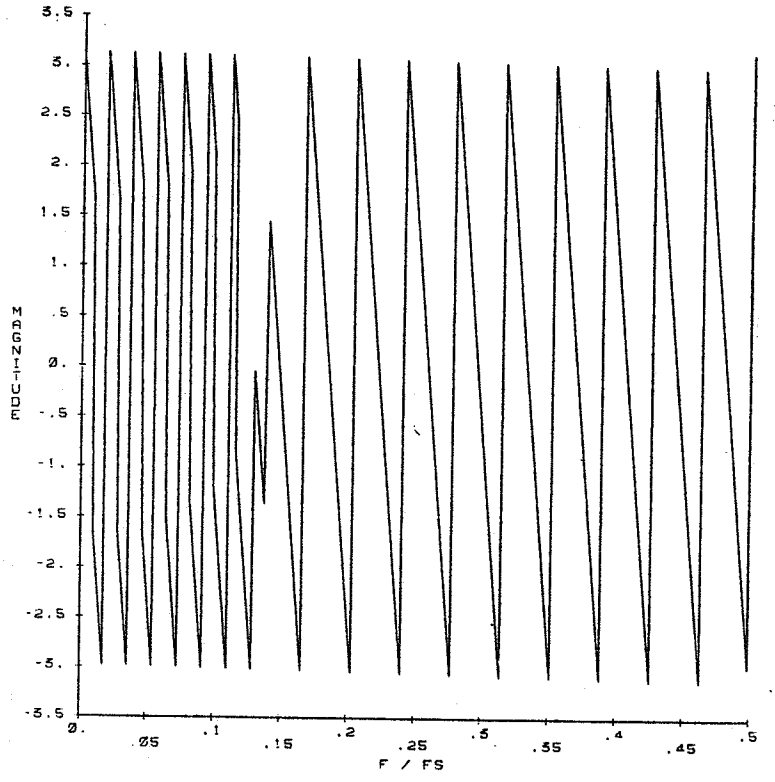

(b)

Figure 27. (a) Magnitude of the frequency response for the interpolation filter and (b) phase of the frequency response for the interpolation filter.

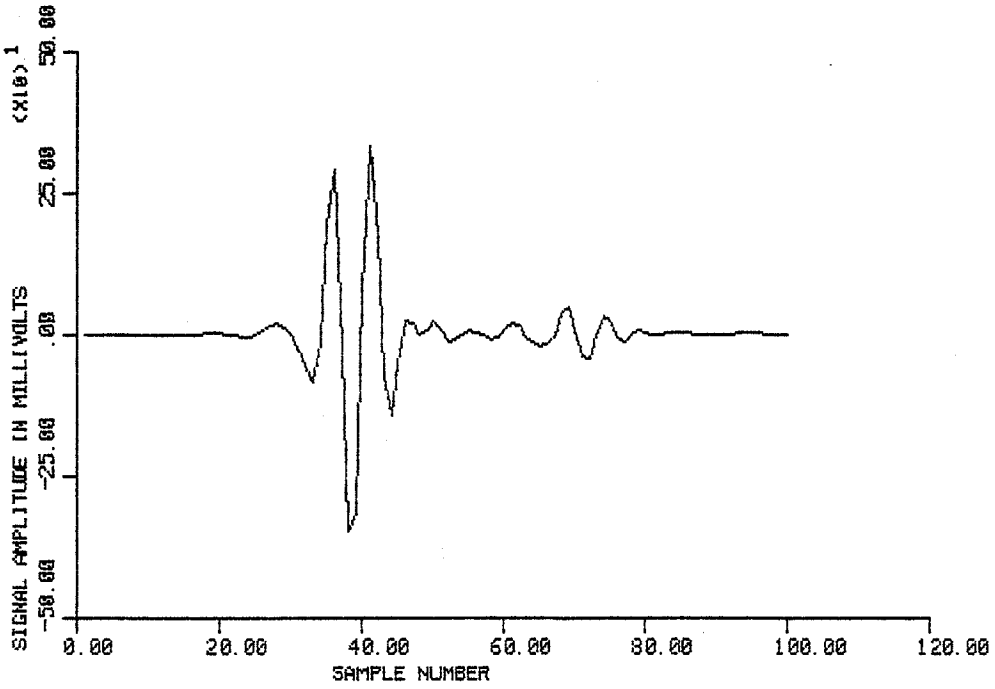

(a)

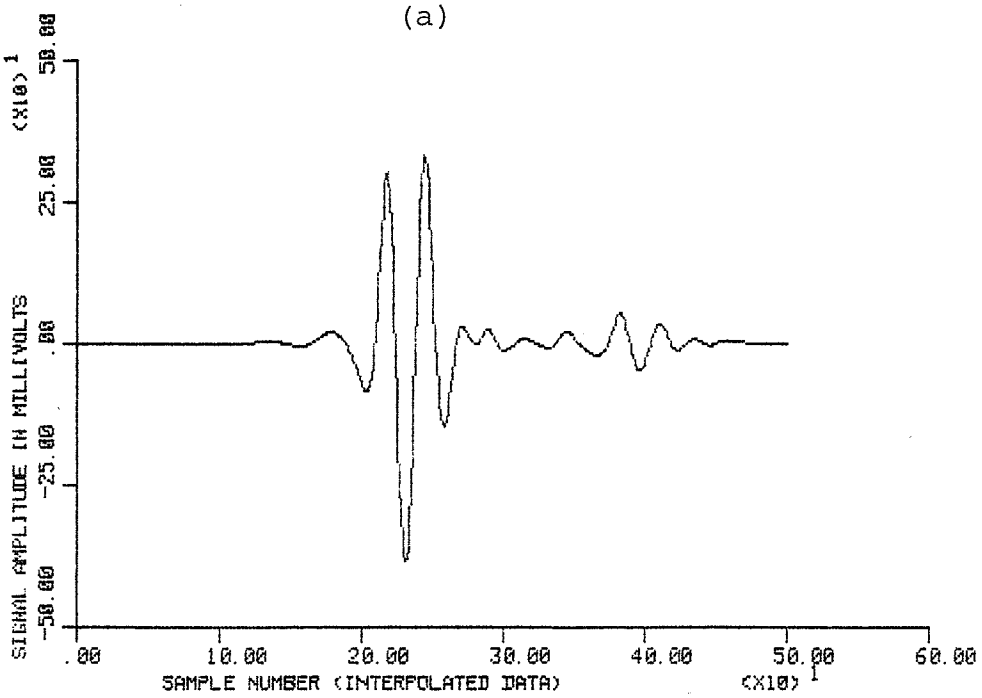

(b)

Figure 28. (a) Signal input to the filter and (b) interpolated signal.

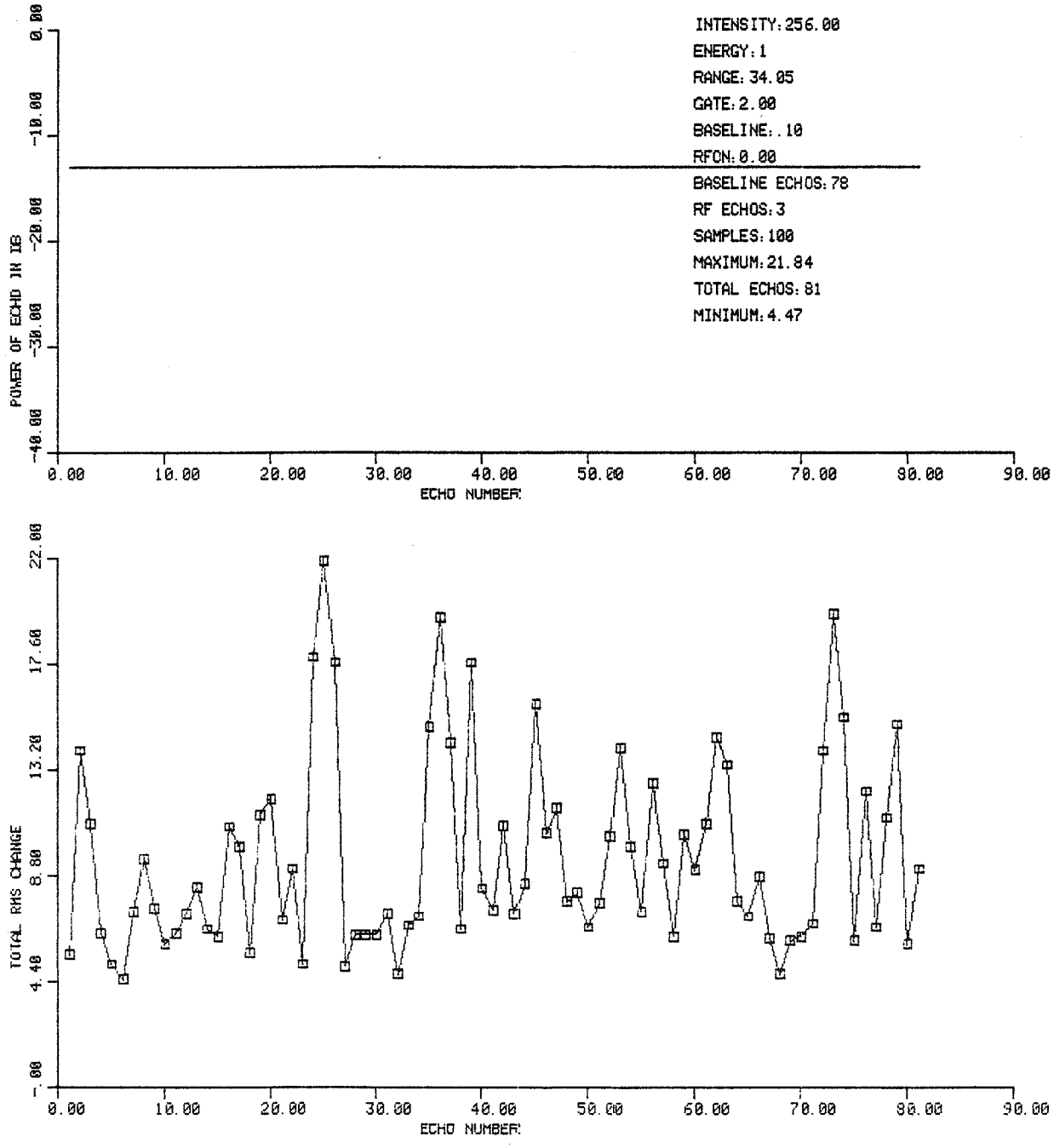

Figure 29. Plot of RMS difference and power generated when all the echoes are acquired during the baseline.

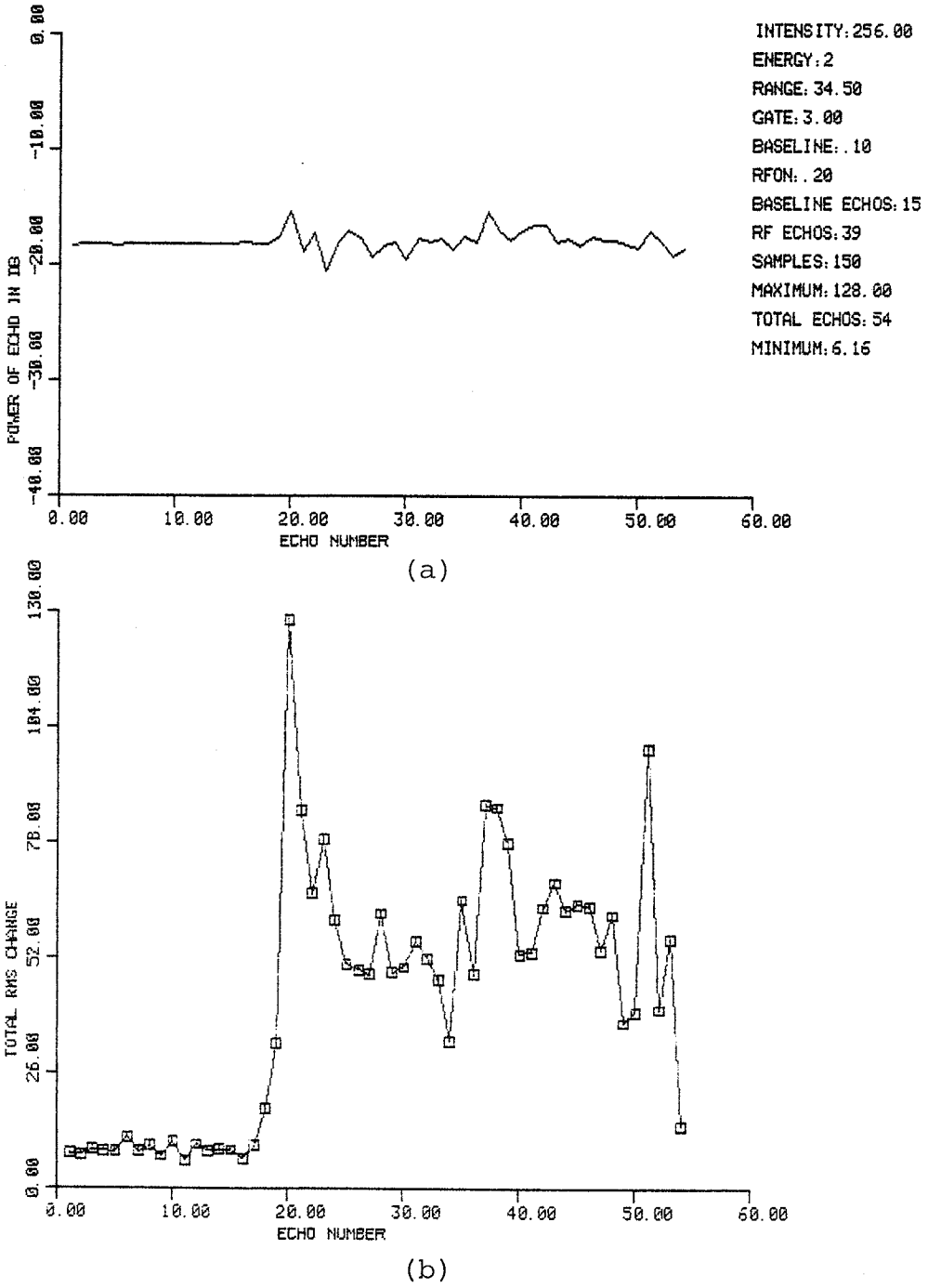

Figure 30. Plot of RMS difference and power generated by program ANALYZ.

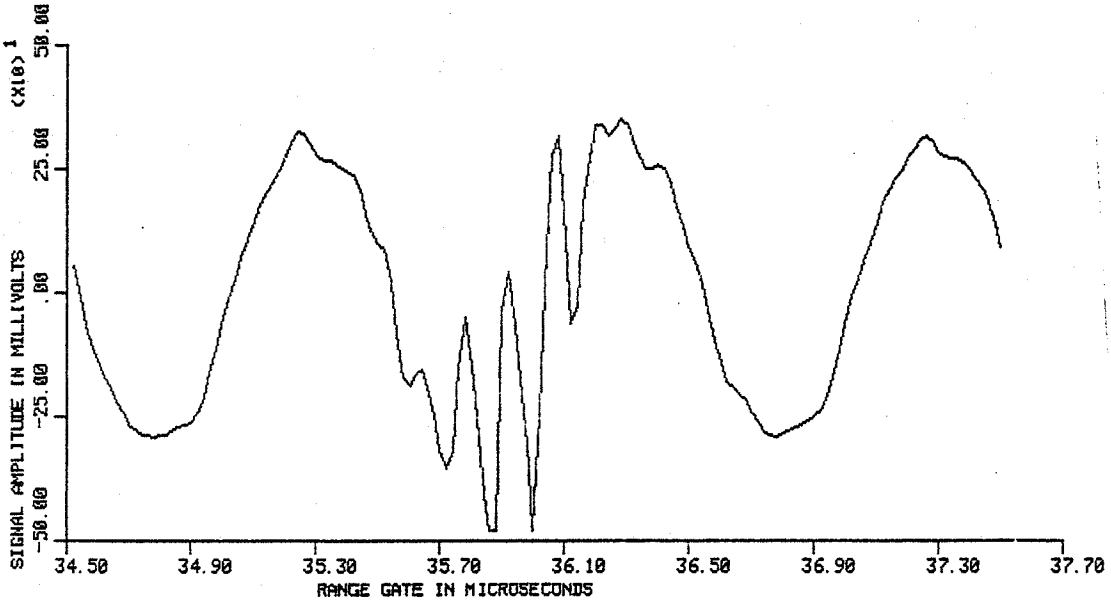

(a)

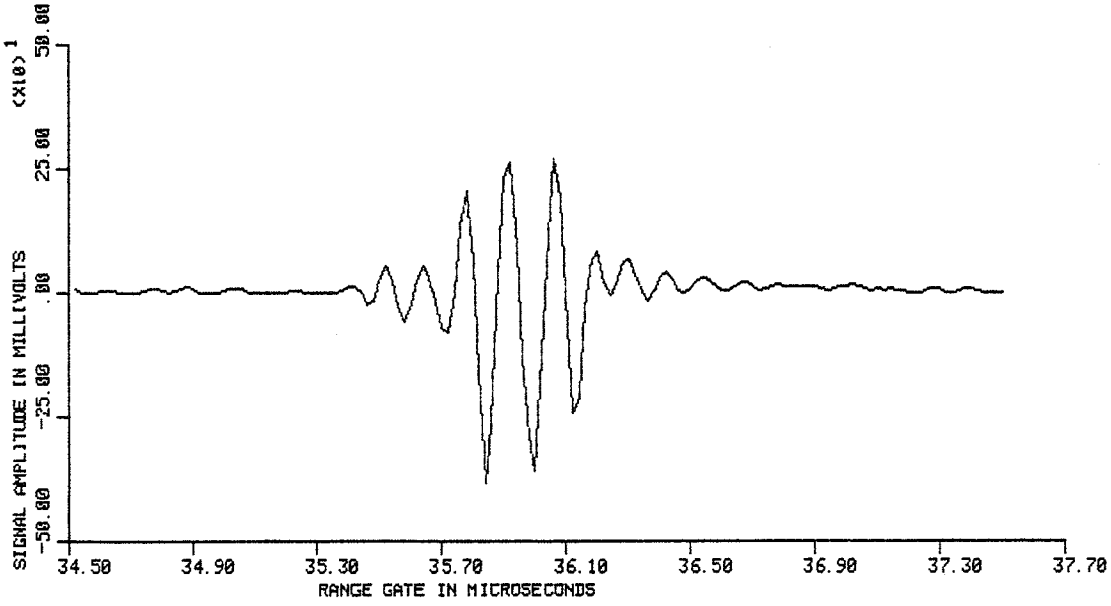

(b)

Figure 31. (a) Echo obtained during ultrasonic exposure and (b) same echo obtained during the baseline.

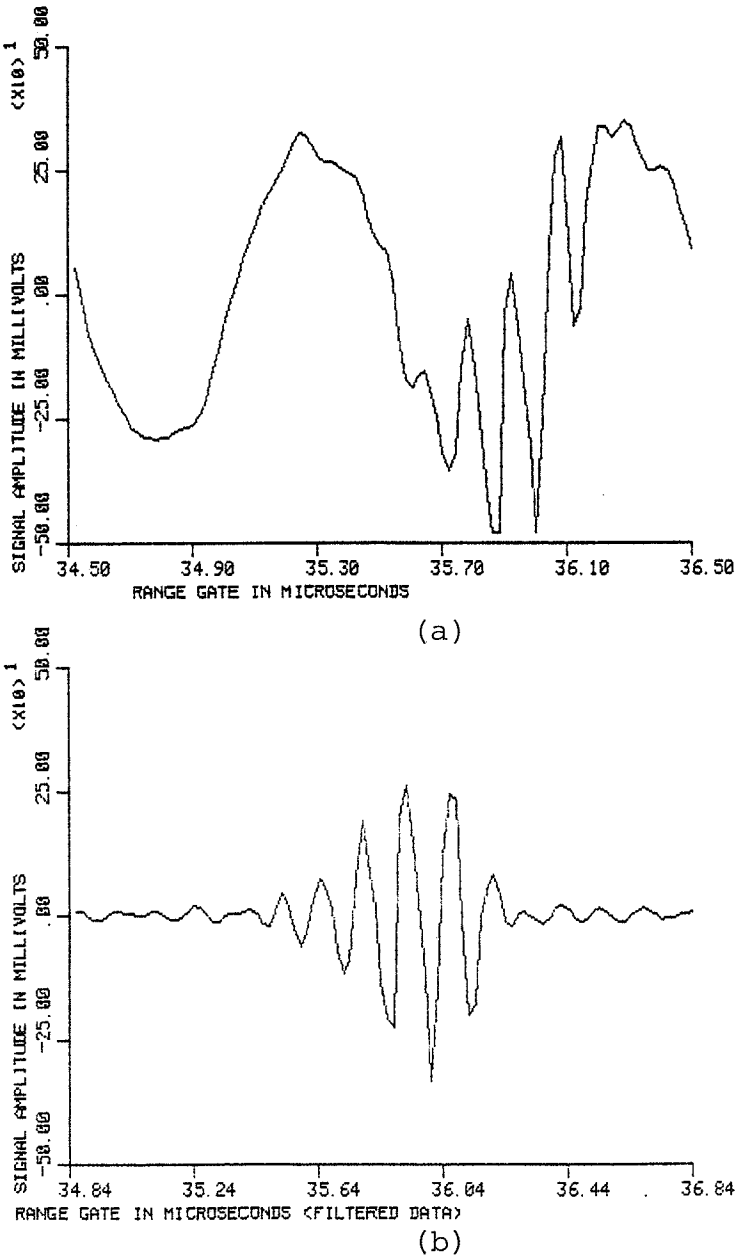

Figure 32. (a) Signal input to the digital filter and (b) output of digital filter with bandedges at 2.5/7.5 MHz.

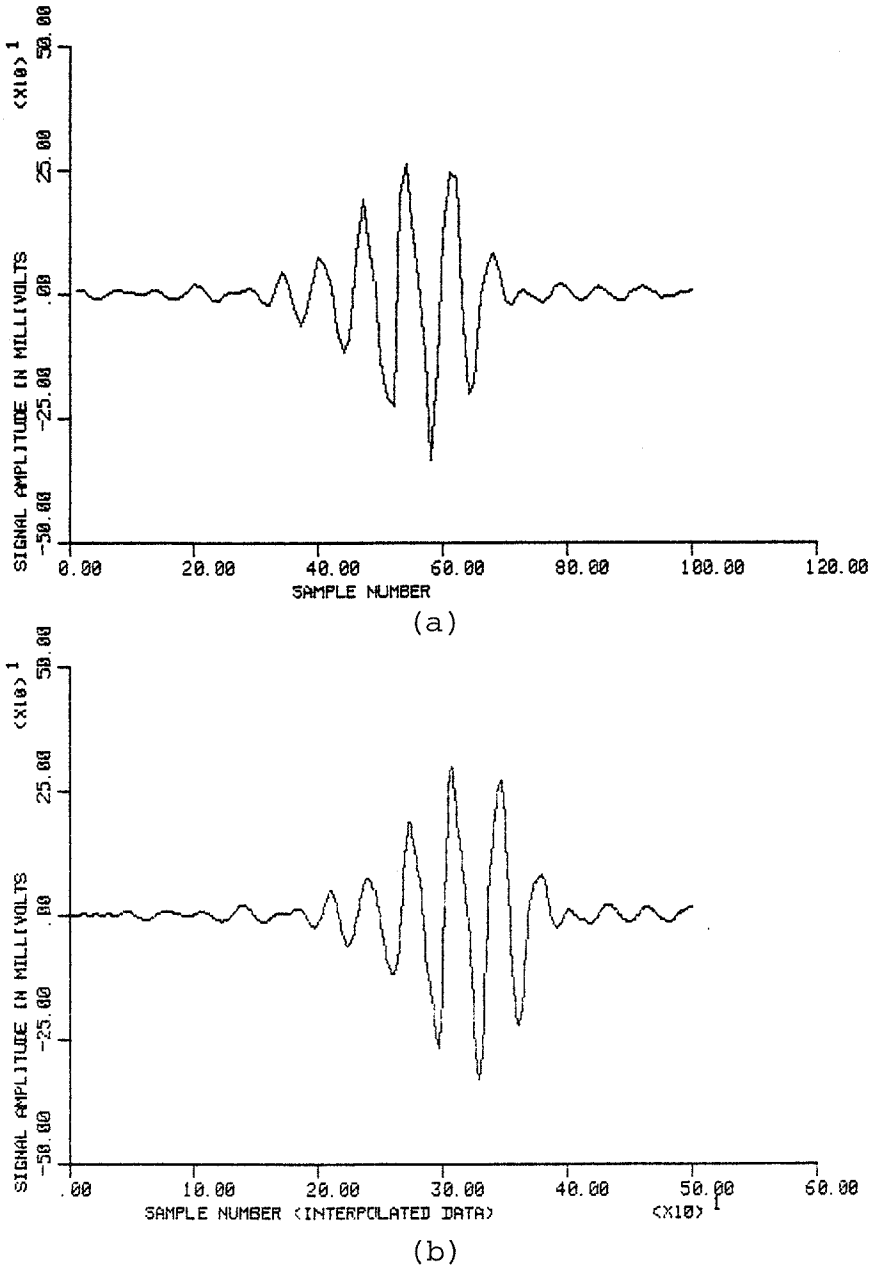

Figure 33. (a) Signal input to interpolating filter and (b) output of interpolating filter.

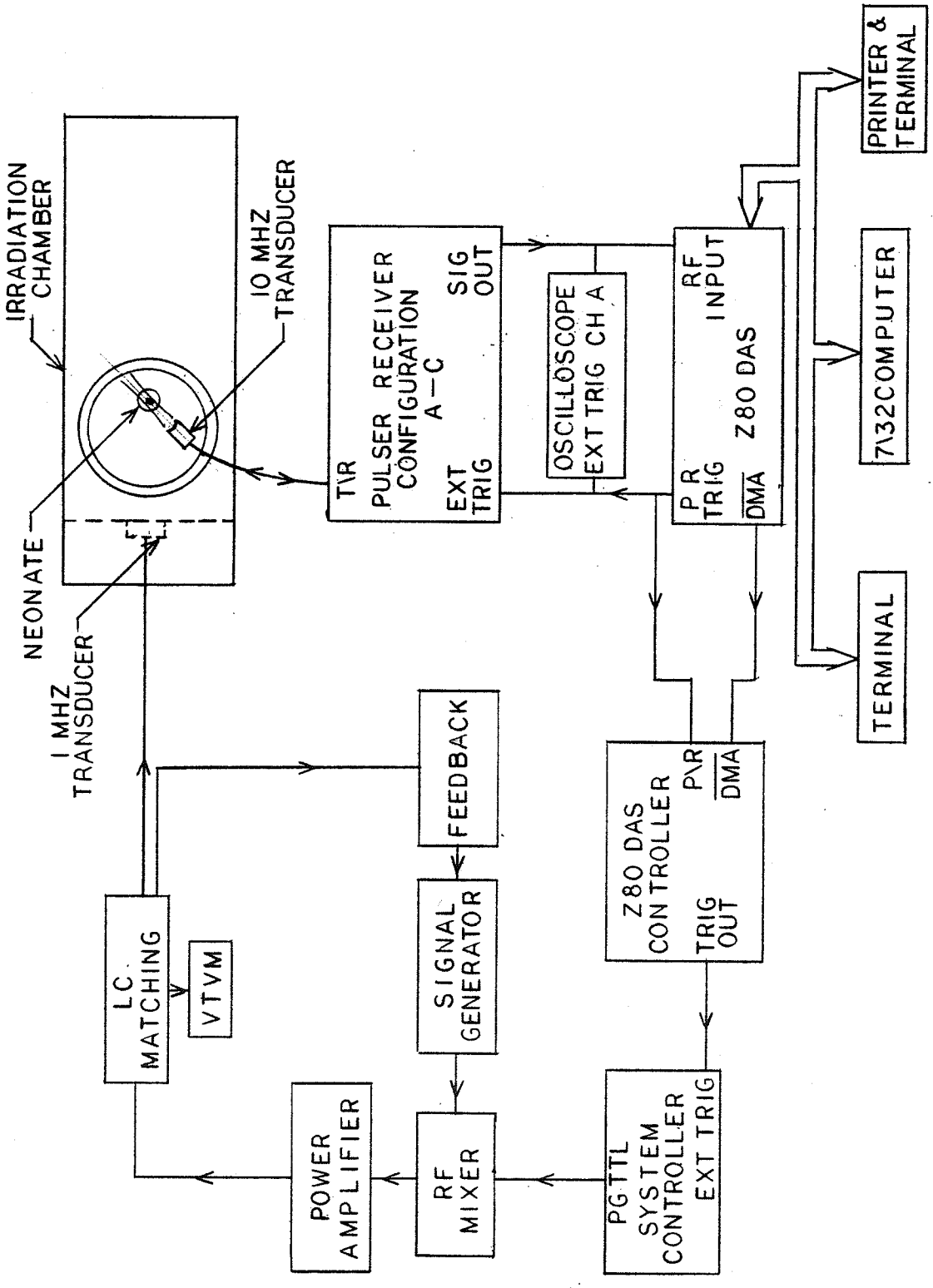

Figure 34. Block diagram of the pulsed ultrasonic exposure system hardware.

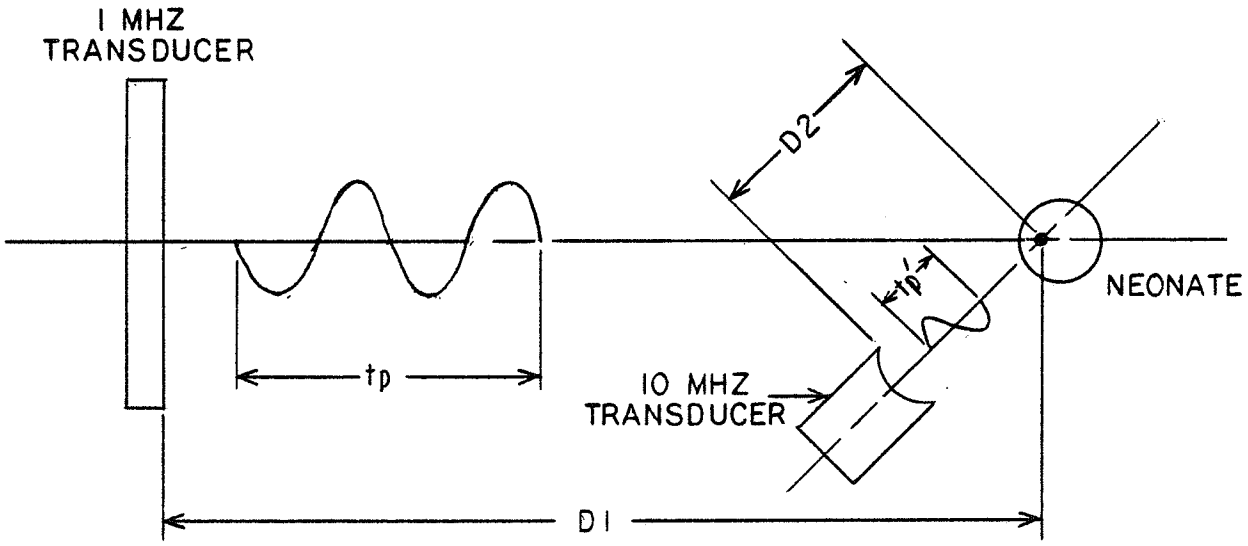

Figure 35. Relation among the parameters characterizing the pulsed ultrasonic exposure technique.

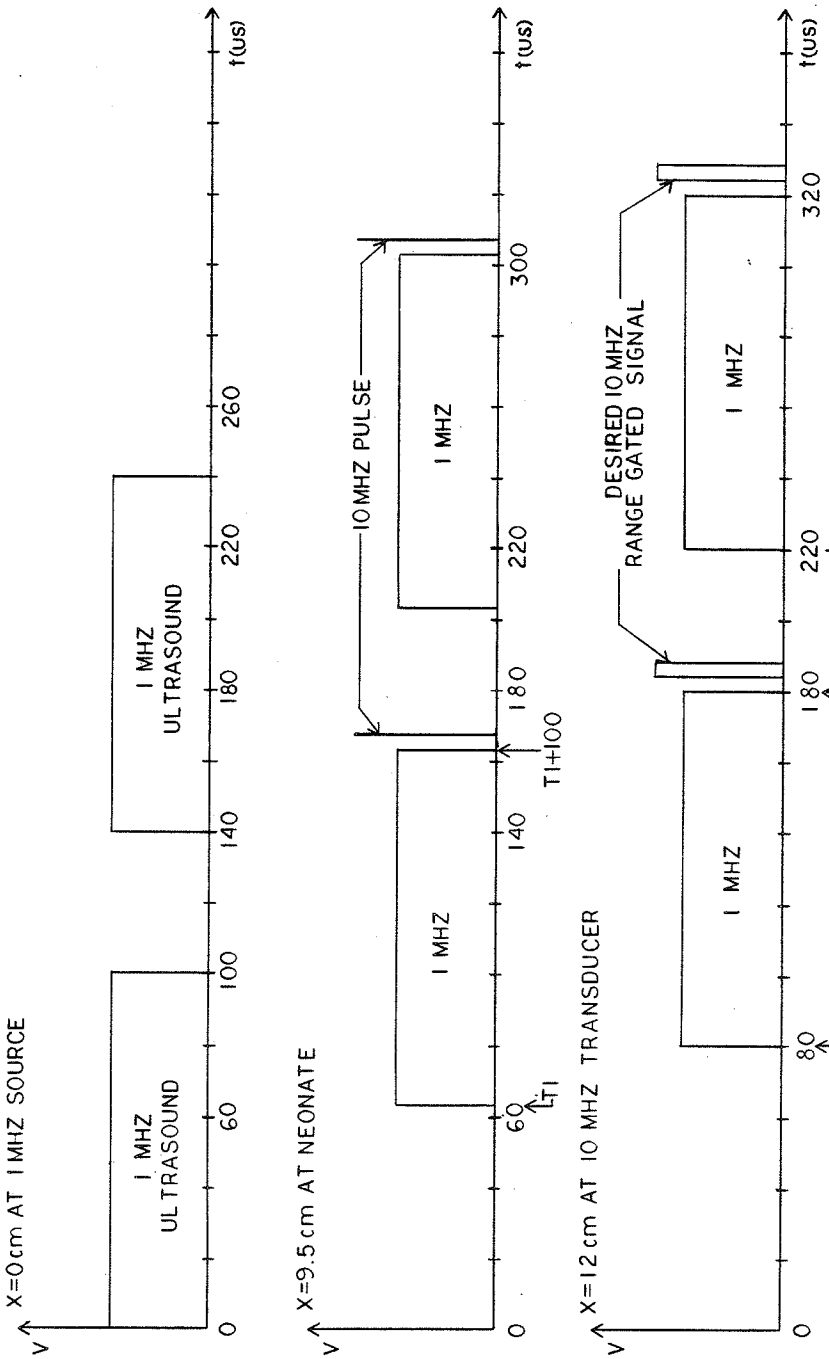

Figure 36. Time variation of acoustic signals detected at the 1 MHz source, neonate, and 10 MHz imaging transducer source.

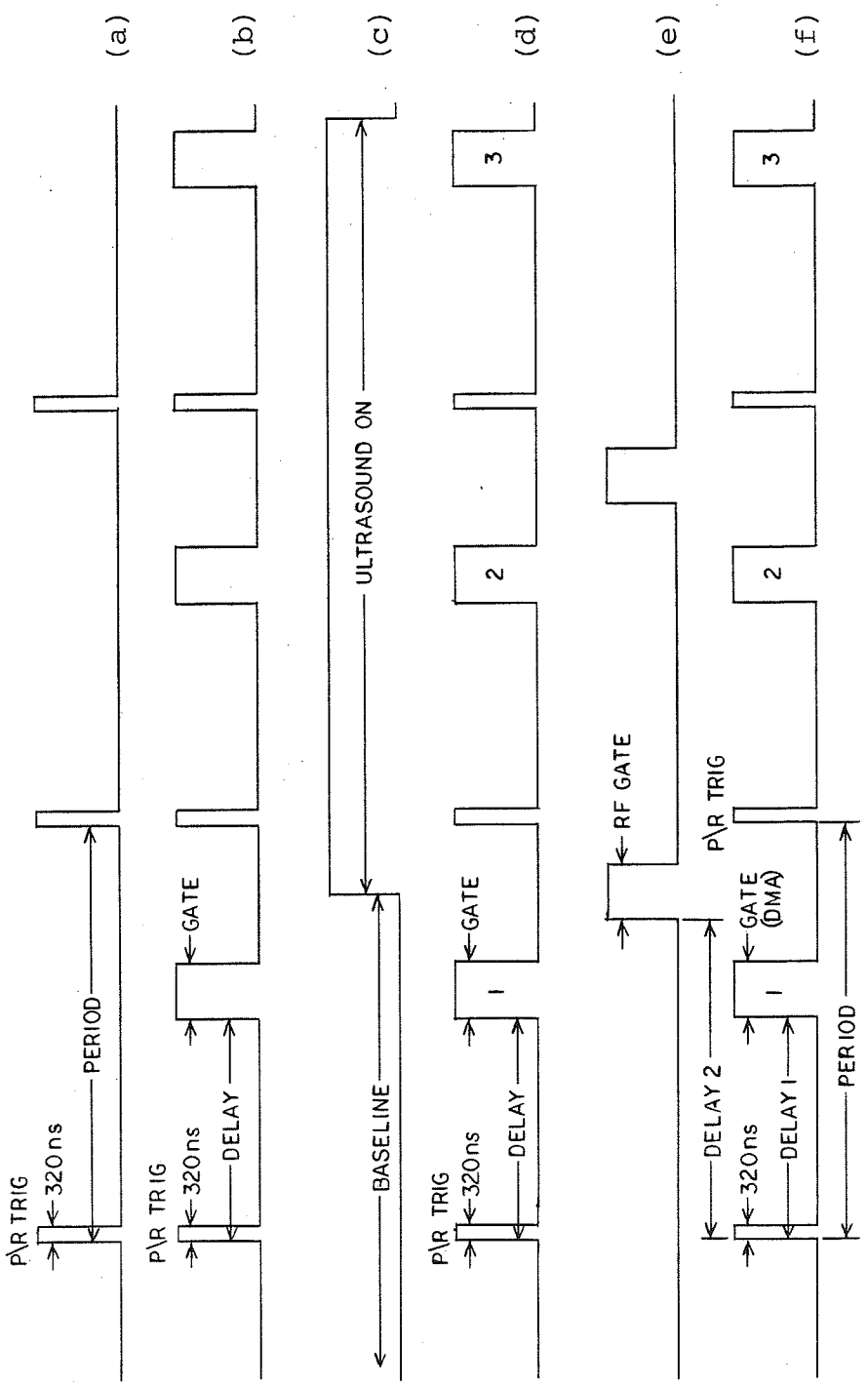

Figure 37. (a) P/R trigger signal generated by the 280 DAS, (b) P/R trigger signal and range gage signal generated by the 280 DAS during data aquisition, (c) required control signal for continuous ultrasonic exposures, (d) signal timing corresponding to the control signal in (e), (e) required control signal for pulsed ultrasonic exposures, and (f) signal timing corresponding to the control signal shown in (e).

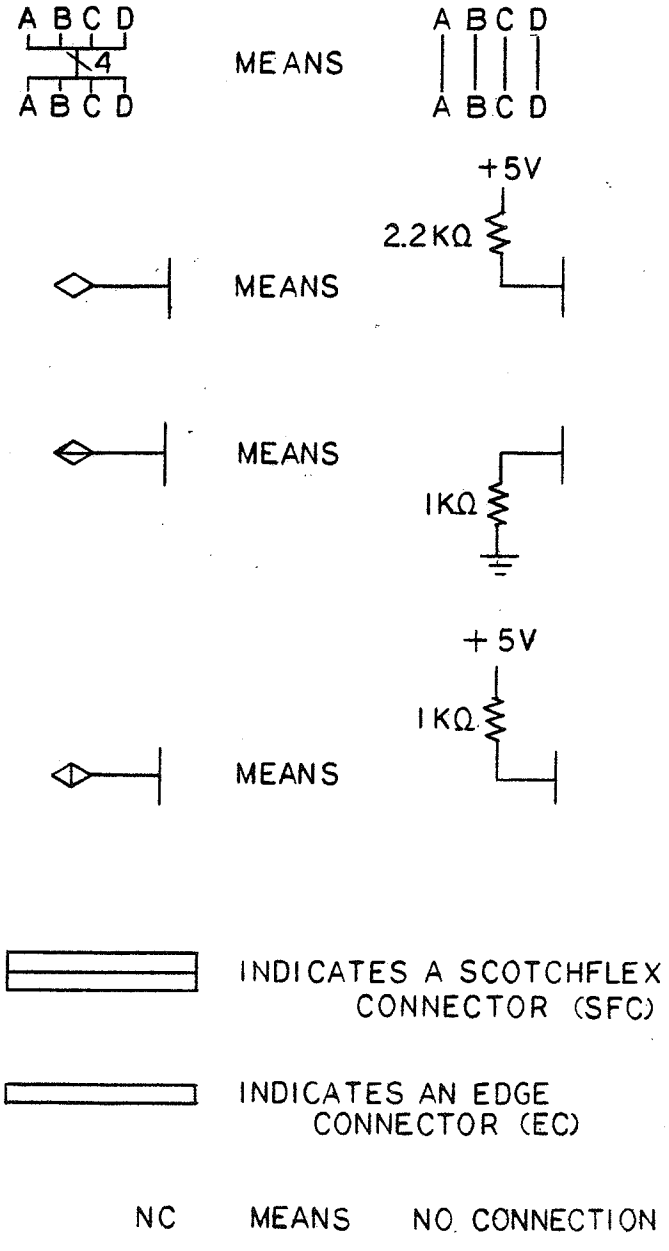

Figure 38. Schematic symbols.

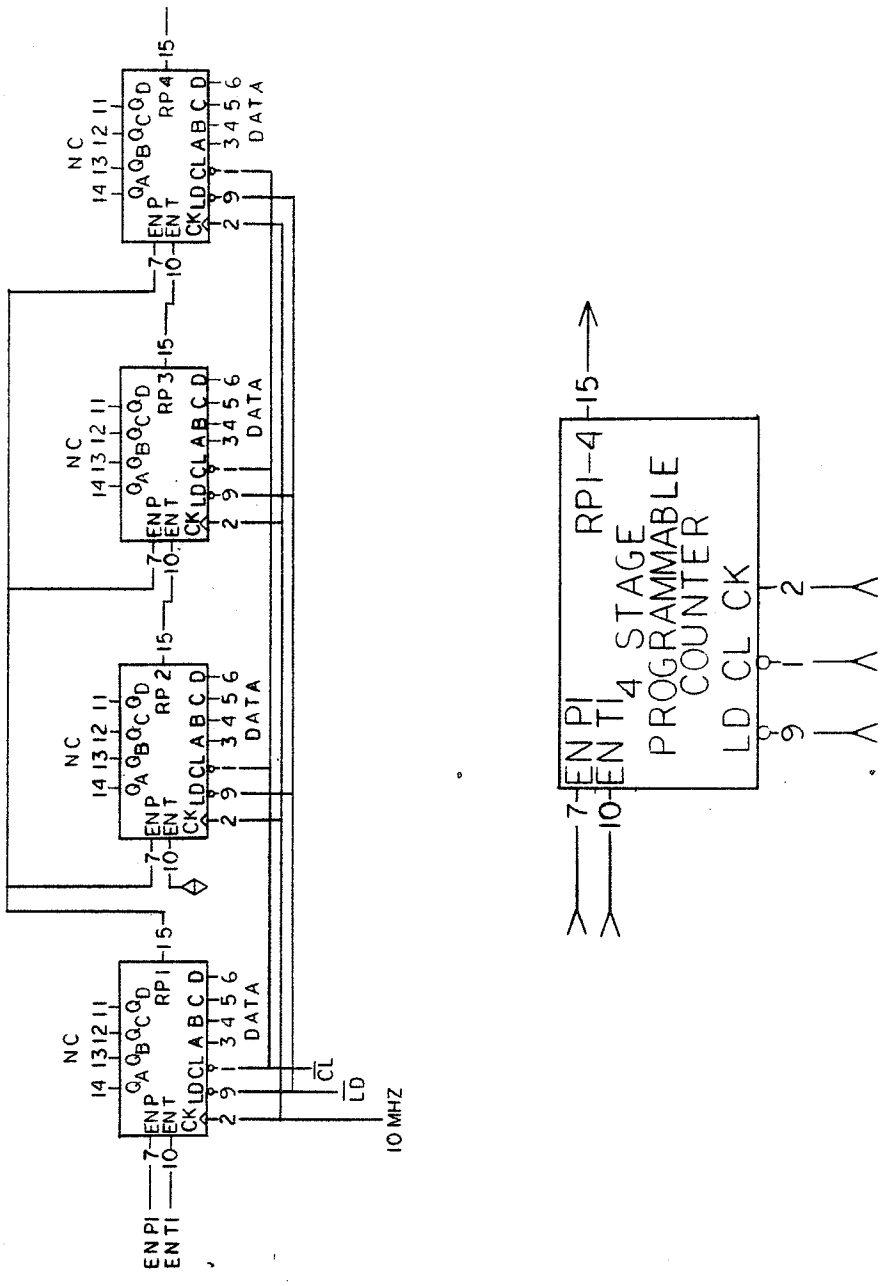

Figure 39. Four stage programmable counter.

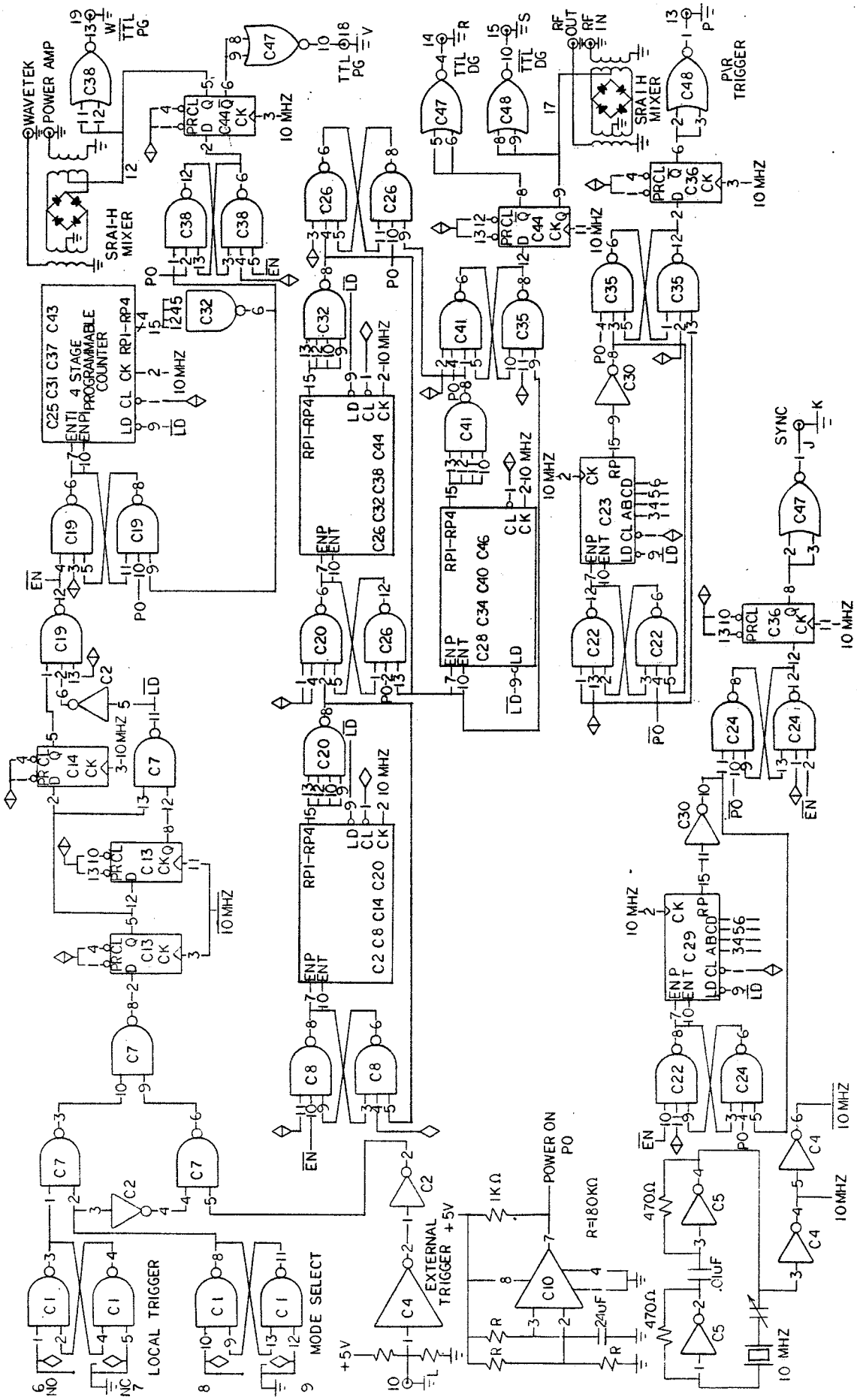

Figure 40. Counter and timing circuit schematic.

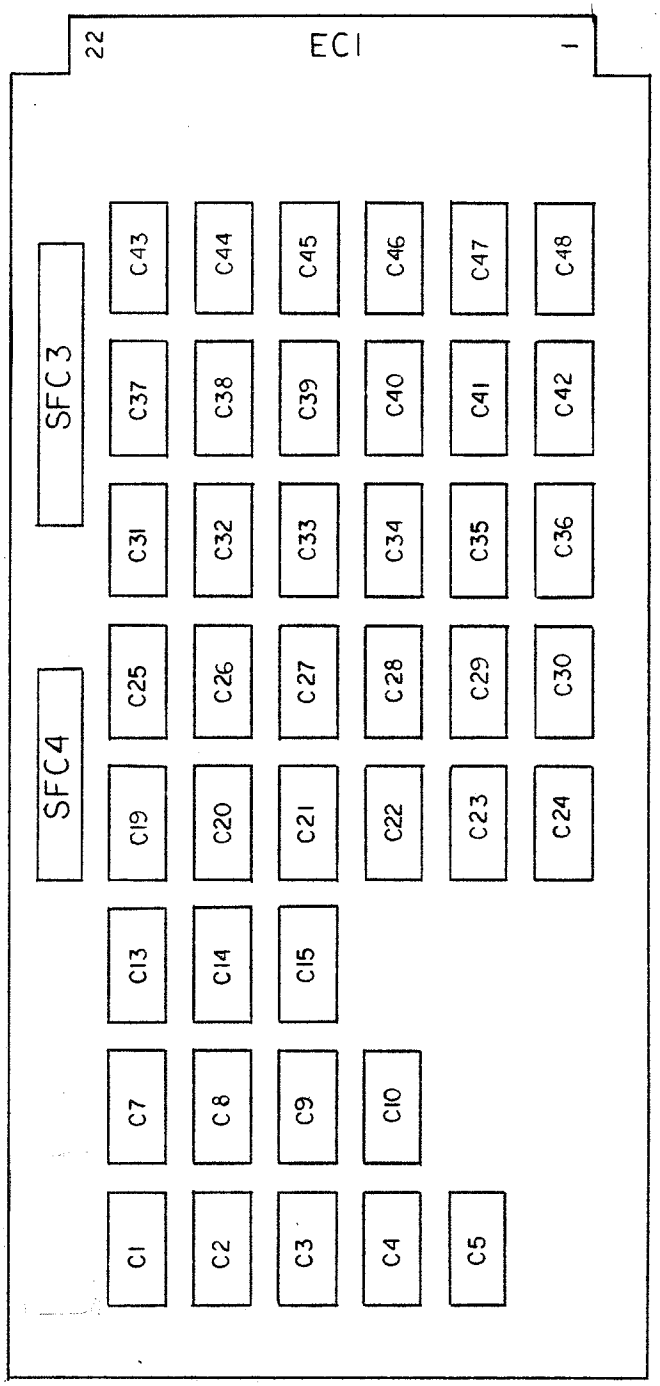

Figure 41. Component layout for the counter and timing circuit board. (Refer to Tables 1-3 for IC identification, ECI pinout, and SFC 3 and 4 pinout.)

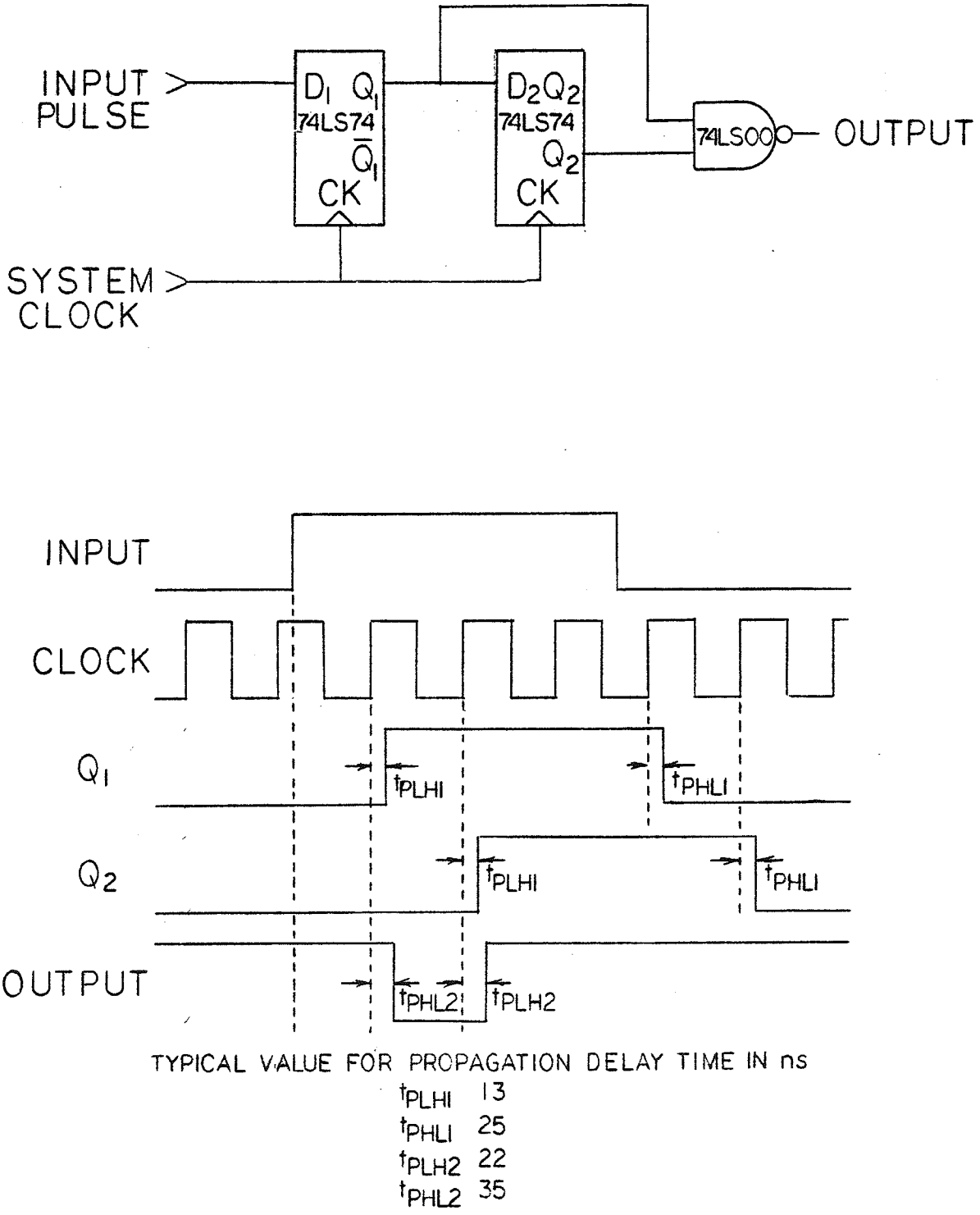

Figure 42. Synchronous single shot device.

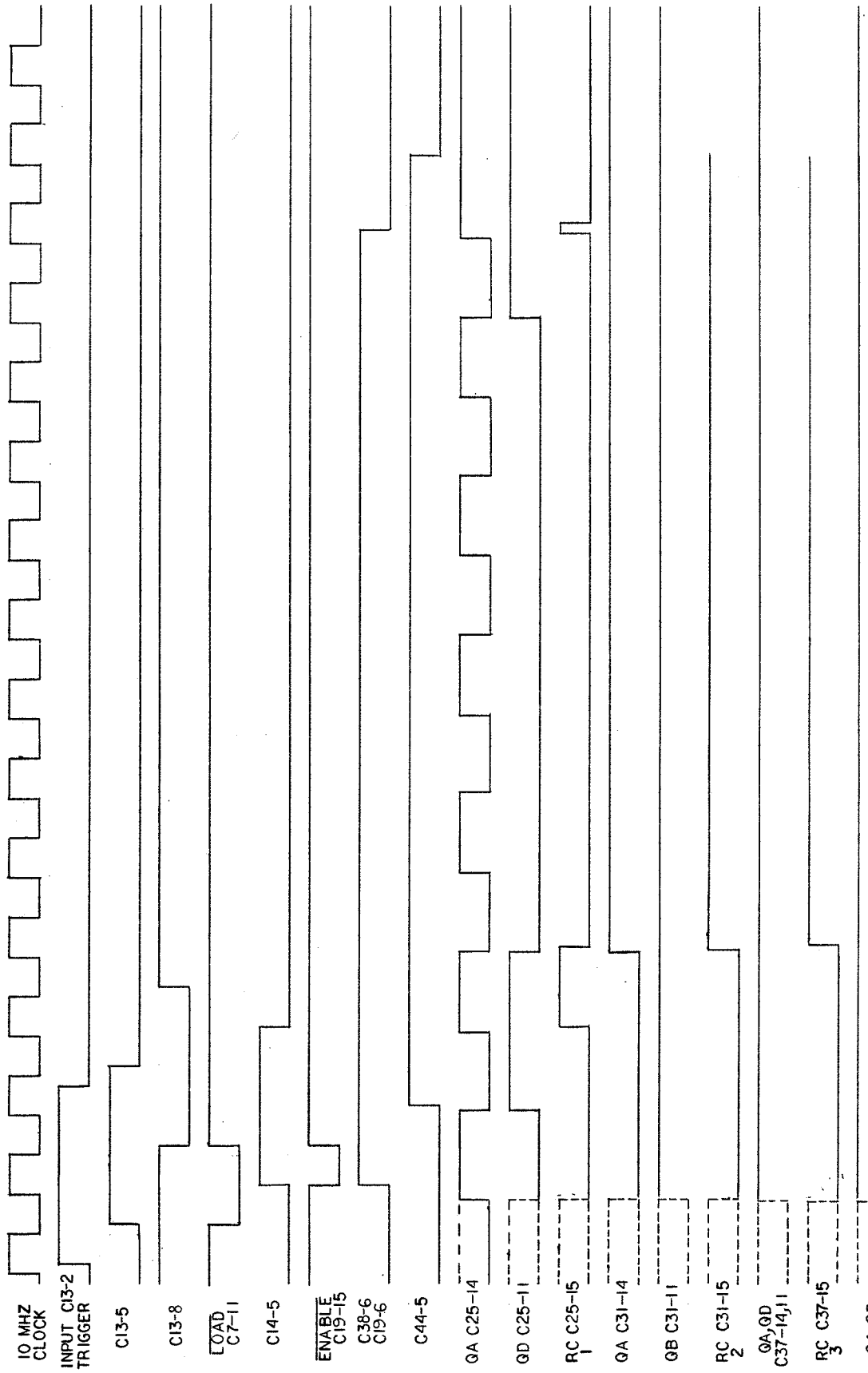

Figure 43. Timing diagram for the counter and timing circuit.

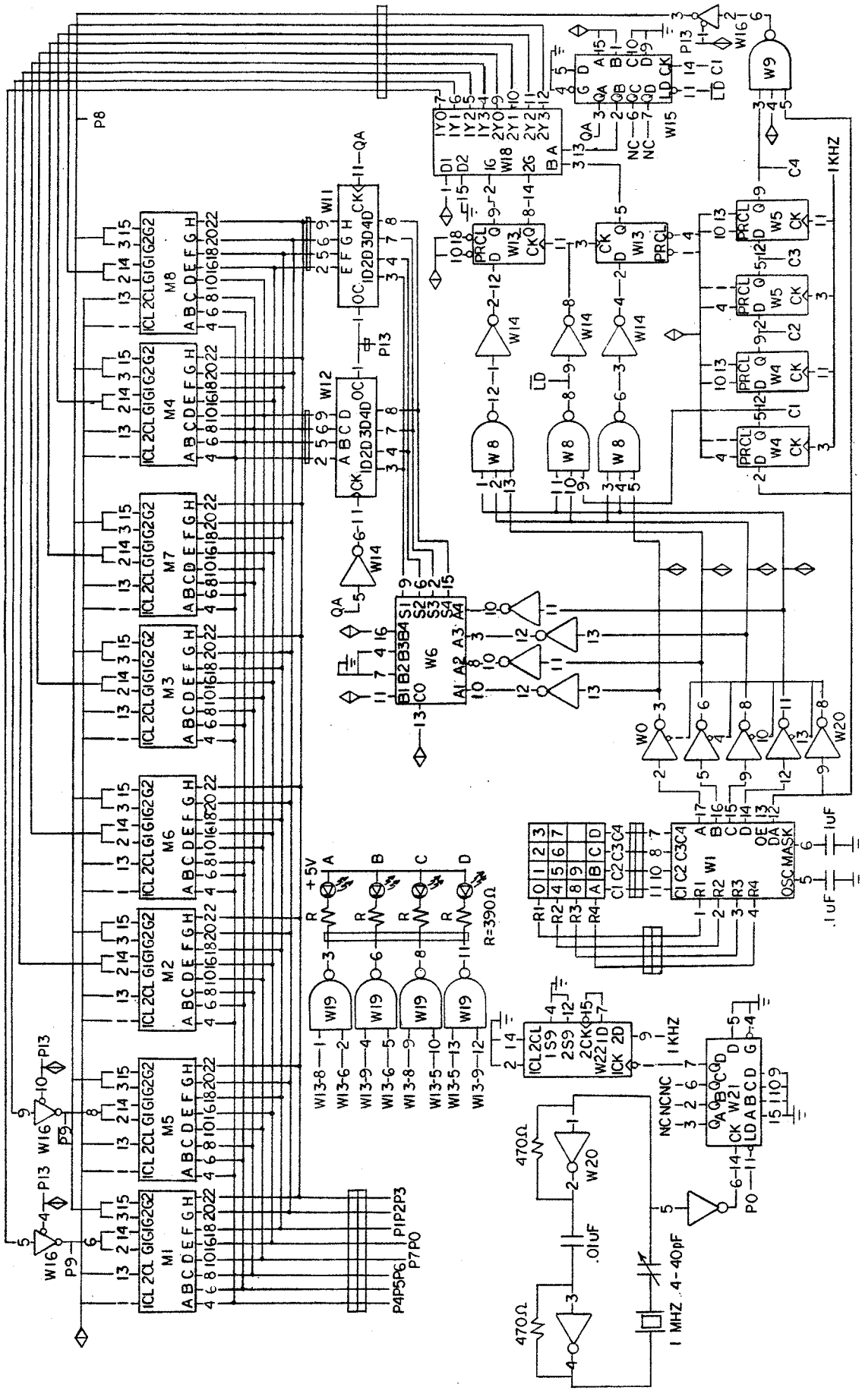

Figure 44. Data entry circuit schematic.

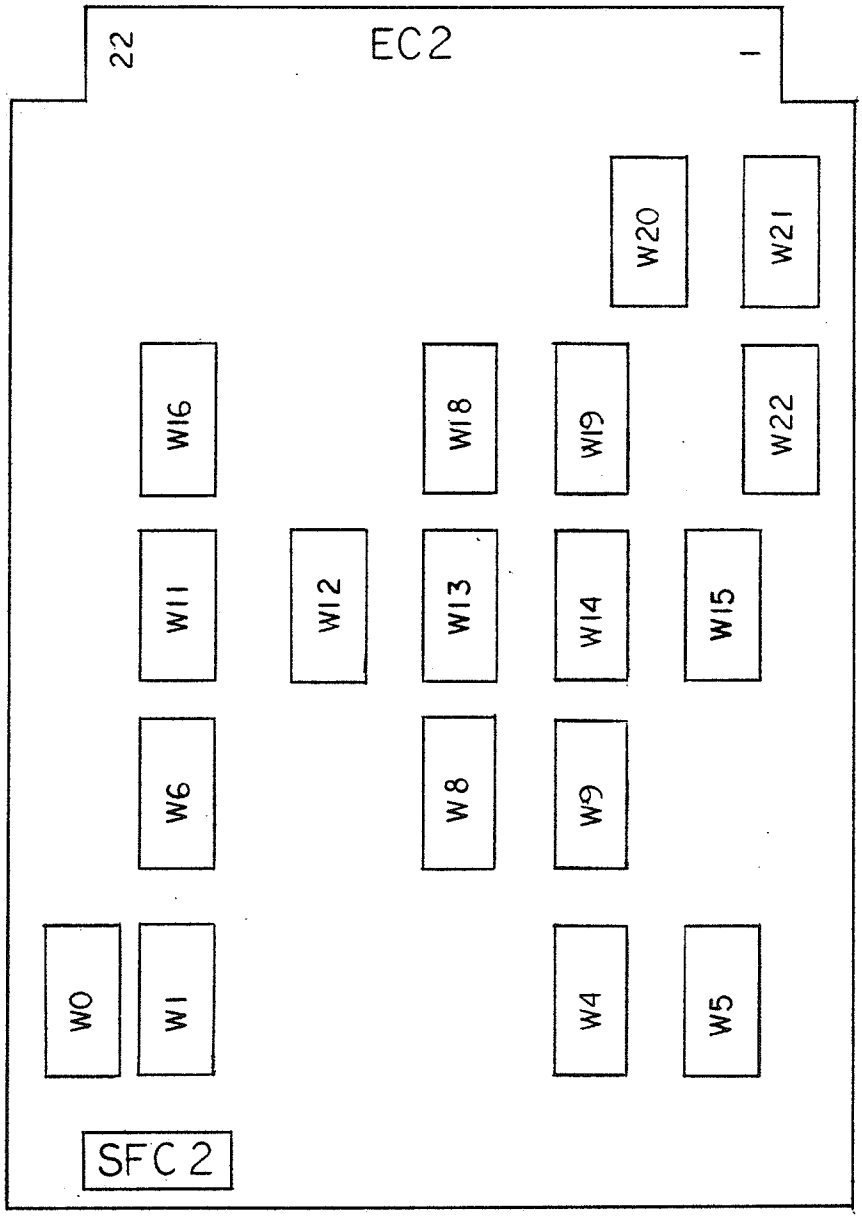

Figure 45. Component layout for the data entry circuit board. (Refer to Tables 4-6 for IC identification, SFC2 pinout, and EC2 pinout.)

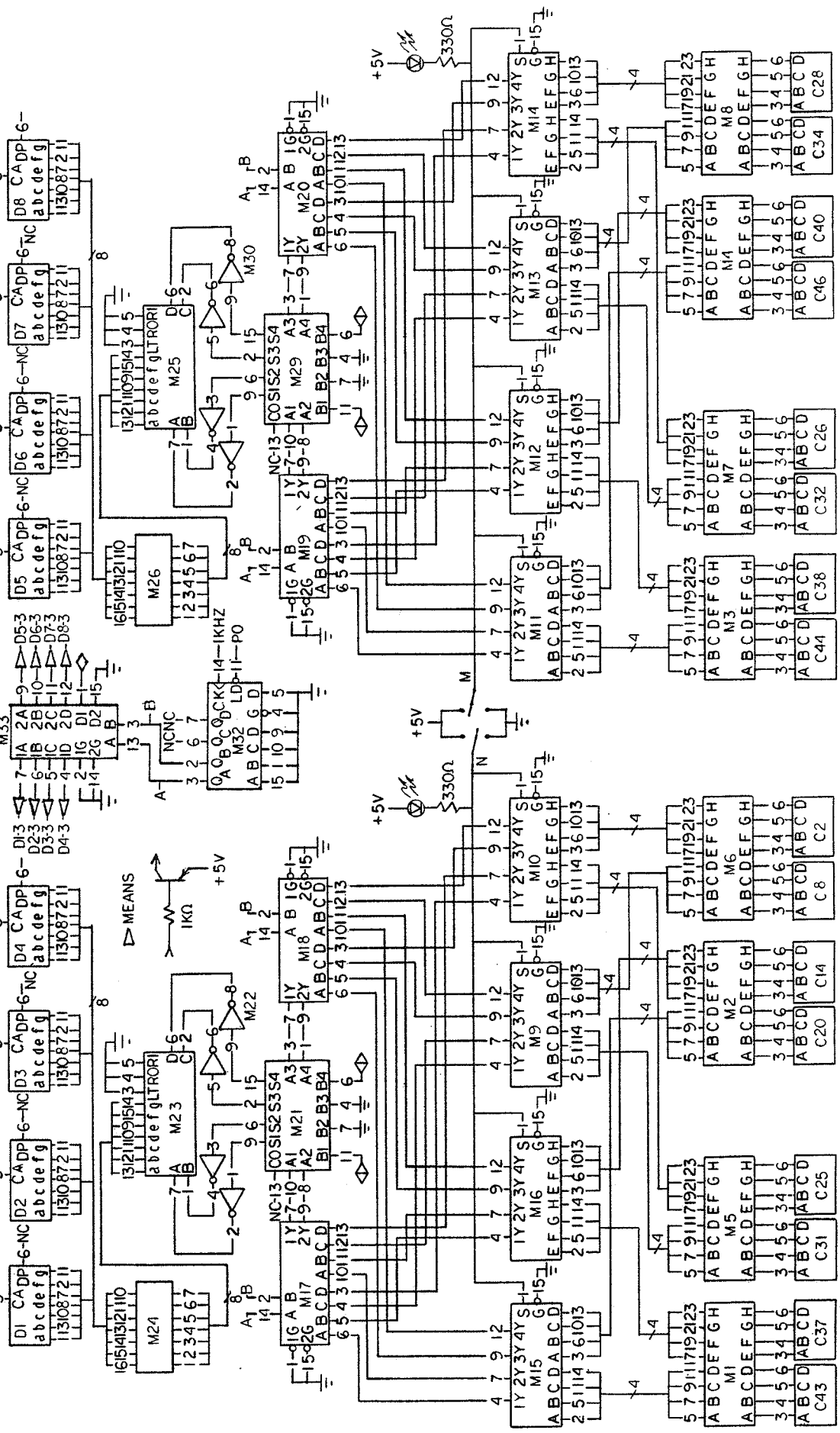

Figure 46. Display circuit schematic.

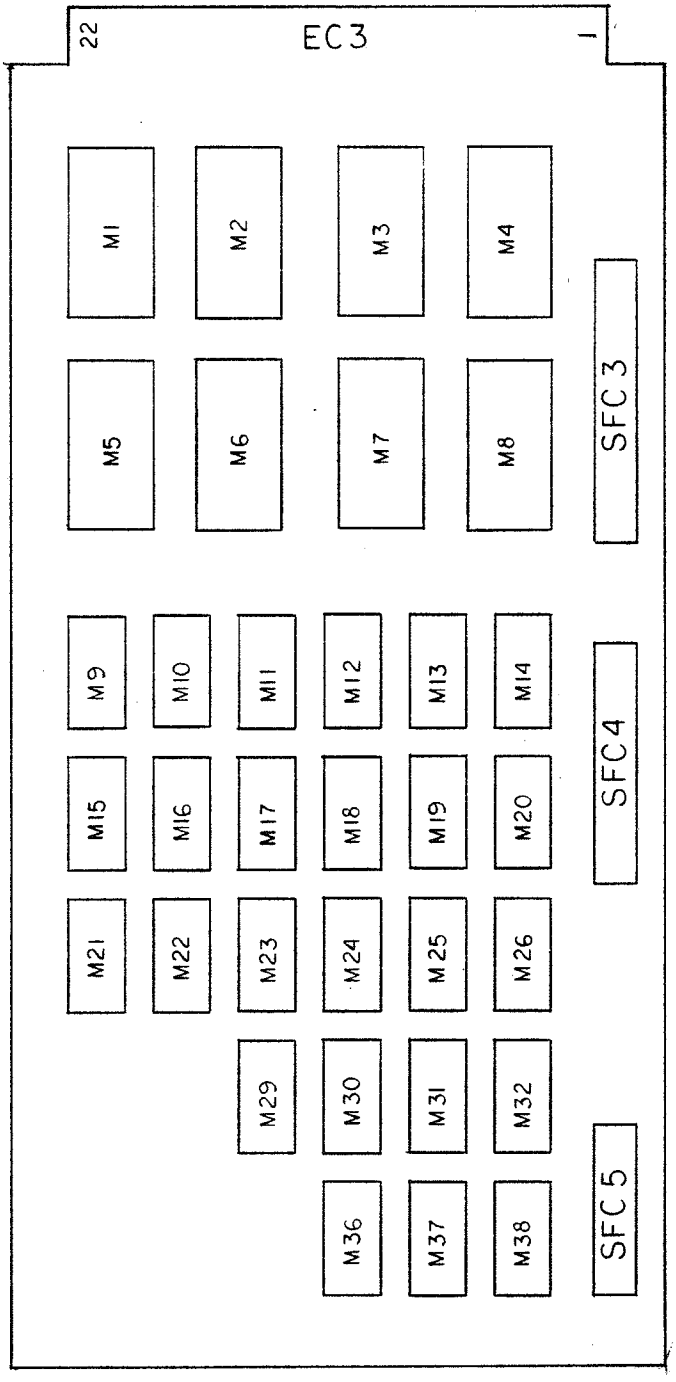

Figure 47. Component layout for the display circuit board. (Refer to Tables 8-10 for IC identification, SFC4 pinout, and EC3 pinout.)

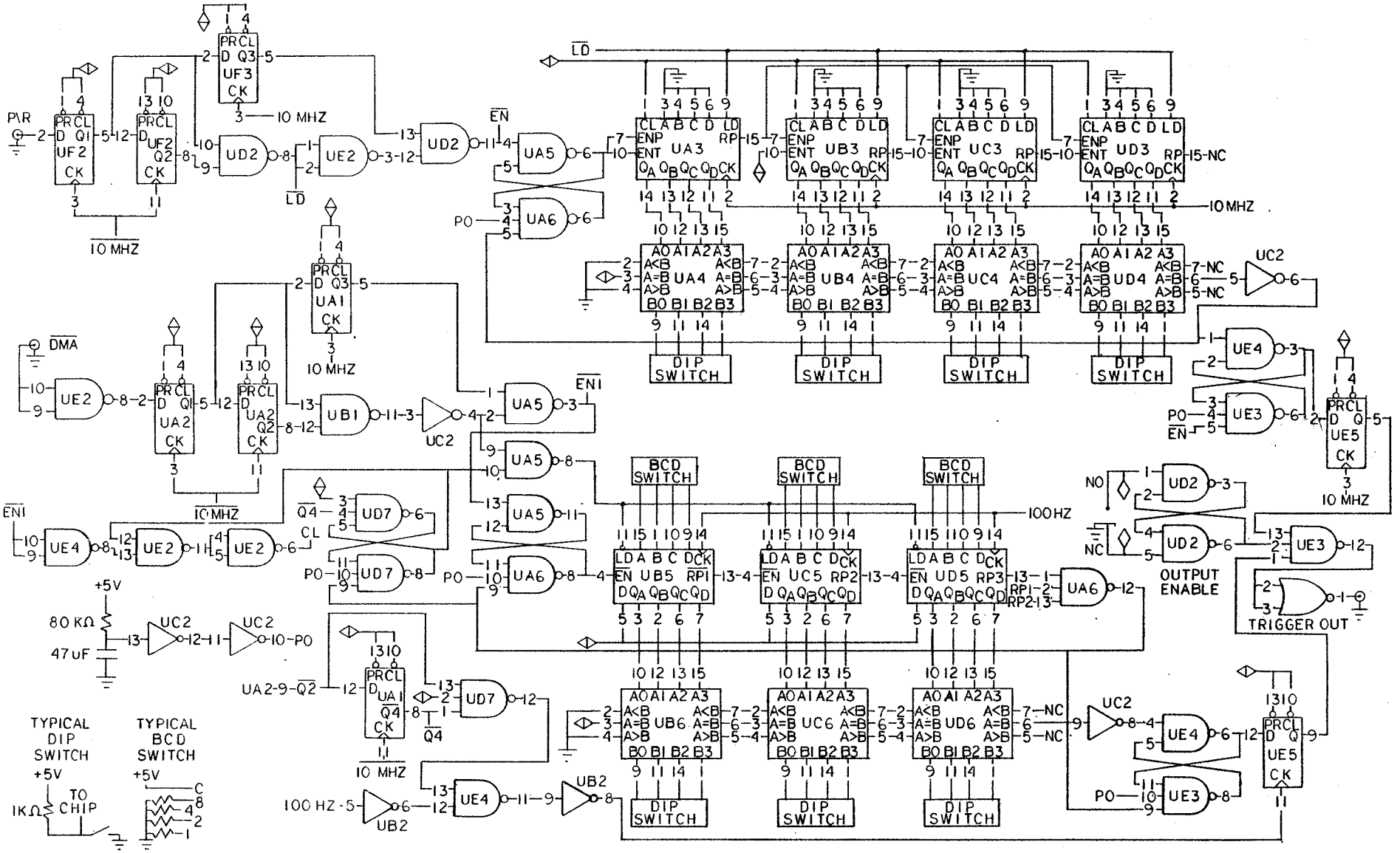

Figure 48. The 280 DAS RF controller circuit schematic.

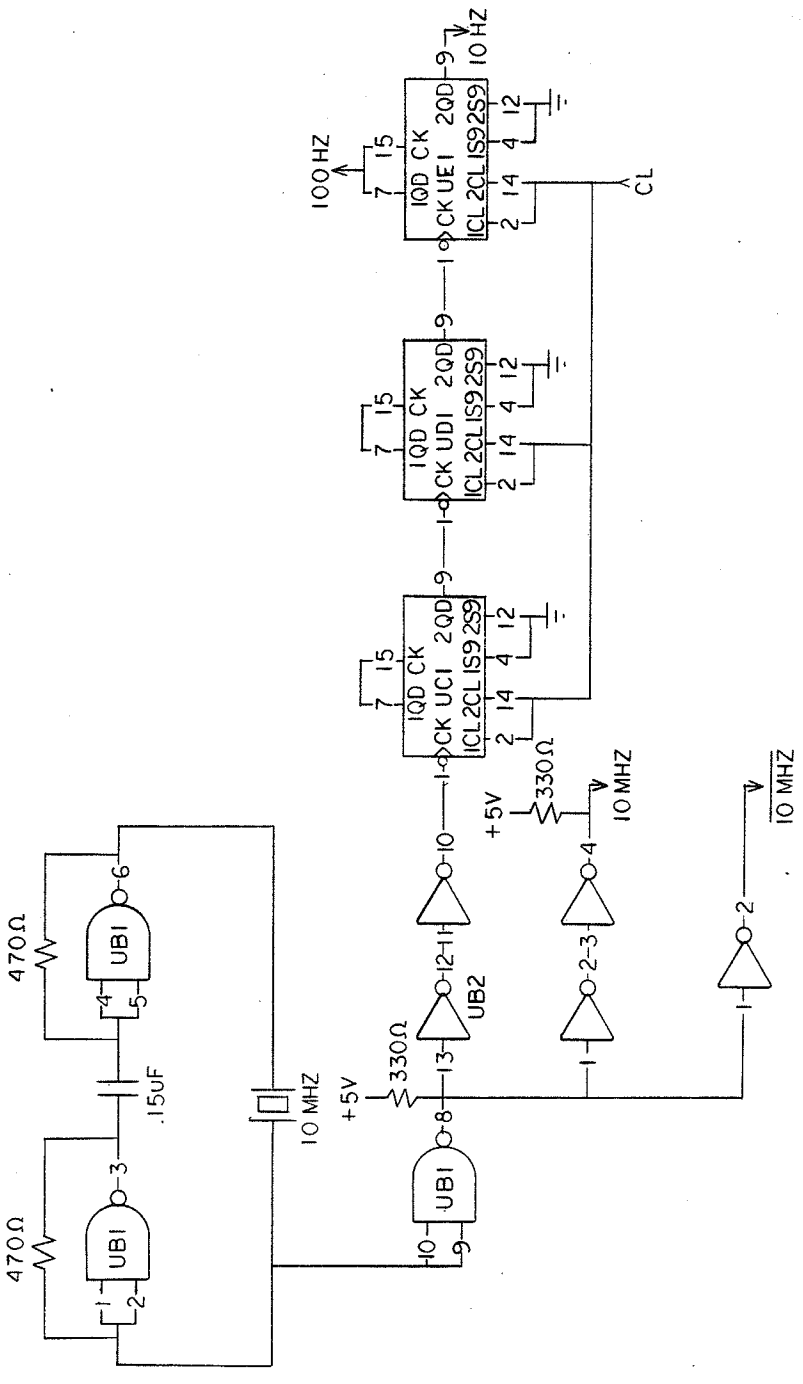

Figure 49. Clock circuit for the 280 DAS RF controller.

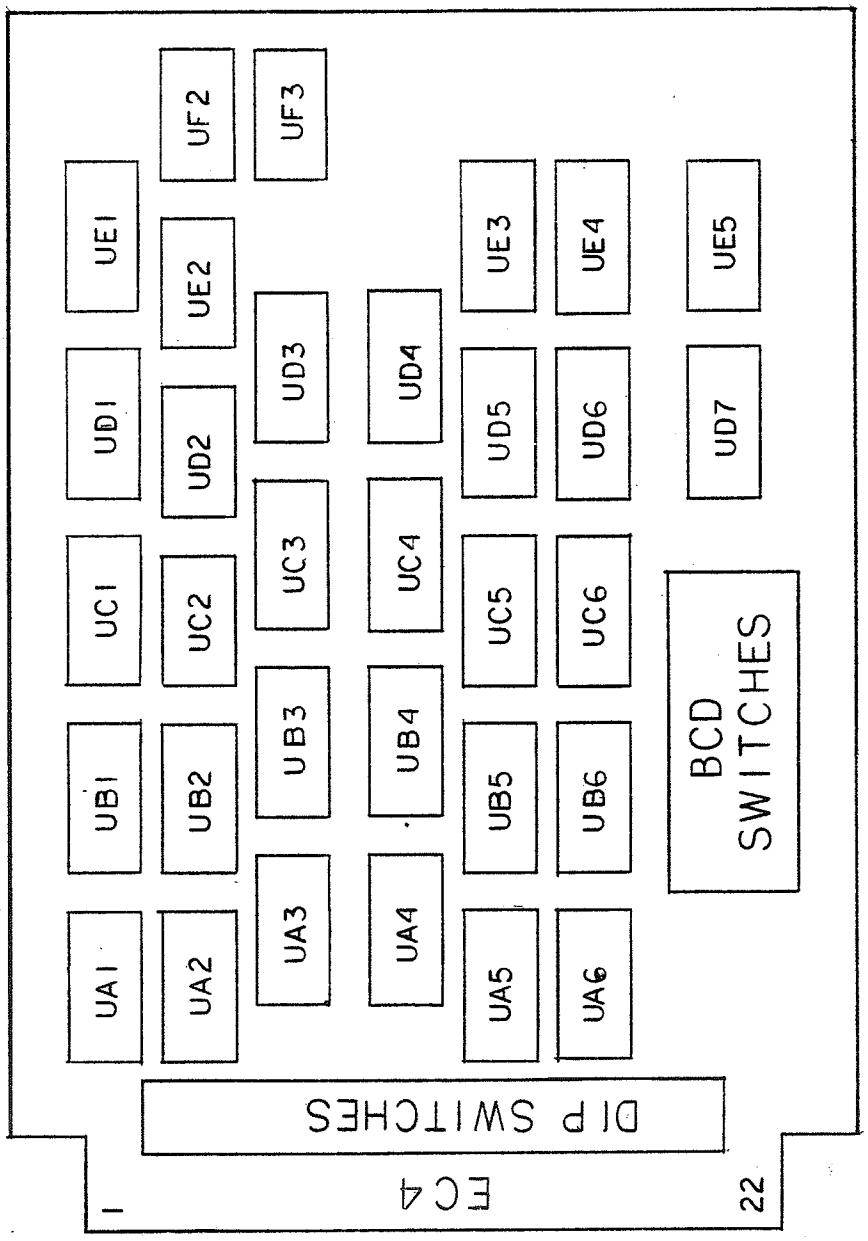

Figure 50. Component layout for the 280 DAS RF controller circuit board. (Refer to Table 11 for IC identification and Table 12 for EC4 pinout.)

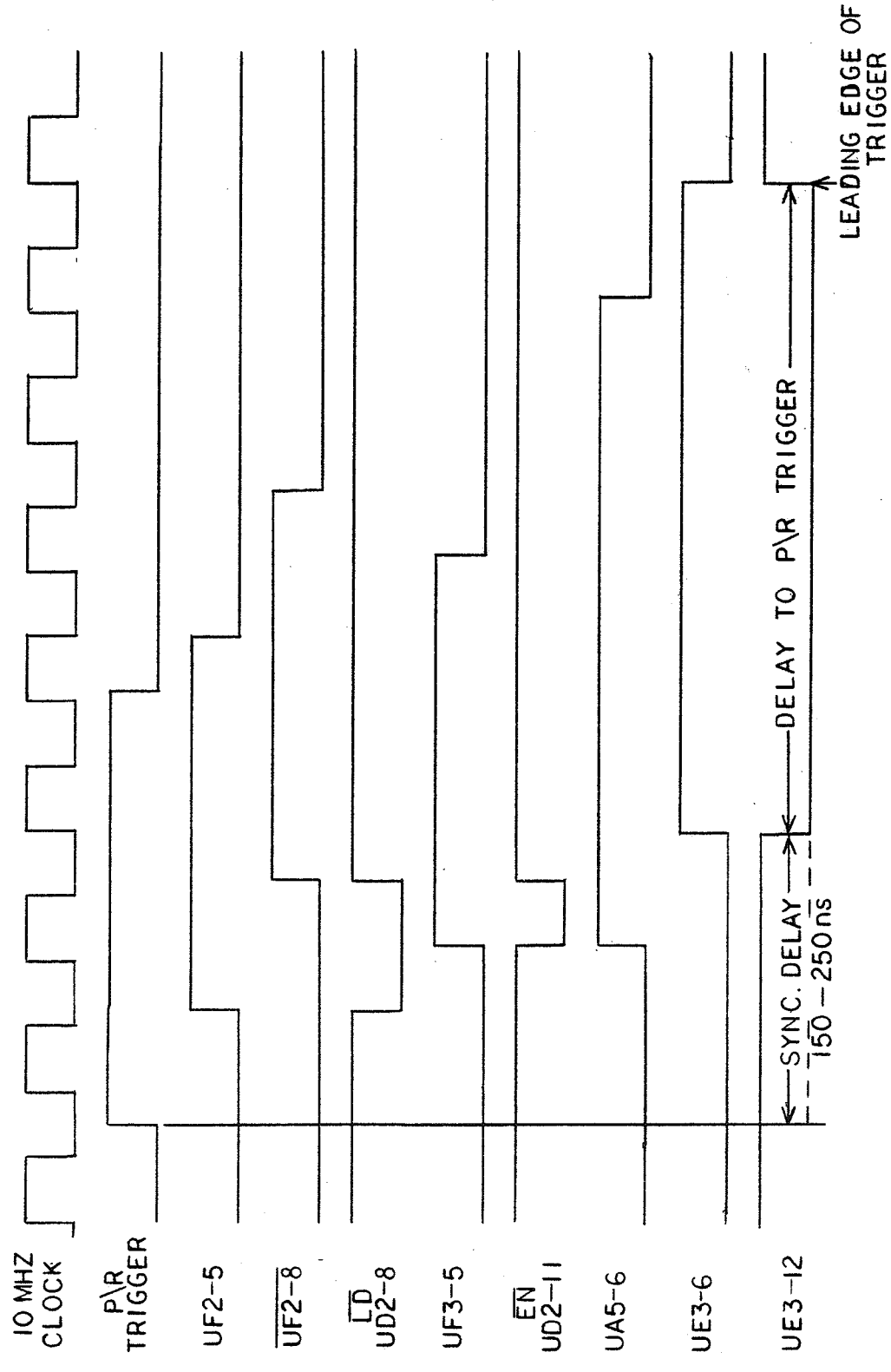

Figure 51. Timing diagram of the hardware generating the trigger signal.

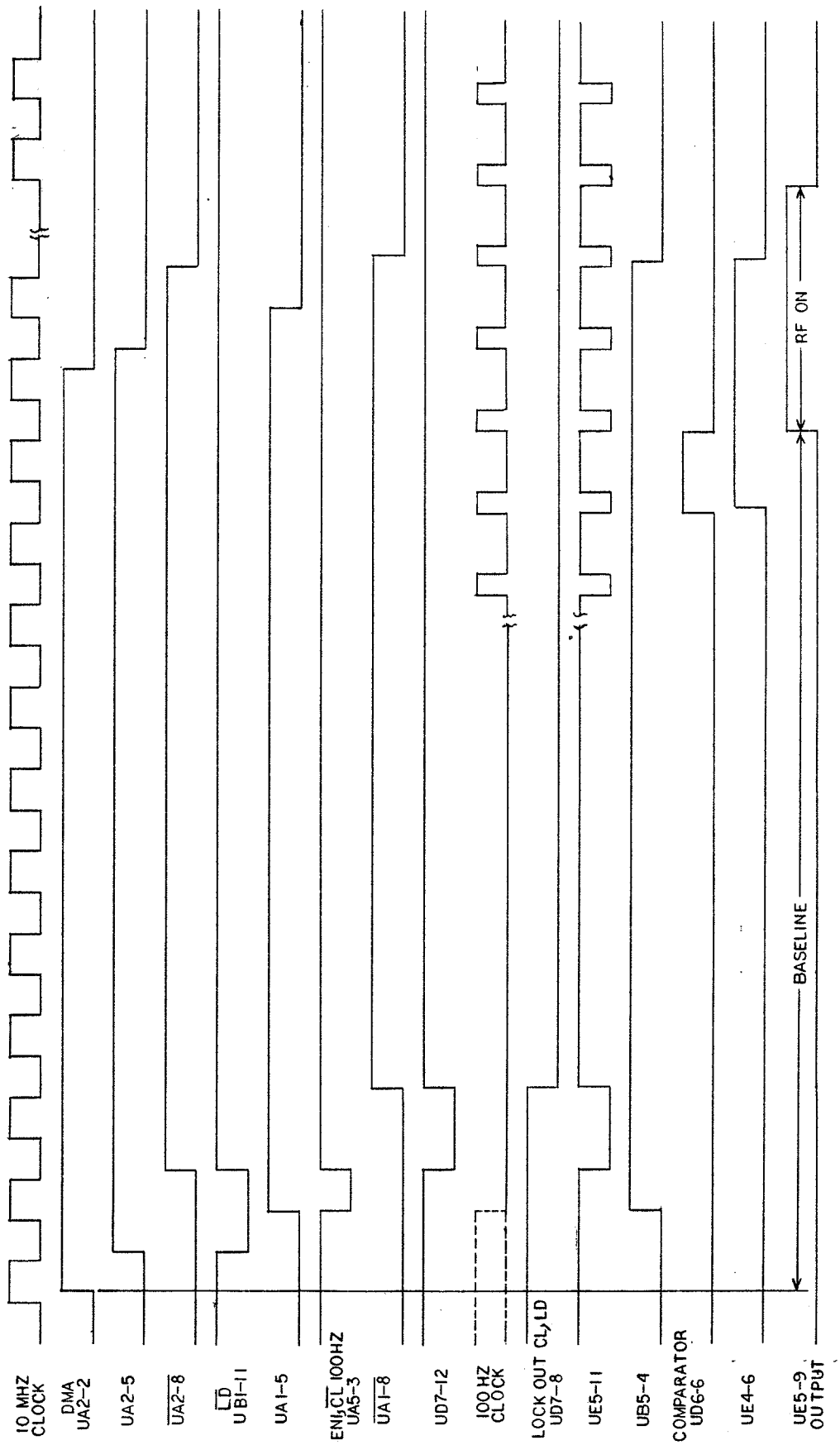

Figure 52. Timing diagram of the hardware generating the output enable signal.

APPENDIX A

SYSTEM CONTROLLER HARDWARE

Each of the three subcircuits: (1) control and timing, (2) data entry, and (3) display and data storage comprising the system controller is discussed. Each subcircuit is implemented on a separate circuit board, and interfaced together via signal busses. Component designation is achieved by prefixing the IC number with a letter identifying the circuit board. The prefixes C, W, and M correspond to the control and timing board, data entry board, and display and data storage board, respectively. To identify a specific output of an IC, the prefixed, IC number is followed by a pin number. For example, C10-7 refers to pin 7 of IC 10, located on the control and timing circuit board. For each subcircuit, the design philosophy and circuit design are explained. The circuit schematic, component layout and pinout for all connectors are included, and timing diagrams are supplied when necessary. Figure 38 illustrates the symbols used throughout the circuit schematics.

A.1 Control and timing subcircuit

To accurately generate the required timing signals with the desired 100 ns resolution, the control and timing circuit operates at 10 MHz. Each timing channel is programmable, allowing selection of any timing duration within the specified 100 ns to 999.9 microsecond range. Cascaded BCD counters implement the timing function for each of the four programmable channels. It can be shown that four cascaded BCD counters are required to

produce the maximum count via the relation

$$T = \sum_{i=1}^{N} \frac{9 \times 10^{(i-1)}}{f}$$

where T is the maximum count in seconds, f is the clock frequency in hertz, and N is the number of cascaded counters. For N=4, the maximum count is

$$T = \sum_{i=1}^{N} \frac{9 \times 10^{(i-1)}}{1 \times 10^{7}} = 999.9 \text{ microseconds}$$

Each of the N-1 counters operates as though its respective clock frequency is one-tenth the frequency of its preceding neighbor.

An appropriate decade counter, the 74LS162 chip, implements a synchronous positive edge triggered up counter when both count enable inputs (P and T) are high. The counter is fully programmable, and outputs may be preset to either level by applying a low level to the load input after presenting the desired data to the data inputs. The outputs will change to agree with the data inputs after the next clock pulse regardless of the levels of the enable inputs. In addition, these counters feature internal carry look ahead circuitry for high speed counting designs when cascading counters for n-bit synchronous operation. The output used to provide the cascading function is the ripple clock. It produces a high level output with a duration approximately equal to the high level portion of the Qa output when an overflow condition exists. The keyboard data entry and storage circuit provide the data to each counter. The schematic of the four counters comprising each 4 stage counter block is shown in Figure 39. Referring to Figure 40, the schematic of the control and timing board, one counter block is used to generate the PULSE GATE signal, and three counter blocks are used to generate the DELAYED GATE signal and the P/R TRIGGER signal. Of these three counter blocks, those designated as D1 and D2 generate

delays, and RG generates the control signal for the range gate RF mixer. Figure 41 illustrates the component layout of the control and timing circuit board. Refer to Tables 1-3 for IC identification, EC1 pinout, and SFC(3&4) pinout, respectively.

The control logic produces the load and enable signal for each counter block when either the manual pushbutton is activated or an external trigger signal is detected. Since there are two modes of operation, each generating the same control signals, one circuit generates the control signals and an electronic switching network determines which trigger signal is gated to trigger the control circuit. A 74LS14 Schmitt trigger waveshapes the input trigger signal (C4-2) to sharpen its edges. The manual pushbutton and trigger select switch are debounced to eliminate false triggering of the control logic. Since neither of the trigger signals is synchronized to the 10 MHz system clock; the selected trigger signal must be synchronized. A synchronous single shot device generates a negative pulse one period long synchronized to the system clock; the operation of this device is illustrated in Figure 42. This device exploits the propagation delay from input to output of the 74LS74 D-type flipflop to generate the one shot output.

The 10 MHz and 10 MHz* clock signals are generated by a standard oscillator circuit, deriving the timebase from a 10 MHz crystal. To prevent undesired outputs after power up, an LM311 comparator generates a negative level for a short period after power up so that the output signals are set to the correct state.

Figure 43 illustrates the timing of the control signals when a 1.2 microsecond ultrasonic pulse is desired. This example

serves to illustrate the important timing signals and applies to the delayed gate subcircuit where three timing blocks are cascaded together. When the selected trigger signal is detected at C13-2, the synchronous single shot device generates the LOAD* signal (C7-11) and an NAND gate generates the ENABLE* signal (C19-12). The trigger signal must be at least 100 ns long to guarantee that the synchronous single shot device detects the input trigger. The delay from the leading edge of the trigger pulse to an output is greater than 150 ns but less than 250 ns. The leading edge of the negative enable pulse sets a latch (C19-6) enabling the first stage of the PG block of counters on the next positive clock edge. The ENABLE* pulse is fed foward setting a latch controlling the input to a synchronizing flipflop (C38-6). The same clock edge that initiates operation of the counters clocks the flipflop, generating the initial edge of the PULSE GATE signal (C44-5). Assuming the correct data are present at each counter's data inputs, the LOAD* signal will result in a synchronous preset of each counter. Since the first counter is loaded with 7 for reasons to be discussed later, an overflow state occurs after two clock transitions. When enable T, Qa and Qd are all high, a RIPPLE CARRY (RP1) is generated. Since enable T of the second stage is always high, and enable P is high for the duration of the ripple clock, the second counter senses a high enable P because of the 17-25 ns propagation delay of the ripple clock relative to the system clock. The second counter which was loaded with eight, thus enabled, counts to nine creating an overflow condition. A RIPPLE CLOCK (RP2) is generated by the second counter, but since the last two stages are loaded with 9, an overflow condition

immediately exists for the last two counters and a RIPPLE CLOCK (RP4) is generated by the last stage. A NAND gate decodes the status of the ripple clock signal from each counter, creating a short pulse when all the counters overflow. This pulse (C32-6) resets the latch controlling the enable signal of the first counter, disabling the rest of the counters, and resets the latch controlling the input to the synchronizing flipflop. This causes the PG output to change to the low state after the next positive clock edge. The TTL and TTL* output signals synchronized by the flipflop are buffered to drive RG58U coax cable using a 74128 line driver chip.

The buffered TTL DG output and TTL* DG output are synchronized to the system clock by a flipflop. The P/R TRIGGER pulse is generated after delay 1 by a 74LS163 binary version of the previously discussed counter. The counter can be preset to generate a minimum trigger pulse length of 100 ns and a maximum pulse length of 1600 ns, depending on the external trigger requirements of the ultrasonic pulser. A SYNC pulse is provided for monitoring the output signals on an oscilloscope. A 74LS163 counter preset to the desired pulse length generates the output pulse. The oscilloscope is positive edge triggered so that the oscilloscope initiates its sweep at the same time that the pulse gate and delayed gate signals are initiated.

A. 2 Data entry subcircuit

Each of the four counter blocks, PG, D1, D2, and DG is programmed via a keyboard. The keyboard data entry circuit decodes the keyboard entry and stores the data in the designated

set of storage devices. Each counter block has an associated set of storage latches, to store the binary data entered with the keyboard. The schematic of the data entry circuit is shown in Figure 44. Figure 45 shows the component layout of the data entry circuit board. Refer to Tables 4-6 for IC identification, SFC 2 pinout, and EC2 pinout, respectively.

The keyboard, a 4X4 tactile membrane switch, has contact bounce characteristics of less than 5 ms and generates a matrix encoded output. A CMOS 16-key decoder (MM74C922) provides the necessary logic to fully decode the keyboard and generate TTL compatible outputs. The keyboard scan and internal debounce circuit are implemented using external capacitors. The debounce period as implemented by the external capacitor is approximately 10 ms, meeting the 5 ms minimum debounce period required by the keyboard. The DATA AVAILABLE (DA) signal goes to a high level when a valid keyboard entry has been made after a debounce period. A two key rollover is provided between every two switches. The TRI-STATE outputs provide for bus operation and are LPTTL compatible. Storage of the programmed data are accomplished using 8 bit latches. Each counter block incorporates two 74116 devices within the storage block. This device provides two independent 4-bit latches in a single package with dual gated enable inputs, simplifying register inplementations.

The four data outputs of the decoder are TRI-STATE buffered to increase the driving capability of the device. Since the 74LS162 counter counts up, the decoded keyboard data are modified before storage in the latches. For example, if zero counts are desired, a nine is loaded into each counter so that the ripple

clock is generated immediately. If 999.9 counts are desired, a zero is loaded into each counter. The modified count is generated via the Boolean expression

MODIFIED COUNT = DECODED DATA * +10

The complement of the decoded data are generated by inverters and the sum is generated by a full adder (74LS83) device. Since each storage latch contains 8 bits, two 4-bit intermediate storage devices store the programmed data until a full byte of data are entered. The two storage devices each utilize 4 bits of an 8 bit TRI-STATE flipflop, because separate clocks are necessary to latch each nibble of data. The equivalent 8-bit storage device is connected in parallel to each of the eight 8-bit storage devices. The control circuit enables the appropriate latch storing the data contained in the intermediate storage devices.

A synchronous control circuit operating at 1 kHz generates the control pulses synchronizing the various stages of data processing. Of the 16 keyboard keys, 10 are designated as numerical keys representing 0-9, and four keys are designated as control keys. The remaining two keys are not decoded and can be used to expand the control operations of the circuit. Each of the four control keys, labeled A-D, respectively, set up the required signals so that only the desired set of latches can accept the data. Control keys A-D correspond to counter blocks PG, D1, D2, and DG, respectively. When a control key is depressed, one of four LED's is activated, confirming detection of the control key. A delay line constructed using four D type flipflops generates sequential copies of the DA signal, each delayed by 1 ms. A dual 2-4 line decoder (74LS156) generates the strobe signal for each

latch, only activating one 8-bit latch at a time. Each decoder operates independently, controlling four 8-bit latches. The decoder control logic determines which latch is enabled when a counter block is programmed. The outputs of the first decoder (1Y0-1Y3) selectively enable each latch storing the data for the PG and D1 counter blocks. This decoder is activated when control keys A or B are used. The other decoder (2Y0-2Y3) controls the latches associated with the D2 and DG counter blocks and are activated when control keys C or D are used. Each enabled latch accepts one byte of data, two decoded numeric keyboard entries. The data decoded as four nibbles of data are converted to two byte long data words by the intermediate storage device. Since the byte of programmed data are available at each latch's input, the decoders determine which latch is enabled to accept the data. A counter and flipflop generate the select signal for the decoder, generating a specific 2-bit code during the sequence of data storage. The control signals 1G, 2G, B, and A determine which set of latches and which of the two latches comprising each set is enabled; 1G and its complement 2G are the decoder's enable signals, always enabling only one decoder. Select input B is preset to a level depending on the counter block selected, and select input A determines which of the two latches is enabled. The 74LS190 counter generating select input B is preset to 0011 when a control key is detected and increments each time a numeric data entry is made. Output Qa of the counter toggles each time a data entry is made, clocking the intermediate storage latch storing a nibble of data. When the first numeric data entry is detected, the data are stored in the intermediate storage device

(W11) and later latched into the 8-bit latch. The second nibble of data is stored in W12 and later latched into the other half of the 8-bit latch. The same operations occur when the third and fourth entries are made, but the second latch is activated, storing the second byte of data.

When the system controller is operated under microprocessor control, the BCD data for the PG channel is uploaded from the microprocessor. The system controller is interfaced to the microprocessor via a 40 conductor bus. The signals communicating between the two devices are identified in Table 7.

A.3 Display subcircuit

A digital multiplexed display provides visual verification of the data programmed into each block of counters. The schematic for the display circuit is shown in Figure 46. Figure 47 shows the component layout of the display circuit board. Refer to Tables 8-10 for IC identification, SFC5 pinout and EC3 pinout, respectively.

To display the data programmed into each of the four channels simultaneously, a direct inplementation would utilize one decoder and display element for each counter. Implementation of this design would require at least 32 chips, disregarding the resistor packages necessary to currently limit the common anode display devices. This circuit would draw a considerable amount of power, and in the worst case would draw approximately 12.5 W. By displaying only two channels at any one time, the chip count is reduced to approximately 24, the number of decoders and seven segment displays is reduced by half; however, multiplexers are

required to implement the switching function, and they select the data from the desired set of latches.

A more efficient design in terms of power and chip count, implemented in the system controller, utilizes a display multiplexing system where only one decoder is used to drive four seven segment displays. Rather than using one display system for each channel, two multiplexed displays are used where the data for each display are selected from two sources. In this case, the chip count is still approximately 24, but the power requirement is reduced to approximately 1 W. The four bits of data corresponding to each digit of the displayed data are scanned rapidly in sequence. If the scanning rate is faster than the response time of the eye, the display will be flicker free even though it is being scanned. Since each of the two display channels derives its data from two possible sources, a 2-1 multiplexer (74LS157) electronically selects one set of data. A switch driving the select line to the multiplexer selects one set of data to be electronically gated to the second stage of multiplexers. The multiplexing of the data to the decoder is accomplished using 4-1 multiplexers (74LS153). A free running counter generates the two bit code driving the select inputs to the 4-1 multiplexers and the 2-4 demultiplexer. The demultiplexer generates the strobe signal supplying power to the display elements, matching the appropriate counter and digit of the display. Since common anode displays are utilized as the display element, sufficient current must be supplied by the strobe signal to achieve the desired average intensity. A transistor amplifier circuit, operating in a switching mode, supplies the current pulse. The data stored in

the latches were modified to produce the correct counting sequence for an up counter. Therefore, the reverse transformation must be applied to the stored data before being displayed. A full adder and inverters are used to generate the modified data, implementing the reverse transformation

$$BINARY^* = DATA + 6$$

APPENDIX B

Z80 DATA ACQUISITION SYSTEM RF CONTROLLER HARDWARE

The Z80 DAS RF controller digital circuit generates the required external trigger signal for the system controller. The schematic of the RF controller circuit is shown in Figure 48, and the schematic for the clock circuit which generates the required clock signal is shown in Figure 49. Figure 50 illustrates the component layout of the RF controller circuit board. Refer to Tables 11 and 12 for IC identification and EC4 pinout, respectively. This circuit has two inputs, P/R TRIGGER and DMA*, and generates one output signal buffered to drive 50 ohm coax cable. The OUTPUT ENABLE signal and TRIGGER signal discussed below are mixed to generate the external trigger signal for the system controller.

The TRIGGER signal is generated by four stages of cascaded 74LS162 BCD counters. Since the maximum period between P/R triggers is 1.31 ms, four stages of counters are used to generate a maximum delay of 999.9 us at the 10 MHz operating frequency. The counters are cascaded for carry look ahead operation for the high speed application. After a P/R trigger is detected, the counters are parallel loaded with zeros and enabled to count. The four outputs of each counter drive the data inputs to one of four cascaded high speed comparators (74LS85). The other set of data inputs to each of the four comparators is programmed by dipswitches. The desired delay is specified using the dipswitches; when the counter counts up to the programmed value, the comparators sense a match and the TRIGGER signal changes

state, triggering the system controller. To guarantee that an ultrasonic pulse is generated, the external trigger signal for the system controller must be longer than 100 ns. This is guaranteed because the TRIGGER signal does not reset until the next P/R TRIGGER signal is detected.

The OUTPUT ENABLE signal, which controls the baseline and ultrasonic exposure periods of the experiment, is controlled by another set of counters. In this case, the counters are operated at a much lower clock frequency because the experiment duration varies between 0.01 s and 1.0 s. A three stage programmable down counter, operating at 100 Hz, in conjunction with three comparators (74LS85), generates the OUTPUT ENABLE signal. By driving one input of a NAND gate with the OUTPUT ENABLE signal, the second input (TRIGGER) to the gate is selectively gated to the output of the device. In this way, the TRIGGER signal is enabled to trigger the system controller whenever the OUTPUT ENABLE signal is high. For the duration of the baseline exposure, the OUTPUT ENABLE signal is low, but during the ultrasonic exposure portion of the experiment, the signal is high. When continuous ultrasonic exposures are desired, the OUTPUT ENABLE signal directly drives the control input to the RF mixer. When the first DMA* signal is detected, indicating initiation of data acquisition, the counters are loaded and enabled. The counters are loaded with data programmed by three BCD thumbwheel switches set to the sum of the baseline and ultrasonic exposures. The length of the ultrasonic exposure is provided to the three cascaded comparators by dipswitches. The baseline must be less than the experiment duration for proper operation. From the time that the counters

are first enabled until the baseline count is detected, a low signal is generated. After the comparators detect a match, this signal changes to the high state and remains in this state until the counters all underflow. When the counter reaches the underflow state, the counters are disabled until the next DMA* signal is detected.

The timing of the internal control signals generating the TRIGGER signal is now discussed. Figure 51 shows a timing diagram illustrating the relation among the control signals. The 10 MHz clock driving the control logic and 74LS162 counters is derived from an oscillator circuit driven by a 10 MHz crystal oscillator. The P/R TRIGGER signal, a 320 ns pulse is synchronized to the system clock by a synchronous single shot device. The LD* signal, the output of a NAND gate (UD2-8), parallel loads each set of counters with zeros every time P/R TRIGGER is detected. The EN* signal, (UD2-11) approximately 50 ns wide, sets a latch generating the enable signals for the first stage of the counters and sets the TRIGGER signal to a low state. When the comparators detect a match between the current count and the desired count, the latch is reset, changing the TRIGGER signal to a high level. The output of the synchronizing flipflop (UE5-5) remains in a low state from P/R TRIGGER detection until the comparators detect a match; then the output switches to a high state until the next P/R TRIGGER is detected. The transition of the TRIGGER signal from low to high triggers the system controller. The delay between detection of the positive edge of the P/R TRIGGER pulse and a state transition at the output of the synchronizing flipflop has an approximate minimum value of 150 ns and a maximum value of 250 ns. The delay

from P/R TRIGGER detection to output transition must be less than the P/R TRIGGER period for proper circuit operation. The TRIGGER signal is generated every time a P/R TRIGGER is detected.

The OUTPUT ENABLE signal, gating the TRIGGER signal, is generated by three 74LS190 BCD counters operating at 100 Hz; the outputs of each counter generate the data inputs to a comparator. The timing diagram shown in Figure 52 illustrates the operation of the circuit.

The 100 Hz clock driving the 74LS190 counters is generated by three dual divide by 10, 74LS490 decade counters. A 10 Hz clock is available, thereby allowing a 0.1 s to 10.0 s range in the experiment duration. To synchronize the clocks driving the two sets of counters, a CLEAR* signal is generated which clears the 74LS490 counters achieving synchronization of the two clocks to within 100 ns. The synchronizing and control circuit generates the LD* and EN* signals for the counters. The DMA* signal triggering this set of counters has a variable length equal to the width of the range gate. Therefore, the control logic must trigger off the positive edge of the DMA signal so that the control signals are independent of the length of the gate. Even though the counters operate at 100 Hz, the control circuitry operates at 10 MHz to guarantee that both sets of counters are triggered within 100 ns of each other. The LD* signal parallel loads the counters with the data programmed by the BCD thumbwheel switches. The EN* signal sets a latch controlling the enable of the first stage of counters; the counters count down from the preset value until the underflow condition is achieved. When the underflow is detected, a 100 ms negative pulse is generated

(UA6-12) which resets the output to a low state and disables the counters. Since these counters are triggered by the DMA* signal, which occurs each time an echo is taken, the first detection of the signal enables the counters; all subsequent DMA* signals must have no effect on the circuit. The LD* and CL* signal must be locked out after the 74LS490 counters are cleared and the 74LS190 counters are loaded after the first trigger signal. Since a latch is used to control the enable to the counters, only the first DMA* signal affects the output of the latch, until the reset signal is detected. Selective control over the LD* and CL* signals is achieved by gating each signal with a NAND gate, where the second input to each gate determines when the respective signal is allowed to propagate. The 10 MHz synchronizing flipflop is updated approximately 10 us after the 10 MHz counters are enabled. Since the 100 Hz synchronizing flipflop is updated approximately 0.01 s later, the OUTPUT ENABLE signal is delayed by 0.01 s relative to the first DMA signal. To eliminate this problem, and provide control logic for the lockout circuit, an artificial clock edge is generated. A flipflop generates a copy of UA2-9 delayed by 100 ns; the NAND of this signal and the original signal generates a 100 ns pulse. The negative edge of the inverted and delayed signal sets a latch, the output of which (UD7-8) controls the enable input to the two NAND gates which, respectively, generate the CL* and LD* lockout signal. After the latch is set, the CL* and LD* signals are locked out until the counters have reset. The positive edge of the negative pulse provides the artificial clock edge necessary to set the output of the synchronizing flipflop (UE5-9). If the experiment duration is

longer than the ultrasonic exposure duration, the output of the synchronizing flipflop remains in a low state until the baseline ends. Then the output changes state and remains high for the duration of the ultrasonic exposure. This signal drives the input to a NAND gate, allowing the TRIGGER signal generated by the 10 MHz counters to be gated to the output when the OUTPUT ENABLE signal is high. The Trigger signals are gated to the system controller only during the ultrasonic exposure duration.

APPENDIX C

NEO PROGRAM

```
C     PROGRAM NEO USES THE TRW A/D TO COLLECT ANALOG DATA
C     WITHIN A SPECIFIED RANGE GATE.  THE DATA CORRESPONDING
C     TO ECHOS RECIEVED AFTER THE MAIN BANG PULSE ARE
C     DIGITIZED AND STORED IN FILES SCRT:01-05, FOR FURTHER
C     PROCESSING.  THE PARAMETERS ARE STORED IN FILE SCRT:PARAM.
C
      INTEGER*2 VIDEO(8192),NUM,POINT,IDUM
      INTEGER*4 LU
      REAL INTEN,ENERGY,RDUM,RDUM1,RF1,RF2
      NUM=1
      LU=6
 100  CONTINUE
      WRITE(1,190)NUM
 190  FORMAT(1X,'SHOT NUMBER:',I1,' (MAX OF 5 SHOTS)')
      WRITE(1,200)
 200  FORMAT(1X,' 1) TAKE ANOTHER SHOT WITH THE SAME PARAMETERS'
     1/1X,' 2) TAKE A SHOT WITH NEW PARAMETERS'
     2/1X,' 3) TERMINATE PROGRAM')
      WRITE(1,210)
 210  FORMAT(1X,'WHICH FUNCTION?')
      READ(1,90)IDUM
      IF(IDUM .EQ. 1)GOTO 300
      IF(IDUM .EQ. 2)GOTO 400
      IF(IDUM .EQ. 3)GOTO 500
 90   FORMAT(I1)
 400  CONTINUE
C
C     ENTER INTENSITY, ENERGY, RANGE AND WIDTH PARAMETERS
C
      WRITE(1,110)
 110  FORMAT(1X,'FOR EACH OF THE FOLLOWING PARAMETERS,'
     1/1X,'ENTER THE NEW VALUE OR <CARRAGE RETURN>'
     2/1X,'TO KEEP OLD VALUE')
      WRITE(1,120)INTEN
 120  FORMAT(1X,'INTENSITY:',F6.2,'  WATTS/(CM)**2')
      READ(1,130)RDUM
 130  FORMAT(F10.5)
      IF(RDUM .EQ. 0.0)GOTO140
      INTEN=RDUM
 140  WRITE(1,150)ENERGY
 150  FORMAT(1X,'ENERGY:',F3.1,'  MICROVOLTS')
      READ(1,130)RDUM
      IF(RDUM .EQ. 0.0)GOTO160
      ENERGY=RDUM
 160  CONTINUE
C
C     ENTER PARAMETERS OF RANGE GATE AND MODIFY PARAMETERS. TO
C     CONTINUE, ENTER A NUMBER LARGER THAN 100 FOR THE RANGE AND
C     WIDTH INCREMENT
C
      WRITE(1,2000)RANGE,WIDTH
```

```
 2000 FORMAT(1X,'CURRENT RANGE (uS):',F6.2,'CURRENT WIDTH (uS):'
     /     ,F6.2)
      READ(1,2010)RDUM.RDUM1
 2010 FORMAT(F16.8)
      IF (RDUM .EQ. 0.0)GOTO 2020
      RANGE=RDUM
 2020 IF (RDUM1 .EQ. 0.0)GOTO 2030
      WIDTH=RDUM1
 2030 CONTINUE
C
C     NUMBER OF SAMPLES TAKEN WITHIN THE RF GATE
C
      IWIDTH=IFIX(50.05*WIDTH+0.5)
      IF(MOD(IWIDTH,2).EQ.1) IWIDTH=IWIDTH+1
 3    CONTINUE
      IRANGE=IFIX(25.025*RANGE+0.5)
C
C     GENERATE CURSOR SIGNAL (RANGE GATE)
C
      CALL CURSOR(IRANGE,IWIDTH)
      WRITE(1,4)RANGE
 4    FORMAT('PRESENT RANGE = ',F6.2,3X,'ENTER RANGE INCREMENT')
      READ(1,2)T
  2   FORMAT(F16.8)
      IF(ABS(T).GT.100.0) GOTO 5
      IF(T.NE.0.0) DR=T
      RANGE=RANGE+DR
      GOTO 3
 5     CONTINUE
      WRITE(1,6)WIDTH
 6     FORMAT('PRESENT WIDTH = ',F6.2,3X,'ENTER WIDTH INCREMENT')
      READ(1,2)T
      IF(ABS(T).GT.100.0) GOTO 7
      IF(T.NE.0.0) DW=T
      WIDTH=WIDTH+DW
      IWIDTH=IFIX(50.05*WIDTH+0.5)
      IF(MOD(IWIDTH,2).EQ.1) IWIDTH=IWIDTH+1
      CALL CURSOR(IRANGE,IWIDTH)
      GOTO 5
 7    CONTINUE
 12   CONTINUE
C
C     ENTER DURATION OF BASELINE AND EXPERIMENT
C
      WRITE(1,8)
8     FORMAT('ENTER DURATION OF BASELINE (SECONDS)')
      READ(1,2)RF1
      WRITE(1,9)
9     FORMAT('ENTER DURATION OF EXPERIMENT (SECONDS)')
      READ(1,2)RF2
C
C     NUMBER OF ECHO FRAMES DIGITIZED
C
      NECHOS=IFIX(8192.0/FLOAT(IWIDTH))
      ISYNC=IFIX(5.005E+06*RF2/FLOAT(NECHOS-1)+0.5)
```

```
      IF(ISYNC.LT.8388607) GOTO 13
      WRITE(1,14)
 14   FORMAT('LENGTH OF SHOT TOO LONG, TRY AGAIN')
      CALL SYSIO(PBLK,Y'29',1,Y'07070707',2,0)
      GOTO 12
 13   CONTINUE
 300  CONTINUE
      IF(IDUM .EQ. 1)CALL CURSOR(IRANGE,IWIDTH)
C
C     GENERATE CONTROL SIGNAL FOR RF MIXER
C
      CALL RF(142,RF1,RF2)
C
C     ACTIVATE A/D CONVERTOR
C
      CALL ATD3(ISYNC.IRANGE,IWIDTH,NECHOS,VIDEO)
C
C     GENERATE OUTPUT FILES
C
      WRITE(LU,346)RANGE,WIDTH
346   FORMAT(F10.3)
      POINT=IWIDTH*NECHOS
      DO 3456 I=1,POINT
      WRITE(LU,3457)VIDEO(I)
 3457 FORMAT(I3)
 3456 CONTINUE
C
C     STORE DATA FOR PROGRAM PLOT, DATA STORED IN FILE SCRT:05
C
      WRITE(10,102)RANGE,WIDTH
      I2=IFIX(NECHOS*RF1/RF2+1.5)
      I3=I2-4
      DO 1113 I=1,IWIDTH
      NB=(I2-10)*IWIDTH+I
      NC=I3*IWIDTH+I
      ND=(I3+1)*IWIDTH+I
      NE=(I3+2)*IWIDTH+I
      NF=(I3+3)*IWIDTH+I
      NG=(I3+4)*IWIDTH+I
      NH=(NECHOS-10)*IWIDTH+I
      NI=(NECHOS-1)*IWIDTH+1
      WRITE(10,1114)VIDEO(I),VIDEO(NB),VIDEO(NC),VIDEO(ND),
     /              VIDEO(NE),VIDEO(NF),VIDEO(NG),VIDEO(NH),
     /              VIDEO(NI)
 1114 FORMAT(I3,9(3X,I3))
 1113 CONTINUE
      WRITE(2,102)RANGE,WIDTH,ENERGY,INTEN,RF1,RF2
 102  FORMAT(F10.5)
      NUM=NUM+1
      LU=LU+1
      GOTO 100
 500  CONTINUE
      STOP
      END
```

APPENDIX D

ATD3, RF, AND CURSER ASSEMBLY CODE

```
$BATCH
      SUBROUTINE ATD3(PRF,RANGE,WIDTH,BLOCK,VIDEO)
      INTEGER*4 PRF,RANGE,WIDTH,BLOCK,R(16)
      INTEGER*2 VIDEO(1)
      CALL GETDIO
$ASSM
DIOUT    EQU   0
DIOIN    EQU   1
TEMP1    EQU   2
TEMP2    EQU   3
INDEX    EQU   4
REM      EQU   7
BLK      EQU   8
OFF      EQU   9
         STM   0,R
         LHI   DIOUT,X'00A8'
         LHI   DIOIN,X'00A9'
         LHI   TEMP1,X'8000'
         L     TEMP2,RANGE
         S     TEMP1,0(TEMP2)
         EXBR  TEMP2,TEMP1
         NHI   TEMP1,X'00FF'
         OHI   TEMP1,X'E000'
         WHR   DIOUT,TEMP1
         NHI   TEMP2,X'00FF'
         OHI   TEMP2,X'E100'
         WHR   DIOUT,TEMP2
         LHI   TEMP1,X'8001'
         L     TEMP2,WIDTH
         L     TEMP2,0(TEMP2)
         AIS   TEMP2,1
         SRLS  TEMP2,1
         SR    TEMP1,TEMP2
         EXBR  TEMP2,TEMP1
         NHI   TEMP1,X'00FF'
         OHI   TEMP1,X'E200'
         WHR   DIOUT,TEMP1
         NHI   TEMP2,X'00FF'
         OHI   TEMP2,X'E300'
         WHR   DIOUT,TEMP2
         LI    TEMP1,Y'00010000'
         L     BLK,BLOCK
         L     BLK,0(BLK)
         SR    TEMP1,BLK
         EXBR  TEMP2,TEMP1
         NHI   TEMP1,X'00FF'
         OHI   TEMP1,X'E400'
         WHR   DIOUT,TEMP1
         NHI   TEMP2,X'00FF'
         OHI   TEMP2,X'E500'
         WHR   DIOUT,TEMP2
```

```
        LHI   TEMP1,X'E601'
        WHR   DIOUT,TEMP1
        LHI   TEMP1,X'E800'
        WHR   DIOUT,TEMP1
        LI    TEMP1,Y'01000000'
        L     TEMP2,PRF
        S     TEMP1,0(TEMP2)
        EXHR  TEMP2,TEMP1
        NHI   TEMP2,X'00FF'
        OHI   TEMP2,X'EB00'
        WHR   DIOUT,TEMP2
        EXBR  TEMP2,TEMP1
        NHI   TEMP1,X'00FF'
        OHI   TEMP1,X'E900'
        WHR   DIOUT,TEMP1
        NHI   TEMP2,X'00FF'
        OHI   TEMP2,X'EA00'
        WHR   DIOUT,TEMP2
        LHI   TEMP1,X'EC00'
        WHR   DIOUT,TEMP1
        RHR   DIOIN,TEMP1
        LHI   TEMP1,X'E700'
        WHR   DIOUT,TEMP1
BUSY    SSR   DIOIN,TEMP1
        BTBS  8,BUSY
        LHI   TEMP1,X'E801'
        WHR   DIOUT,TEMP1
        LHI   TEMP1,X'EC01'
        WHR   DIOUT,TEMP1
        L     INDEX,VIDEO
        LIS   INDEX+1,4
        LIS   REM,0
        L     INDEX+2,WIDTH
        L     INDEX+2,0(INDEX+2)
        SRLS  INDEX+2,1
        BNCS  JUMP1
        LIS   REM,1
JUMP1   SLLS  INDEX+2,2
        LR    OFF,INDEX+2
        SIS   INDEX+2,4
        AR    INDEX+2,INDEX
LOOP    RHR   DIOIN,TEMP1
        EXBR  TEMP2,TEMP1
        NHI   TEMP2,X'00FF'
        STH   TEMP2,0(INDEX)
        NHI   TEMP1,X'00FF'
        STH   TEMP1,2(INDEX)
        BXLE  INDEX,LOOP
        LR    REM,REM
        BZS   JUMP3
        RHR   DIOIN,TEMP1
        EXBR  TEMP1,TEMP1
        NHI   TEMP1,X'00FF'
        STH   TEMP1,0(INDEX)
        AIS   INDEX,2
```

```
          AIS    INDEX+2,2
JUMP3     AR     INDEX+2,OFF
          SIS    BLK,1
          BNZ    LOOP
          LM     0,R
$FORT
      CALL DIODUN
      RETURN
      END



      SUBROUTINE RF(RM,RFON,RFOFF)
      INTEGER*4 RM,R(3)
      N=IFIX(4*RFOFF)
      IF(FLOAT(N).EQ.4*RFOFF) N=N-1
      IF(N.LT.0) N=0
      M1=IFIX(32768.0/FLOAT(N+1)*RFON-0.5)
      M2=IFIX(32768.0/FLOAT(N+1)*RFOFF-0.5)
$ASSM
          STM    13,R
          LHI    15,X'00A8'
          LHI    14,X'DA00'
          WHR    15,14
          LHI    14,X'D908'
          WHR    15,14
          L      14,N
          EXBR   13,14
          NHI    14,X'00FF'
          OHI    14,X'DB00'
          WHR    15,14
          NHI    13,X'00FF'
          OHI    13,X'DC00'
          WHR    15,13
          L      14,M1
          EXBR   13,14
          NHI    14,X'00FF'
          OHI    14,X'D300'
          WHR    15,14
          NHI    13,X'001F'
          OHI    13,X'D400'
          WHR    15,13
          L      14,M2
          EXBR   13,14
          NHI    14,X'00FF'
          OHI    14,X'D500'
          WHR    15,14
          NHI    13,X'001F'
          OHI    13,X'D620'
          WHR    15,13
          L      14,RM
          L      14,0(14)
          CHI    14,224
          BNES   JUMP1
```

```
          LHI   13,X'DF01'
          B     JUMP3
JUMP1     CHI   14,142
          BNES  JUMP2
          LHI   13,X'DF02'
          B     JUMP3
JUMP2     LHI   13,X'DF00'
JUMP3     WHR   15,13
          LHI   14,X'DEFF'
          WHR   15,14
          LHI   14,X'D922'
          WHR   15,14
          STM   13,R
$FORT
      RETURN
      END



      SUBROUTINE CURSOR(RANGE,WIDTH)
      INTEGER*4 RANGE,WIDTH,R(3)
$ASSM
          STM   13,R
          LHI   15,X'00A8'
          LHI   14,X'8000'
          L     13,RANGE
          S     14,0(13)
          EXBR  13,14
          NHI   14,X'00FF'
          OHI   14,X'E000'
          WHR   15,14
          NHI   13,X'00FF'
          OHI   13,X'E100'
          WHR   15,13
          LHI   14,X'8001'
          L     13,WIDTH
          L     13,0(13)
          SRLS  13,1
          SR    14,13
          EXBR  13,14
          NHI   14,X'00FF'
          OHI   14,X'E200'
          WHR   15,14
          NHI   13,X'00FF'
          OHI   13,X'E300'
          WHR   15,13
          LHI   14,X'E400'
          WHR   15,14
          LHI   14,X'E580'
          WHR   15,14
          LHI   14,X'E601'
          WHR   15,14
          LHI   14,X'E900'
          WHR   15,14
```

```
          LHI    14,X'EAF0'
          WHR    15,14
          LHI    14,X'EBFF'
          WHR    15,14
          LHI    14,X'E700'
          WHR    15,14
          LM     13,R
$FORT
      RETURN
      END
$BEND
```

APPENDIX E

DIGFIL PROGRAM

```
C     PROGRAM DIGFIL IMPLEMENTS A DIGITAL FILTER IN THE SEQUENCE
C     DOMAIN USING LINEAR CONVOLUTION.   THE DATA FILE CONTAINING
C     THE COEFFICIENTS IS SCRT:COEFF (LU=2).  THE OUTPUT FILE IS
C     STORED IN SCRT:DIGFIL.DTA (LU=3).  THE DATA IS STORED IN
C     SCRT:02 (LU=4).
C
      REAL RESULT(2000),ANS,COEFF,NUM,RANGE,POINT,WIDTH
      INTEGER*2 LINE,END,X,L,TNUM,TTNUM,DATA(2000)
      INTEGER ISAMP,INUM,OFFSET
      REAL H(55)
C
C     SELECT THE SET OF FILTER COEFFICIENTS
C
      WRITE(1,1)
1     FORMAT('ENTER REAL NUMBER CORRESPONDING TO DESIRED SET '
     /  'OF FILTER COEFFICIENTS (1-5)')
      READ(1,2)ANS
2     FORMAT(F16.8)
      WRITE(1,33)
33    FORMAT('ENTER DC OFFSET OF A/D (I3)')
      READ(1,14)OFFSET
14    FORMAT(I3)
      DO 3 I=1,120
      READ(2,2)COEFF
      IF(COEFF.EQ.ANS)GOTO 25
3     CONTINUE
25    CONTINUE
      READ(2,2)NUM
      X=1
      INUM=NUM
C
C     READ HALF OF SYMMETRIC COEFFICIENTS
C
      DO 5 I=1,INUM
      READ(2,2)COEFF
      H(X)=COEFF
      X=X+1
5     CONTINUE
C
C     CREATE SECOND HALF OF COEFFICIENTS
C
      TNUM=NUM*2-1
      DO 6 I=X,TNUM
      L=TNUM-I+1
      H(I)=H(L)
6     CONTINUE
      DO 7 I=1,TNUM
      WRITE(1,22)H(I)
22    FORMAT(E16.8)
7     CONTINUE
C
```

```
C     READ DATA FROM FILE
C
      READ(4,2)RANGE,WIDTH
      IF(ANS.EQ.1.0)RANGE=RANGE+.34
      IF(ANS.EQ.2.0)RANGE=RANGE+.44
      IF((ANS.EQ.3.0).OR.(ANS.EQ.4.0))RANGE=RANGE+.54
      WRITE(1,26)
26    FORMAT('ENTER REAL NUMBER OF DATA POINTS')
      READ(1,2)SAMP
      ISAMP=SAMP
      DO 9 I=1,ISAMP
      READ(4,10)DATA(I)
10    FORMAT(I3)
9     CONTINUE
      JSAMP=ISAMP-TNUM
C
C     CONVOLUTION OF FILTER COEFFICIENTS AND DATA
C
      DO 11 I=1,JSAMP
      RESULT(I)=0.0
      DO 11 J=1,TNUM
      N=I+J-1
      RESULT(I)=RESULT(I)+H(J)*(DATA(N)-OFFSET)
11    CONTINUE
C
C     GENERATE OUTPUT FILE
C
      WRITE(1,21)
21    FORMAT('ENTER NUMBER OF POINTS TO BE PLOTTED (F16.8)')
      READ(1,2)POINT
      WRITE(3,2)RANGE
      WRITE(3,2)POINT
      DO 13 I=1,JSAMP
      RES=RESULT(I)+OFFSET
      WRITE(3,2)RES
13    CONTINUE
      STOP
      END
```

```
C       FILE SCRT:COEFF CONTAINS THE COEFFICIENTS FOR FOUR
C       DIGITAL HIGHPASS FILTERS
C
C       COEFFICIENTS FOR A 35 TAP DIGITAL HIGHPASS FILTER WITH
C       BANDEDGES AT 2.5/7.5 MHZ.
1.0
18.0
0.0011670382
0.0022733025
0.0014087021
-0.00042468278
-0.0046194638
-0.0083601606
-0.0094631306
-0.0046112661
0.0064628973
0.020877089
0.031456049
0.029491673
0.0079105256
-0.034540296
-0.091458944
-.14962047
-.19319749
0.79064562
C
C      COEFFICIENTS FOR A 45 TAP DIGITAL HIGHPASS FILTER WITH
C      BANDEDGES AT 4.0/6.0 MHZ
C
2.0
23.
-0.0099650732
-0.0051432772
0.00084968389
0.0022157481
0.0092060758
0.0088052572
0.0089592737
0.00057756828
-0.0067073012
-0.016650571
-0.018580881
-0.015405847
-0.0013005553
0.015519770
0.033163506
0.039357802
0.031164683
0.0017017084
-0.043155080
-0.098850435
-.15046187
-.1889004
0.79816604
C
```

```
C       COEFFICIENTS FOR A 55 TAP DIGITAL HIGHPASS FILTER WITH
C       BANDEDGES AT 6.0/8.0 MHZ.
3.0
28.0
0.00081921011
0.0060260495
-0.00030934593
-0.0026744865
-0.0047991165
-0.0034096307
0.0014272046
0.0065896310
0.0076374972
0.0023923620
-0.0064699994
-0.012352578
-0.0093442622
0.0024930704
0.015575802
0.019129744
0.0073819796
-0.014224493
-0.030394115
-0.025598362
0.0033893129
0.040998539
0.058503635
0.030273460
-0.048594168
-.15486548
-.24608637
0.71802075
C
C       COEFFICIENTS FOR A 55 TAP DIGITAL HIGHPASS FILTER WITH
C       BANDEDGES AT 7.0/9.0 MHZ.
C
4.0
28.
-0.000029422376
-0.0060434917
-0.0000881001
0.0031288846
0.0045763015
0.0015567063
-0.0042156640
-0.0072119688
-0.0031743453
0.0055870723
0.010830424
0.0057844232
-0.0070088339
-0.015838237
-0.010004083
0.0083744246
0.023036984
```

0.017005822
-0.0095777529
-0.034474427
-0.029868479
0.10519566
0.057297444
0.060842634
-0.011115663
-.14213185
-.2693567
0.67798822

APPENDIX F

INTERP PROGRAM

```
C     PROGRAM INTERP IMPLEMENTS A LOW PASS DIGITAL FILTER USING
C     THE CONVOLUTION TECHNIQUE.  THE INPUT SAMPLES ARE STORED IN
C     SCRT:DIGFIL.DTA (LU=2). BETWEEN EVERY TWO SAMPLES, FOUR ZERO
C     VALUED SAMPLES ARE INSERTED.  THE FILTERED OUTPUT IS 1:5
C     INTERPOLATED AND STORED IN FILE SCRT:INTERP.DTA (LU=3).
C     THIS PROGRAM IS SET UP FOR THE 7/32 DAS DATA FORMAT
C
C
      REAL H(85),RESULT(1002),NUM(1002),FREQ,SAMP,SAMP1,R1(1002)
      REAL NUM1(202),INT,INT1,DATA1(202)
      REAL POINT,PLOTT,DATA(1000)
      INTEGER*2 U,K
C
C     INITILIZE ARRAY WITH FILTER COEFFICIENTS
C
      DATA(H(I),I=1,43)/-.5307162E-04,-.4418324E-03,-.6479009E-03
     : ,-.8737527E-03,-.87009235E-03,-.54003669E-03,.12197497E-03,
     : .96195331E-03,.16810201E-02,.19233260E-02,.14232084E-02,
     : .15878757E-03,-.15593413E-02,-.31256601E-02,-.38234319E-02,
     : -.31103576E-02,-.90558714E-03,.22515912E-02,.52742115E-02,
     : .68576326E-02,.59837405E-02,.24235130E-02,
     : -.29800894E-02,-.84155321E-02,-.1163468E-01,-.10799120E-01,
     : -.53046013E-02,.36676551E-02,.13244553E-01,.19635294E-01,
     :.19434907E-01,.11055239E-01,-.42335211E-02,-.22105995E-01,
     :-.36036139E-01,-.39066765E-01,-.26010597E-01,.46067520E-02,
     : .49534201E-01,.10113543,.14909011,.18301707,.19526359/
C
C     CREATE OTHER HALF OF FILTER COEFFICIENTS.
C
      DO 1 I=44,85
      L=85-I+1
      H(I)=H(L)
 1    CONTINUE
      DO 2 I=1,85
      H(I)=5*H(I)
      WRITE(1,300)H(I)
 300  FORMAT(E16.8)
 2    CONTINUE
      WRITE(1,200)
 200  FORMAT('ENTER FREQUENCY IN MHZ')
      READ(1,250)FREQ
 250  FORMAT(F6.2)
      READ(2,6)RANGE,POINT
C
C     PAD THE INPUT SAMPLES WITH ZEROS.
C
      WRITE(1,10)
10    FORMAT('ENTER REAL NUMBER OF INPUT POINTS')
      READ(1,250)POINT
      IPOINT=POINT*5
      DO 4 I=1,IPOINT
```

```
      DATA(I)=0
 4    CONTINUE
      DO 5 I=1,IPOINT,5
      READ(2,6)DATA(I)
      DATA(I)=-(DATA(I)-132.0)*3.922
 6    FORMAT(F16.8)
 5    CONTINUE
C
C     CREATE AN ARRAY CONTAINING THE ORIGINAL SAMPLES.
C
      WRITE(1,11)
11    FORMAT('ENTER REAL NUMBER OF PLOTTING POINTS (INTER.)')
      READ(1,250)PLOTT
      IPLOT=PLOTT
      JPLOT=PLOTT/5
      DO 350 I=1,JPLOT
      N=I+(I-1)*4
      DATA1(I)=DATA(N)
 350  CONTINUE
C
C     N POINT CONVOLUTION OF FILTER COEFFICIENTS AND DATA
C     SAMPLES.
C
      DO 7 I=1,IPOINT
      RESULT(I)=0.0
      JPOINT=IPOINT/5+1
      DO 8 J=1,JPOINT
      U=(5*(J-1))+1
      K=I-5*(J-1)
      IF((K.LE.0).OR.(K.GE.86))GOTO 8
      RESULT(I)=RESULT(I)+H(K)*DATA(U)
 8    CONTINUE
 7    CONTINUE
      DO 88 I=1,IPOINT
      WRITE(3,89)RESULT(I)
 89   FORMAT(F16.8)
 88   CONTINUE
      DO 112 I=1,IPLOT
      R1(I)=RESULT(I)
 112  CONTINUE
C
C     CREATE ARRAY CONTAINING SAMPLE NUMBERS FOR PLOTTING.
C
      DO 100 I=1,IPLOT
      NUM(I)=FLOAT(I)
 100  CONTINUE
      DO 450 I=1,JPLOT
      NUM1(I)=FLOAT(I)
 450  CONTINUE
C
C     CREATE PLOT OF ORIGINAL SAMPLES AND FILTERED OUTPUT.
C
      CALL PLOTS(0.0,10)
      CALL PLOT(2.0,2.0,-3)
      SAMP=(1/(FREQ*.02))*4
```

```
 SAMP1=(SAMP*5)
 INT=(JPLOT/SAMP)+1
 INT1=(IPLOT/SAMP1)+1
 NUM(IPLOT+1)=0.0
 NUM(IPLOT+2)=SAMP1
 R1(IPLOT+1)=-500.0
 R1(IPLOT+2)=250.0
 CALL AXIS(0.0,0.0,'SAMPLE NUMBER (INTERPOLATED DATA)'
/,-33,INT1,0.0,0.0,SAMP1)
 CALL AXIS(0.0,0.0,'SIGNAL AMPLITUDE IN MILLIVOLTS',30,4.0,
/   90.0,-500.0,250.0)
 CALL LINE(NUM,R1,IPLOT,1,0,0)
 CALL PLOT(0.0,5.0,-3)
 DATA1(JPLOT+1)=-500.
 DATA1(JPLOT+2)=250.0
 NUM1(JPLOT+1)=0.0
 NUM1(JPLOT+2)=SAMP
 CALL AXIS(0.0,0.0,'SAMPLE NUMBER',-13,INT,0.0,0.0,SAMP)
 CALL AXIS(0.0,0.0,'SIGNAL AMPLITUDE IN MILLIVOLTS',30,4.0,
/   90.0,-500.,250.)
 CALL LINE(NUM1,DATA1,JPLOT,1,0,0)
 CALL PLOT(0.0,0.0,10)
 CALL PLOT(0.0,0.0,11)
 STOP
 END
```

APPENDIX G

PLOT PROGRAM

```
C     FORTRAN PROGRAM PLOT GENERATES A HARD COPY PLOT OF ANY
C     FRAME OR FRAMES OF ECHOS.  THE DESIRED DATA TO BE PLOTTED
C     IS GENERATED BY NEO.FTN AND IS STORED IN FILE SCRT:05.
C     THE OUTPUT FILE CONTAINING THE PLOTTING DATA IS STORED
C     IN A BUFFER FILE.  THE PROGRAM CAN BE MODIFIED TO WRITE
C     TO THE GRAPHICS TERMINAL IN ROOM 224 BY CHANGING THE
C     LOGICAL UNIT IN THE CALL PLOTS ARGUMENT FROM 10 TO -10
C
C
C     VARIABLE DECLARATIONS
C
      REAL NUM(603), DATA(603), RANGE, WIDTH, L
      INTEGER ENUM,IWIDTH,LIM,DATA1(9),OFFSET,SIGN
C
C     ENTER PARAMETERS
C
      WRITE(1,21)
21    FORMAT('ENTER OFFSET OF A/D (I3)')
      READ(1,22)OFFSET
22    FORMAT(I3)
      IF(OFFSET.EQ.128)SIGN=1
      IF(OFFSET.GT.128)SIGN=-1
      READ(9,10)RANGE,WIDTH
 10   FORMAT(F6.2)
      WRITE(1,10)RANGE,WIDTH
      IWIDTH=IFIX(50.05*WIDTH+0.5)
      WRITE(1,13)IWIDTH
 13   FORMAT(I3)
      WRITE(1,1)
 1    FORMAT('ENTER ECHO NUMBER TO BE PLOTTED: (I1)')
      READ (1,2)ENUM
 2    FORMAT(I1)
C
C     READ THE DATA TO BE PLOTTED.
C
      DO 7 I=1,IWIDTH
      READ(9,8)(DATA1(J),J=1,9)
 8    FORMAT(I3,8(3X,I3))
      DATA(I)=DATA1(ENUM)
      WRITE(1,12)DATA(I)
12    FORMAT(F6.2)
      WRITE(1,4)(DATA1(J),J=1,9)
 7    CONTINUE
 4    FORMAT(9(3X,I3))
C
C     CONVERT THE QUANTIZED SAMPLE VALUE TO AN EQUIVALENT VOLTAGE
C
      DO 6 I=1,IWIDTH
      DATA(I)=(DATA(I)-OFFSET)*3.922*SIGN
 6    CONTINUE
 3    CONTINUE
```

```
      DO 5 I=1,IWIDTH
      NUM(I)=RANGE+.02*I
 5    CONTINUE
C
C     SET UP THE PARAMETERS FOR THE PLOTTING SOFTWARE
C
      CALL PLOTS(0.0,10)
      CALL PLOT(2.0,2.0,-3)
      NUM(IWIDTH+1)=RANGE
      NUM(IWIDTH+2)=.4
      DATA(IWIDTH+1)=-500.0
      DATA(IWIDTH+2)=250.0
      L=IWIDTH/20
      IF(MOD(IWIDTH,20).GE.1)L=L+1
      CALL AXIS(0.0,0.0,'RANGE GATE IN MICROSECONDS',-26,
     /   L,0.0,RANGE,.4)
      CALL AXIS(0.0,0.0,'SIGNAL AMPLITUDE IN MILLIVOLTS',30,
     /   4.0,90.0,-500.0,250.0)
      CALL LINE(NUM,DATA,IWIDTH,1,0,0)
      CALL PLOT(0.,0.,10)
      CALL PLOT(0.,0.,11)
      STOP
      END
```

APPENDIX H

ECHO PROGRAM

```
C     PROGRAM ECHO GENERATES PLOTS OF THE ECHO DATA BEFORE AND
C     AFTER DIGITAL FILTERING.  THE DATA IS STORED IN SCRT:02
C     AND THE FILTERED DATA IS STORED IN SCRT:DIGFIL.DTA.
C     THE PROGRAM CAN BE MODIFIED TO WRITE TO THE GRAPHICS
C     TERMINAL IN ROOM 224 BY CHANGING THE LOGICAL UNIT IN
C     THE CALL PLOTS ARGUMENT FROM 10 TO -10
C
C
C     VARIABLE DECLARATIONS
C
      REAL WIDTH, NUM(300), DATA(300), RANGE, L
      REAL NUM1(300),POINT,RANGE1,DATA2(300)
      INTEGER DATA1(300)
C
C     READ PARAMETERS OF ORIGINAL AND FILTERED DATA
C
      READ(9,10)RANGE,POINT
      READ(8,10)RANGE1,WIDTH
 10   FORMAT(F16.8)
C
C     READ THE DATA TO BE PLOTTED.
C
      IPOINT=POINT
      DO 7 I=1,IPOINT
      READ(9,10)DATA(I)
      READ(8,13)DATA1(I)
13    FORMAT(I3)
 7    CONTINUE
C
C     OFFSET THE DATA SO THAT A DATA VALUE OF 0 CORRESPONDS TO
C     50.0 MILLIVOLTS AND 255 CORRESPONDS TO -50.0 MILLIVOLTS
C     THIS IS SET UP FOR THE 7/32 DAS DATA FORMAT
C
      DO 6 I=1,IPOINT
      DATA(I)=-(DATA(I)-132.0)*3.922
      DATA2(I)=-(DATA1(I)-132.0)*3.922
 6    CONTINUE
      DO 5 I=1,IPOINT
      NUM(I)=RANGE+.02*I
      NUM1(I)=RANGE1+.02*I
 5    CONTINUE
C
C     SET UP THE PARAMETERS FOR THE PLOTTING SOFTWARE
C
      CALL PLOTS(0.0,10)
      CALL PLOT(2.0,2.0,-3)
      NUM(IPOINT+1)=RANGE
      NUM(IPOINT+2)=.4
      DATA(IPOINT+1)=-500.0
      DATA(IPOINT+2)=250.0
      L=IPOINT/20
```

```
      IF(MOD(IPOINT,20).GE.1)L=L+1
      CALL AXIS(0.0,0.0,'RANGE GATE IN MICROSECONDS (FILTERED)'
     /    ,-37,L,0.0,RANGE,.4)
      CALL AXIS(0.0,0.0,'SIGNAL AMPLITUDE IN MILLIVOLTS',30,
     /    4.0,90.0,-500.0,250.0)
      CALL LINE(NUM,DATA,IPOINT,1,0,0)
      CALL PLOT(0.0,5.0,-3)
      NUM1(IPOINT+1)=RANGE1
      NUM1(IPOINT+2)=.4
      DATA2(IPOINT+1)=-500.0
      DATA2(IPOINT+2)=250.0
      CALL AXIS(0.0,0.0,'RANGE GATE IN MICROSECONDS',-26,L,0.0,
     /    RANGE1,.4)
      CALL AXIS(0.0,0.0,'SIGNAL AMPLITUDE IN MILLIVOLTS',30,4.0,
     /    90.0,-500.0,250.0)
      CALL LINE(NUM1,DATA2,IPOINT,1,0,0)
      CALL PLOT(0.,0.,10)
      CALL PLOT(0.,0.,11)
      STOP
      END
```

APPENDIX I

ANALYZ PROGRAM

```
C     PROGRAM ANALYZ COMPUTES THE TOTAL RMS DIFFERENCE AND POWER
C     FOR EACH FRAME OF ECHOES.  THE INPUT DATA IS READ FROM FILE
C     SCRT:INTERP.DTA AND THE PARAMETERS OF THE EXPERIMENT ARE
C     READ FROM SCRT:PARAM.  PLOTS OF THE RMS DIFFERENCE AND POWER
C     VERSUS ECHO NUMBER ARE PLOTTED.
C
      INTEGER VIDEO(8192),MEAN(256),POINT
      INTEGER*4 LU
      REAL RMS(256),POW(256),MAX,BLINE,BECHOS,MIN,RECHOS,RWIDTH
      REAL RNCHOS,DIV,L,INTEN,ENERGY,RF1,RF2,RANGE,WIDTH,U(256)
C
C     READ INPUT DATA FROM FILE
C
      WRITE(1,135)
135   FORMAT('ENTER LOGICAL UNIT FOR INPUT FILE (6-10)')
      READ(1,136)LU
136   FORMAT(I1)
C
C     READ DATA PARAMETERS FROM FILE
C
      READ(2,1)RANGE,WIDTH,ENERGY,INTEN,RF1,RF2
1     FORMAT(F16.8)
      IWIDTH=IFIX(50.05*WIDTH+0.5)
      RWIDTH=IWIDTH
      IF(MOD(IWIDTH,2).EQ.1)IWIDTH=IWIDTH+1
      BLINE=RF1
      RFON=RF2-RF1
      NECHOS=IFIX(8192/FLOAT(IWIDTH))
      RNCHOS=NECHOS
C
C     READ DATA FROM FILE SCRT:INTERP.DTA
C
      READ(LU,456)AA,BB
456   FORMAT(F8.2)
      POINT=NECHOS*IWIDTH
      DO 131 I=1,POINT
      READ(LU,132)VIDEO(I)
132   FORMAT(I3)
131   CONTINUE
      DO 20 I=1,IWIDTH
      MEAN(I)=0
20    CONTINUE
      I2=IFIX(NECHOS*RF1/RF2+1.5)
      I3=I2-4
      BECHOS=I3
      RECHOS=NECHOS-I3
C
C     COMPUTE MEAN ECHO
C
      DO 15 I=1,I3
      DO 15 J=1,IWIDTH
```

```
      K=(I-1)*IWIDTH+J
      MEAN(J)=MEAN(J)+VIDEO(K)
15    CONTINUE
      DO 16 I=1,IWIDTH
      MEAN(I)=MEAN(I)/I3
      WRITE(9,1700)MEAN(I)
1700  FORMAT(I3)
16    CONTINUE
C
C     COMPUTE RMS DIFFERENCE AND POWER FOR EACH ECHO FRAME
C
      MAX=0
      DO 17 I=1,NECHOS
      RMS(I)=0.0
      POW(I)=0.0
      DO 18 J=1,IWIDTH
      K=(I-1)*IWIDTH+J
      RMS(I)=RMS(I)+FLOAT2(VIDEO(K)-MEAN(J))**2
      POW(I)=POW(I)+FLOAT2(VIDEO(K)-133)**2
18    CONTINUE
      RMS(I)=SQRT(RMS(I))
      MAX=AMAX1(MAX,RMS(I))
      MAXX=MAX
      POW(I)=POW(I)/FLOAT(IWIDTH)
17    CONTINUE
      MIN=MAX
C
C     SET UP DATA FOR PLOTTING
C
      DO 19 I=1,NECHOS
      U(I)=FLOAT(I)
      MIN=AMIN1(MIN,RMS(I))
      POW(I)=10.0*ALOG10(POW(I)/8192.0)
      IF(POW(I).LT.-40.0) POW(I)=-40.0
19    CONTINUE
      DO 1100 I=1,10
      J=I-1
      P=10**J
      IF((MAX.GE.P).AND.(MAX.LE.P*10))GOTO1101
 1100 CONTINUE
 1101 MAXX=P
      IF(MAX.EQ.0.0)MAX=10.0
      MAG=ALOG10(MAX)
      NUM1=10.0**MAG
      DO 1102 I=1,100
      L=.1*I*NUM1
      IF(L.GE.MAX)GOTO 1103
 1102 CONTINUE
 1103 DIV=L/5
C
C     GENERATE PLOTS OF RMS DIFFERENCE VERSUS ECHO FRAME NUMBER
C     AND POWER VERSUS ECHO FRAME NUMBER
C
      CALL PLOTS(0.0,11)
      CALL PLOT(0.5,0.5,-3)
```

```
      CALL SYMBOL(6.,10.,.1,'INTENSITY:',0.,10)
      CALL WHERE(X,Y,Z)
      CALL NUMBER(X,Y,.1,INTEN,0.,2)
      CALL SYMBOL(6.,9.75,.1,'ENERGY:',0.,7)
      CALL WHERE(X,Y,Z)
      CALL NUMBER(X,Y,.1,ENERGY,0.,-1)
      CALL SYMBOL(6.,9.5,.1,'RANGE:',0.,6)
      CALL WHERE(X,Y,Z)
      CALL NUMBER(X,Y,.1,RANGE,0.,2)
      CALL SYMBOL(6.,9.25,.1,'GATE:',0.,5)
      CALL WHERE(X,Y,Z)
      CALL NUMBER(X,Y,.1,WIDTH,0.,2)
      CALL SYMBOL(6.,9.0,.1,'BASELINE:',0.,9)
      CALL WHERE(X,Y,Z)
      CALL NUMBER(X,Y,.1,BLINE,0.,2)
      CALL SYMBOL(6.,8.75,.1,'RFON:',0.,5)
      CALL WHERE(X,Y,Z)
      CALL NUMBER(X,Y,.1,RFON,0.,2)
      CALL SYMBOL(6.,8.5,.1,'BASELINE ECHOS:',0.,15)
      CALL WHERE(X,Y,Z)
      CALL NUMBER(X,Y,.1,BECHOS,0.,-1)
      CALL SYMBOL(6.,8.25,.1,'RF ECHOS:',0.,9)
      CALL WHERE(X,Y,Z)
      CALL NUMBER(X,Y,.1,RECHOS,0.,-1)
      CALL SYMBOL(6.,8.,.1,'SAMPLES:',0.,8)
      CALL WHERE(X,Y,Z)
      CALL NUMBER(X,Y,.1,RWIDTH,0.,-1)
      CALL SYMBOL(6.,7.75,.1,'MAXIMUM:',0.,8)
      CALL WHERE(X,Y,Z)
      CALL NUMBER(X,Y,.1,MAX,0.,2)
      CALL SYMBOL(6.,7.50,.1,'TOTAL ECHOS:',0.,12)
      CALL WHERE(X,Y,Z)
      CALL NUMBER(X,Y,.1,RNCHOS,0.,-1)
      CALL SYMBOL(6.,7.25,.1,'MINIMUM:',0.,8)
      CALL WHERE(X,Y,Z)
      CALL NUMBER(X,Y,.1,MIN,0.,2)
      CALL PLOT(0.,0.,3)
      S=NECHOS/10.0
      DO 1300 I=1,20
      B=I
      IF((S.GE.B).AND.(S.LE.1+B))GOTO1301
 1300 CONTINUE
 1301 S=1+I
      U(NECHOS+1)=0.0
      U(NECHOS+2)=10.0
      RMS(NECHOS+1)=0.0
      RMS(NECHOS+2)=DIV
      CALL AXIS(0.0,0.0,'ECHO NUMBER',-11,S,0.0,0.0,10.0)
      CALL AXIS(0.0,0.0,'TOTAL RMS CHANGE',16,5.0,90.0
     $,0.0,DIV)
      CALL LINE(U,RMS,NECHOS,1,1,0)
      CALL PLOT(0.0,6.0,-3)
      POW(NECHOS+1)=-40.0
      POW(NECHOS+2)=10.0
      CALL AXIS(0.0,0.0,'ECHO NUMBER',-11,S,0.0,0.0,10.0)
```

```
      CALL AXIS(0.0,0.0,'POWER OF ECHO IN DB',19,4.0,90.0
     / ,-40.0,10.0)
      CALL LINE(U,POW,NECHOS,1,0,0)
      CALL PLOT(0.0,0.0,10)
      CALL PLOT(0.0,0.0,11)
      DO 1600 I=1,NECHOS
      WRITE(9,1601)RMS(I)
1601  FORMAT(F10.1)
1600  CONTINUE
      STOP
      END
```

REFERENCES

Brady, J. K. and Dunn, F., (1974). "Ultrasonically Produced Functional Alterations in Biological Systems," J. Acoust. Soc. Am. 55, s16.

Carson, P. L., Fischella, P. S. and Oughton, T. V., (1978). "Ultrasonic Power and Intensities Produced by Diagnostic Ultrasound Equipment," Ultrasound Med. Biol. 3, 341-350.

Carstensen, E. L., Miller, M. W. and Linke, L. A., (1974). "Biological Effects of Ultrasound," J. Biol. Phys. 2, 173-192.

Carstensen, E. L., Child, S. Z., Law, W. K., Horwitz, D. R. and Miller, M. W., (1979). "Cavitation as a Mechanism for the Biological Effects of Ultrasound on Plant Roots," J. Acoust. Soc. Am. 66, 1285-1291.

Carstensen, E. L., (1982). "Biological Effects of Low Temporal, Average Intensity, Pulsed Ultrasound," Bioelectromagnetics 3, 147-156.

Carstensen, E. L. and Gates, A. H., (1984). "The Effects of Pulsed Ultrasound on the Fetus," J. Ultrasound Med. 3, 145-147.

Chan,S. K. and Frizzell, L. A., (1977). "Ultrasonic Thresholds for Structural Changes in the Mammalian Liver," 1977 Ultrasonic Symposium Proceedings, IEEE Cat.# 77CH1264-1SU, 153-156.

Child, S. Z., Carstensen, E. L. and Miller, M. W., (1975). " Growth of Pea Roots Exposed to Pulsed Ultrasound," J. Acoust. Soc. Am. 58, 1109-1110.

Child, S. Z. and Carstensen, E. L., (1982). "Effects of Ultrasound on Drosophilia-IV," Ultrasound Med. Biol. 8, 311-312.

Coakley, W. T. and Dunn, F., (1971). "Degradation of DNA in High Intensity Focused Ultrasonic Fields at 1 MHZ," J. Acoust. Soc. Am. 50, 1539-1545.

Coakley, W. T. and Nyborg, W. L., (1978). "Cavitation; Dynamics of Gas Bubbles; and Applications," Chapter II in Ultrasound: Its Application in Medicine and Biology, Fry, F. J. Ed. (Elsevier Publishing Co., New York).

Crochiere, R. E. and Rabiner, L. R., (1975). "Optimum FIR Digital Filter Implementations for Decimation, Interpolation, and Narrow Band Filterings," IEEE Trans. Acoust., Speech, Signal Processing ASSP-23, 444-456.

Crum,L. A. and Hanson, G. M., (1982). "Generalized Equations for Rectified Diffusion," J. Acoust. Soc. Am. 75, 1586-1592.

Dunn,F., (1956). PH.D. Thesis, University of Illinois, Urbana, Illinois.

Dunn,F. and Fry, F., (1971). "Ultrasonic Threshold Dosages for the Mammalian Central Nervous System," IEEE Trans. Biomed. Eng. BME-18, 253-256.

Dunn,F., Lohnes, J. E. and Fry, F. J., (1975). "Frequency Dependence of Threshold Ultrasonic Dosages for Irreversible Structual Changes in Mammalian Brain," J. Acoust. Soc. Am. 58, 512-514.

Dunn,F. and O'Brien, W. L., Jr., Eds., (1976). Ultrasonic Biophysics, (Dowden, Hutchinson and Ross, Inc., Stroudsbrug, Pa.).

Eller, A., (1969). "Growth of Bubbles by Rectified Diffusion," J. Acoust. Soc. Am. 46, 1246-1250.

Esche, R., (1952). "Investigation of Vibratory Cavitation in Liquids," Akust. Beih. 4, 208.

Flynn, H. G., (1964). "Physics of Acoustic Cavitation in Liquids," in Physical Acoustics, Vol. 1B, ed. by W. P. Mason, Academic Press, New York.

Flynn, H. G., (1982). "Generation of Transient Cavities in Liquids by Microsecond Pulses of Ultrasound," J. Acoust. Soc. Am. 6, 1926-1932.

Foster, S. G., (1984). Ph.D. Thesis, University of Illinois, Urbana, Illinois.

Frizzell, L. A., Linke, C. A., Carstensen, E. L. and Fridd, C. W. , (1979). "Thresholds for Focal Ultrasonic Lesions in Rabbit Kidney, Liver, and Testicle," IEEE Trans. Biomed. Eng. BME-24, 393-396.

Frizzell, L. A., Lee, C. S., Aschenbach, P. D., Borrelli, M. J., Morimoto, R. S. and Dunn, F., (1983). "Involvement of Ultrasonically Induced Cavitation in the Production of Hind Limb Paralysis of the Mouse Neonate," J. Acoust. Soc. Am. 74, 1062-1065.

Fry, W. J. and Dunn, F., (1962). "Ultrasound: Analysis and Experimental Methods in Biological Research," Chapter 6 in Physical Techniques in Biological Research, (Academic Press Inc., New York).

Fry, F. J., Kossoff, G., Eggleton, R. C. and Dunn, F., (1970). "Threshold Ultrasonic Dosages for Structual Changes in the Mammalian Brain," J. Acoust. Soc. Am. 48, 1413-1417.

Fry, F. J., (1979). "Biological Effects of Ultrasound," Proc. IEEE 67, 604.

Goss,S. A., Johnston, R. L. and Dunn, F., (1978). "Comprehensive Compilation of Empirical Ultrasonic Properties of Mammalian Tissues," J. Acoust. Soc. Am. 64, 423-457.

Goss,S. A., Johnston, R. L. and Dunn, F., (1980). "Compilation of Empirical Ultrasonic Properties of Mammalian Tissues II," J. Acoust. Soc. Am. 68, 93-108.

Harvey, E. N., (1951). in Decompression Sickness, Eds., Fulton, J. F. and Saunders, W. B., Philadelphia.

Lee, C., (1982). M.S. Thesis, University of Illinois, Urbana, Illinois.

Lewin, P. A. and Bjorno, L., (1981). "Acoustic Pressure Amplitude Thresholds for Rectified Diffusion in Gaseous Microbubbles in Biological Tissue," J. Acoust. Soc. Am. 69, 846-852.

Neppiras, E. A., (1980). "Acoustic Cavitation," Physics Reports 61, 159-251.

O'Brien, W. D., Jr., Christman, C. L. and Dunn, F., (1972). "Ultrasonic Investigation of Aqueous Solutions of Deoxyribose Nucleic Acid," J. Acoust. Soc. Am. 4, 1251-1255.

Parks, T. W. and McClellan, J. H., (1972). "A Program for the Design of Linear Phase Finite Impulse Response Filters," IEEE Trans. Audio Electroacoust. AV-20, 195-199.

Sommer, F. G. and Pounds, D., (1982). "Transient Cavitation in Tissues during Ultrasonically Induced Hyperthermia," Medical Physics 9, 1-3.

ter Harr, G., Daniels, S., Eastaugh, K. C. and Hill, C. R., (1982). "Ultrasonically Induced Cavitation *in vivo*," Br. J. Cancer 45, 151-155.

Wood,R. W. and Loomis, A. L., (1927). "The Physical and Biological Effects of High Frequency Sound Waves of Great Intensity," Philos. Mag. 4, 417.